Kobe University Repository : Kernel

PDF issue: 2025-02-07

Study on development of hollow fiber membrane distillation technology and new applications

須賀，友規

(Degree)
博士（工学）

(Date of Degree)
2022-03-25

(Date of Publication)
2023-03-01

(Resource Type)
doctoral thesis

(Report Number)
甲第8360号

(URL)
https://hdl.handle.net/20.500.14094/D1008360

※ 当コンテンツは神戸大学の学術成果です。無断複製・不正使用等を禁じます。著作権法で認められている範囲内で、適切にご利用ください。

Doctoral Dissertation

Study on development of hollow fiber membrane distillation technology and new applications

中空糸膜蒸留技術の開発および新しい応用に関する研究

January 2022

Graduate School of Engineering
Kobe University

Yuki Suga
須賀　友規

Contents

Chapter I General introduction

Chapter I
General introduction

I. 1. Water treatment technology

Water is an indispensable substance for human life. However, only less than 1% of the water existing on the earth can be used for our lives [1]. We use a large amount of water for domestic water, agriculture, industry, and so on [2–4]. In addition, it is said that daily use of water per person is increasing depending on GDP [5,6]. Therefore, global water use continues to increase due to recent population growth and the development of developing countries [2]. As a result, water shortage has become a global problem. In addition, one of the problems related to water is environmental pollution caused by industrial wastewater [7]. To solve these problems, the process dealing with water treatment, such as seawater desalination and wastewater treatment, are carried out everywhere in the world. Generally, distillation technology, for example vacuum distillation, mechanical vapor recompression, thin film distillation, and so on, is used in this field [8]. However, these technologies have problems such as enormous energy consumption and the need for large-scale equipment [9]. Membrane technology is one of the solutions addressing this issue, because the phase separation of feed is not accompanied in the membrane processes, and thus, the energy consumption is lower than distillation process [10,11]. In general, in membrane processes, the solutes in solutions are separated by size sieving effect, and water permeate through the membrane by using the transmembrane pressure (TMP) as a driving force [9]. In addition, there is an advantage that it is possible to easily scale up by simply increasing the number of membrane modules [11]. Those membranes are classified to Microfiltration (MF), Ultrafiltration (UF), Nanofiltration (NF), and Reverse osmosis (RO), according to the size of membrane pore (Figure I-1).

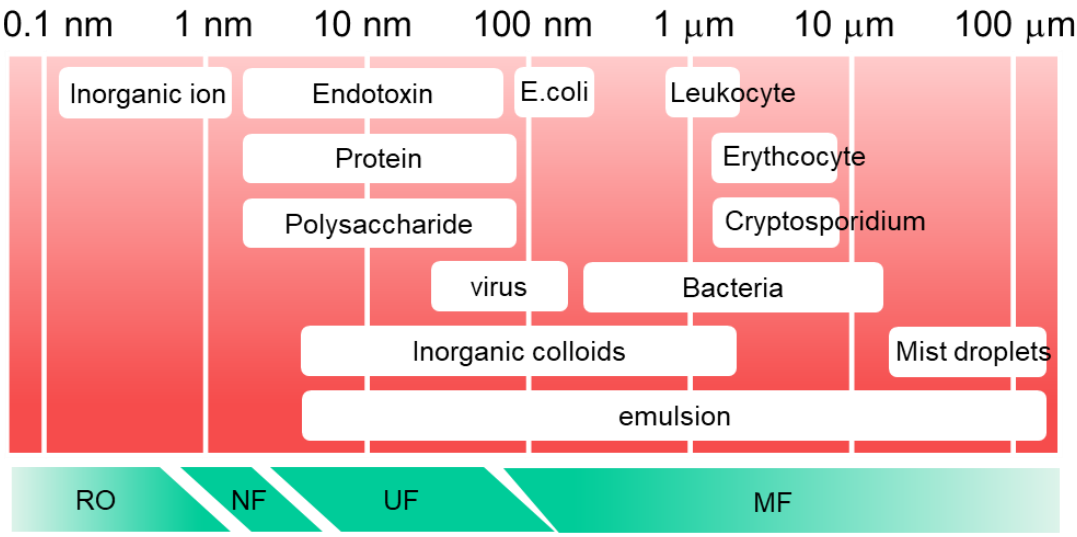

Figure I-1 Membrane classification according to pore size and their separation targets.

I. 2. Membrane separation technology in water treatments

I. 2. 1. Microfiltration (MF)

Microfiltration (MF) is a separation process in which the membranes with 0.05 to 10 μm of pore size are used [11–13]. As a characteristic property of MF membranes, they can separate a variety of insoluble components, such as emulsions, microorganisms, and suspended solids from solutions (Figure I-2). Regarding the applications, MF is widely used industrially, for example, refining fermented liquids, prefiltration of seawater, food process, membrane bioreactor (MBR) for treatment of wastewater and so on [13,14]. Almost all of MF membranes are organic membranes, which are made by various organic polymers such as polyethylene, polysulfone, polyvinylidene fluoride (PVDF), etc. [11,13]. However, some of inorganic membranes have also been commercialized in recent years [15]. They have longer lifetime than that of organic membranes.

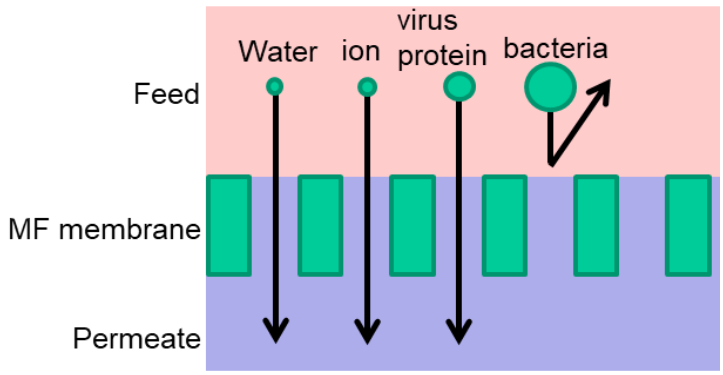

Figure I-2 Schematic of microfiltration (MF).

I. 2. 2. Ultrafiltration (UF)

Ultrafiltration (UF) is a separation process in which the membranes with 0.01 μm to 0.1 μm of pore size are used, and the range of molecular weight cut-off is about 3 to 100 kDa [10,12,16]. UF membranes can separate smaller particles than MF membrane, for examples, enzymes, proteins and virus, etc. (Figure I-3). On the other hand, much smaller molecules such as inorganic ions cannot be separated by UF membranes [17]. Regarding the applications, UF is also widely used industrially, for example, virus removal in pharmaceutical manufacturing and impurity removal in ultrapure water production [11]. It is also used as a pretreatment for the desalination process with reverse osmosis (RO) membrane [18]. Additionally, UF membrane is also used as a microporous support for fabricating thin film composite (TFC) membranes which has ultrathin active layer on the UF [19].

Almost all commercial UF membranes are organic membrane, for example, polyacrylonitrile, polysulfone, and poly ether sulfone, etc [16].

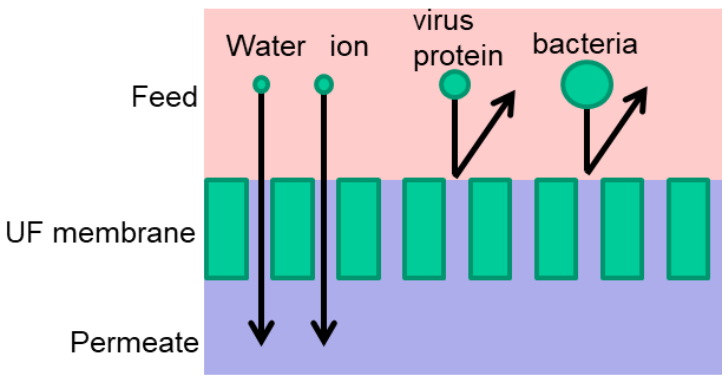

Figure I-3 Schematic of ultrafiltration (UF).

I. 2. 3. Nanofiltration (NF)

The pore size of nanofiltration (NF) membrane is approximately 1 nm [17, 20]. Many of NF membranes are composite or asymmetric membrane, which has an active layer (skin layer) on porous support layer (Figure I-4) [17]. Historically, NF membrane was called as a loose RO. Small molecules such as H_2O and monovalent ions can permeate through the active layer by the dissolution/diffusion mechanism, but some bigger solute such as multivalent ions and proteins cannot. Therefore, NF membranes can separate small compounds that permeate through UF and MF membranes. Regarding the application of NF, NF process is used for water purification for manufacturing electronic devices at first. Now, NF is also applied to water softening, and recovery of valuable resources. Today, most popular NF membranes are TCF membrane with polyamide active layer on polysulfone support, and cellulose acetate asymmetric membrane [20–22].

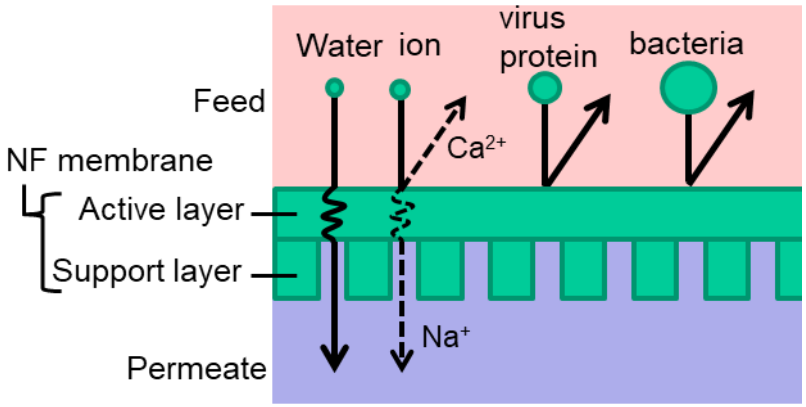

Figure I-4 Schematic of nanofiltration.

I. 2. 4. Reverse osmosis (RO)

RO is a process that separates water and ions with a semi-permeable membrane by applying an external pressure higher than the osmotic pressure difference between feed and permeate to the feed side (Figure I-5) [19]. RO membranes have an active layer on a porous support layer, as well as NF membranes (Figure I-6). However, the active layer of RO membranes is denser than that of NF, so that RO membrane can separate H_2O and monovalent ions, which cannot be separated by NF membranes. Because RO can separate H_2O and Na^+, RO have been applied to many desalination processes such as brackish water and seawater desalination [23]. Furthermore, RO is also applied for recovery of

various valuable resources, for example, in food, chemical and pharmaceutical processes [24–26]. With the progress of RO operation, the osmotic pressure of the feed solution increases as the increasing of concentration of the solute in the feed solution. Therefore, RO membranes are required to have high pressure resistance. Moreover, RO has a limit to the osmotic pressure of feed that can be handled [19]. Recently, research for expanding the applicable concentration range of RO has been conducted [18].

The materials of RO membrane are the same as those of NF membranes [19].

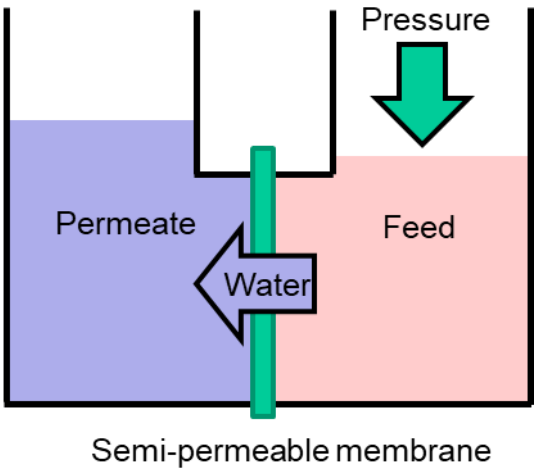

Figure I-5 Mechanism of water permeation in reverse osmosis (RO).

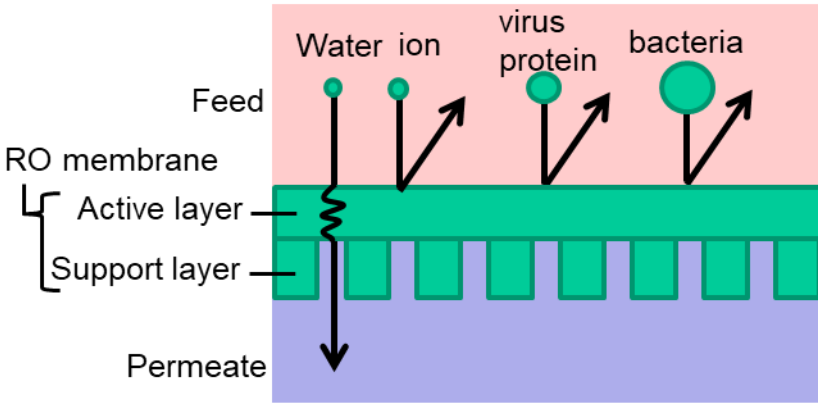

Figure I-6 Schematic of Reverse osmosis (RO).

I. 3. Another membrane separation technology in water treatments

In the membrane processes mentioned above, the principle of membrane separation is the size sieving using TMP as the driving force. However, there are some feed solutions

that cannot be treated by the membrane technologies mentioned above. Thus, in recent years, another membrane separation technologies which use different separation principles and driving force have been studied. In this section, I explain Forward osmosis (FO), Pervaporation (PV), and Membrane distillation (MD) as examples of another membrane technologies.

I. 3. 1. Forward osmosis (FO)

In FO process, a semi-permeable membrane and a high osmotic pressure solution which is called as a Draw solution (DS) are used (Figure I-7) [27, 28]. In FO process, water permeates through the membrane using the osmotic pressure difference between feed solution and DS as a driving force. Therefore, FO does not need applying high TMP to permeate water through the FO membrane, unlike RO [28]. So, FO can save operation energy more than RO because FO consumes less electricity for pump. However, FO needs the recovery of DS, because DS is diluted and decrease its osmotic pressure by permeated water during FO operation.

The materials of FO membrane are the same as those of RO and NF membranes [28–30].

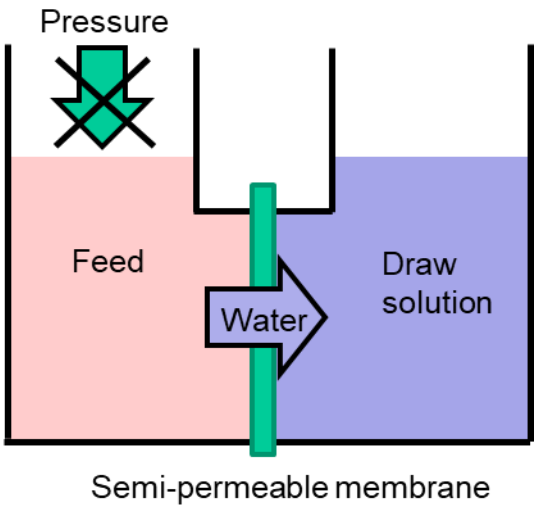

Figure I-7 Mechanism of water permeation in forward osmosis (FO).

I. 3. 2. Pervaporation

Pervaporation (PV) is a technology for separating volatile components from a solution using a dense semipermeable membrane (Figure I-8) [31]. In PV, only volatile

components in the feed solution permeates through the dense active layer of the PV membrane by the dissolution/diffusion mechanism by using vapor pressure difference as a driving force [31]. Due to the differences in solubility and diffusivity between solute (volatile components) and solvent against the active layer of the PV membrane, PV can separate volatile components regardless of molecular size. On the other hand, the permeability of PV membrane tends to be low due to the dense layer. In addition, the system becomes complicate to obtain vapor pressure difference, for example, using vacuum pump or sweep gas on the permeate side of PV membrane [32].

As the material of dense active layer of PV membrane, hydrophilic polymers and hydrophobic polymers are selected according to the target components. For example, poly vinyl alcohol is often used as the hydrophilic polymer, and polydimethylsiloxane is often used as the hydrophobic polymer because of their high permeability for volatile molecules [33,34].

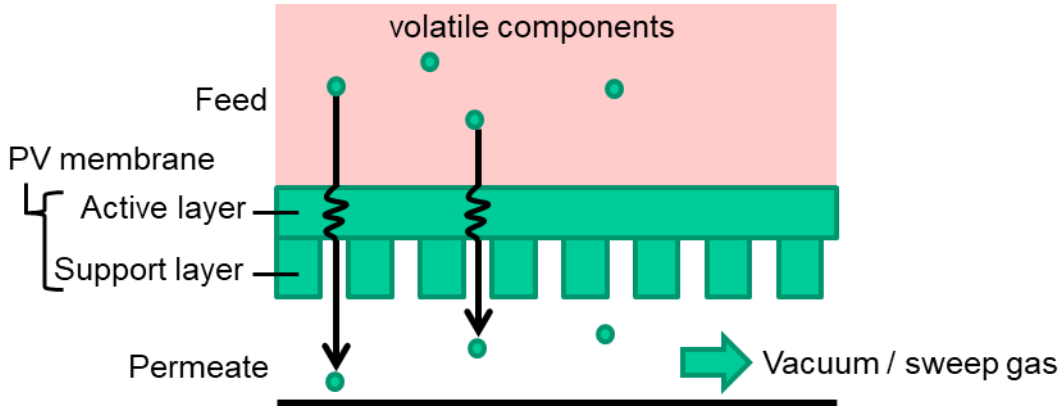

Figure I-8 Schematic of pervaporation (PV).

I. 3. 3. Membrane distillation (MD)

Membrane distillation (MD) is a process that can separate a vapor and a solution by using porous membrane [35–37]. In treating an aqueous solution, hydrophobic porous membrane is used as MD membrane, because an aqueous solution cannot permeate through the membrane due to its hydrophobicity, but vapor can permeate through the membrane pore [37]. In MD, permeability of the vapor becomes much larger than that of PV, due to larger pore size of MD membrane. However, there is the risk of membrane wetting which causes the loss of ability of separating vapor and solution [38].

The details of MD are described in the section I.4, since MD is the membrane process treated in this thesis.

I. 4. Membrane distillation (MD)

I. 4. 1. Principle of membrane distillation

As described at section I.3.3, MD is a process that can separate a vapor and solution using porous membrane. In a water treatment by MD, the water vapor from feed solution permeates through the MD membrane by using the vapor pressure difference as a driving force, and then the permeated vapor is condensed at the permeate side of the membrane [35–37]. Involatile solute such as Na^+ cannot permeate through the membrane, so that the purity of condensed water obtained by MD is very high [36].

The driving force of MD is the vapor pressure difference between feed side and permeate side of MD membrane. Therefore, as long as the vapor pressure difference can be obtained, MD can treat a solution with very high osmotic pressure which cannot be treated by RO [39].

Even for such high performances of MD technologies for water treatment, MD is not still widely commercialized. One of the biggest issues for commercialization of MD is its expensive water production cost [40–42]. In MD process, heat energy and membrane cost are the large portions of the water production cost [41]. MD operation does not require a high TMP like RO, but requires thermal energy for vaporization. Most of the energy consumed by MD is this thermal energy, but it is thought that energy consumption can be reduced by using low-grade waste heat or solar energy [42,43]. Moreover, the severe issue of MD is membrane wetting. If the membrane gets wet, the liquid and solute will permeate through the membrane and contaminate the permeate. In addition, wetting pore cannot permeate the vapor. As a result, wetted membranes will not function as the MD membrane. In this manner, the membrane wetting is closely related to the stable operation of MD and the life of the MD membrane. Thus, various studies for improving the hydrophobicity of the membrane have been conducted in order to avoid membrane wetting. However, the anti-wetting of membrane is still challenging.

I. 4. 2. Theory of membrane distillation

I. 4. 2. 1. Vapor permeability through the membrane

In MD process, the vapor flux, J (kg/m^2·h) is proportional to the vapor pressure difference between the feed side and the permeate side, and is given by Equation (I-1) [44–46]

$$J = \alpha(P_{feed} - P_{permeate}) \quad \text{(I-1)}$$

where, α (kg/m^2·h·kPa), P_{feed} (kPa) and $P_{permeate}$ (kPa) indicate the vapor permeation coefficient, the saturated vapor pressures at membrane surface of the feed side, and of the permeate side, respectively. Many studies of the vapor permeation coefficient, α, have been reported to reveal the mechanism of MD and to improve MD technology. In many previous studies, the Kinetic Theory of Gases is used to explain the behavior of vapor permeation through the MD membranes [47,48]. In this theory, the mass transport of the vapor is explained by several types of flow, Knudsen type of flow, molecular diffusion type of flow, and mixed model of them (Figure I-9).

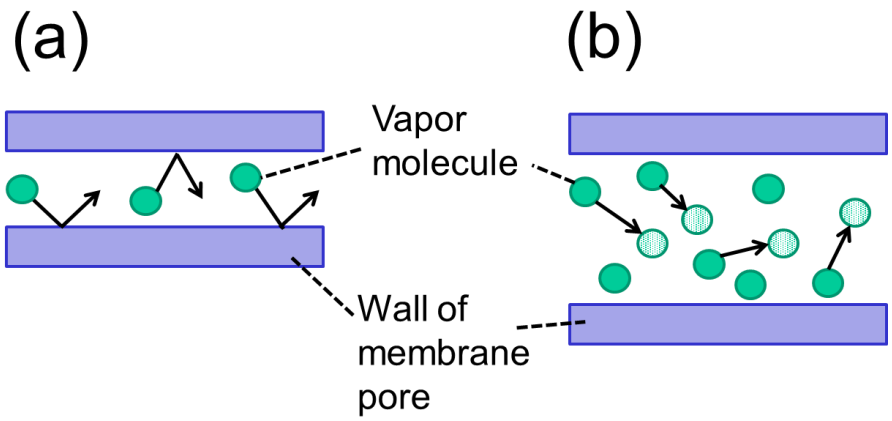

Figure I-9 Schematic of transporting mechanism of vapor permeation in the pore of MD membrane: (a) Knudsen type of the flow, (b) molecular diffusion type of the flow.

The mechanism changes depending on the value of Knudsen number which is determined by the relation between the mean free path of the vapor molecule and the pore size of the membrane as is defined by Equation (I-2),

$$K_n = \frac{\lambda}{d_p} \tag{I-2}$$

where K_n (-), λ (m), and d_p (m) indicate the Knudsen number, the mean free path of vapor molecule, and the membrane pore diameter, respectively. The mean free path is given by Equation (I-3) [7],

$$\lambda = \frac{k_B T}{\sqrt{2}\pi P_m \sigma^2} \tag{I-3}$$

where k_B (-), T (K), P_m (Pa) and σ (m) indicate Boltzmann constant, absolute temperature, mean pressure within the pore, and collision diameter of the vapor molecule, respectively. In the case of water vapor molecule, the mean free path of water vapor is given by Equation (I-4) [9],

$$\lambda_W = \frac{k_B T}{\sqrt{2}\pi P_m (2.641 \times 10^{-10})^2} \tag{I-4}$$

where λ_W (m) indicates the mean free path of water vapor molecule. 2.641 means the collision diameter of water vapor molecule. It is found from Equation (I-4) that λ_W varies depending on the water vapor temperature, and/or the mean pressure within the membrane pore.

If K_n is larger than 10, vapor molecule flows as Knudsen type of flow. If K_n is smaller than 0.01, vapor molecule flows as molecular diffusion type of flow [47,49]. And if Kn is larger than 0.01 and less than 10, vapor molecule flows as the combined flow of these two types of flow. If the membrane is composed of the pores with a uniform pore size r_u (m), the water vapor permeation coefficient of Knudsen type of flow, α_W^K, molecular diffusion type of flow, α_W^D, and combined flow, α_W^C are given by Equations (I-5)–(I-7), respectively [47,49–51],

$$\alpha_W^K = \frac{2}{3RT}\frac{\varepsilon r_u}{\tau\delta}\left(\frac{8RT}{\pi M_W}\right)^{\frac{1}{2}} \tag{I-5}$$

$$\alpha_W^D = \frac{1}{RT\delta}\frac{\varepsilon P D_W}{p_a \tau} \tag{I-6}$$

$$\alpha_W^C = \frac{1}{RT\delta}\left(\frac{3\tau}{2\varepsilon r_u}\left(\frac{\pi M_W}{8RT}\right)^{\frac{1}{2}} + \frac{p_a \tau}{\varepsilon P D_W}\right)^{-1} \tag{I-7}$$

where R (J/K·mol) is the gas constant. δ (m), ε (-) and r_u (m) indicate the membrane thickness, the membrane porosity, and the membrane pore radius, respectively. M_W (g/mol) represents the molecular weight of water. p_a (Pa), τ (-) and P (Pa) indicate the air pressure in the membrane pore, the pore tortuosity of the membrane, and the total pressure in the membrane pore, respectively. D_W denotes the diffusion coefficient of water.

For example, when the P_m is 1.013 x 10^5 Pa, T is 323 K, and d_p is 0.1 μm, λ_W and Kn become 0.14 μm and 0.71. So that the combined flow of Knudsen flow and molecular diffusion flow will occur. If P_m changes to 1.013 x 10^4 Pa, λ_W and Kn become 1.4 μm and 0.071. So that the only Knudsen flow will occur. In order to improve the permeation coefficient of the MD membrane, it is obvious from Equations (I-5)–(I-7) that the required membrane properties are larger membrane porosity, thinner membrane thickness, and smaller tortuosity. In addition, larger pore diameter is also required to improve the permeation coefficient of the MD membrane.

I. 4. 2. 2. Membrane wetting

As mentioned above, MD membrane must separate liquid and vapor. If the membrane gets wet, the liquid and solute will permeate through the membrane and contaminate the permeate. Therefore, membrane wetting is the one of the biggest issues for stable MD operation. In order to avoid membrane wetting, MD membrane must have the property of being hard to be wetted by the liquid. For example, when handling an aqueous solution, a hydrophobic porous membrane is suit for MD membrane. The membrane durability for wetting is evaluated by the liquid entry pressure (LEP (Pa)), which is a pressure required for liquid to penetrate the membrane and is given by Equation (I-8) [36,52,53];

$$LEP = \frac{-2B\sigma_L cos\theta}{r_{max}} \tag{I-8}$$

where, B (-) indicates a geometric factor determined by pore structure, for example, B = 1 for cylindrical pores. σ_L (kg/s^2), θ (°), and r_{max} (m) indicate a surface tension of liquid, a contact angle of liquid, and a maximum pore radius of membrane, respectively.

If TMP excess the LEP of the membrane, liquid will penetrate the membrane and membrane wetting will occur. In order to increase the LEP of the membrane, improving

the hydrophobicity of membrane surface to increase the contact angle, forming the surface shape like the lotus leaf, and reducing the maximum pore size are considered to be effective [54].

I. 4. 3. Development of MD membrane

MD membrane is required to have a high flux and a large LEP. As mentioned above, required properties for ideal MD membrane are as follows [36,48],

- Large mean pore diameter and small maximum pore diameter
- Thin membrane thickness
- High porosity
- Small tortuosity
- High hydrophobicity

In order to develop membrane having these properties, many studies on MD membrane fabrication have been reported. As the material for MD membrane, a polymer having high heat resistance and high hydrophobicity is suitable. Therefore, polyolefins such as polyethylene (PE) and polypropylene (PP), and fluoropolymers such as PVDF and polytetrafluoroethylene (PTFE) are often used [55–58]. Among those polymers, PVDF is one of most reported materials for MD membrane, because of its high chemical resistance, hydrophobicity, and ease of fabrication [57,59].

Regarding the way to fabricate PVDF membrane, non-solvent induced phase separation (NIPS) and thermally induced phase separation (TIPS) (Figure I-10) are often used [12,60]. In NIPS, the phase separation occurs in a uniform polymer solution by penetrating of a non-solvent to the polymer solution [12,59]. In TIPS, phase separation occurs by cooling the uniform polymer solution in which polymer is dissolved at a high temperature [12,57,61] (Figure I-10). In addition, many researches to fabricate composite membrane have been reported.

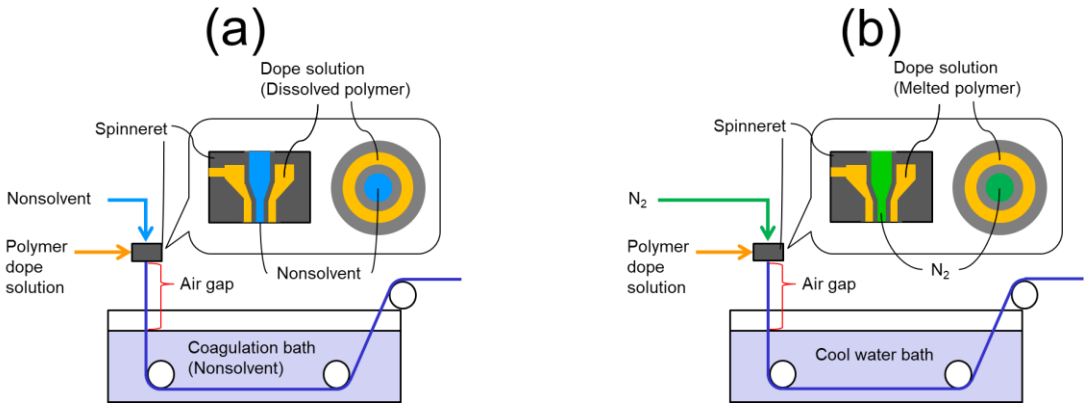

Figure I-10 Schematic of the fabrication of PVDF membrane, (a) NIPS, (b) TIPS.

The shape of the membrane is roughly classified into a flat sheet membrane and a hollow fiber (HF) membrane (Figure I-11) [36]. Flat sheet membrane is easy to fabricate. Therefore, many studies are reported on the fabrication of composite flat sheet membrane using novel materials, such as SiO_2 [62], graphene oxide [63], carbon nanotube [64], and so on. Compared with a flat sheet membrane, the HF membrane has a larger specific membrane surface area per volume [65]. As described at section I. 4. 4, there are various operating methods for MD, and there are suitable operating methods for each of the flat sheet membrane and the hollow fiber membrane.

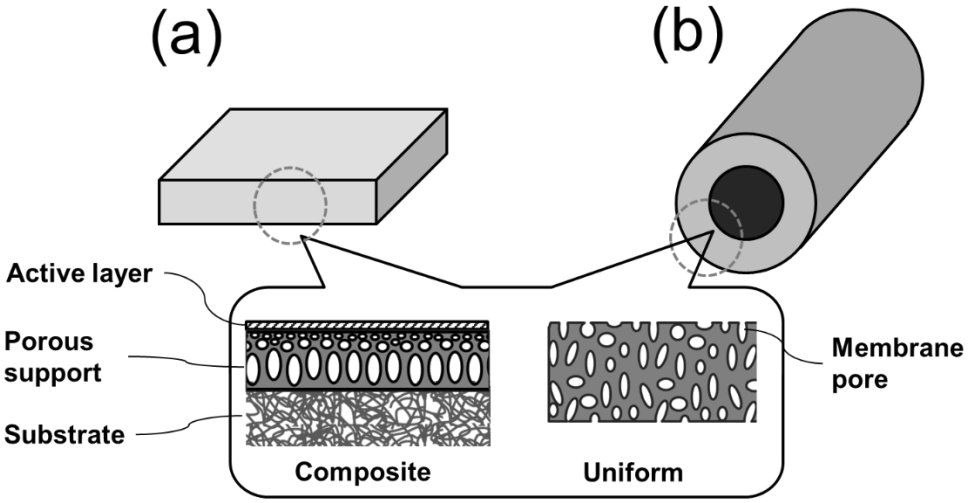

Figure I-11 Schematic of the shape of membrane, (a) flat sheet membrane, (b) hollow fiber membrane.

I. 4. 4. Operation method

In MD, it is important to obtain the high vapor pressure difference between both sides of the membrane to increase the vapor flux. In addition, MD requires thermal energy for vaporization, which accounts for the most of energy consumption of MD [66]. In order to obtain high vapor flux and to save energy consumption, various studies have been reported on MD operating methods [35]. Those operation methods can be roughly classified into four, direct contact MD (DCMD), air gap MD (AGMD), sweep gas MD (SGMD), and vacuum MD (MD) [53]. Details of each operation methods are explained below.

I. 4. 4. 1. Direct contact MD

Direct contact MD (DCMD) is a method in which a feed water flows in one side of the membrane and a cooling water flows in the other side (Figure I-12) [45,67]. Water vapor permeates through the MD membrane from the feed side to the permeate side directly. DCMD is the simplest MD operation method, and it is easy to obtain the vapor pressure difference and generate high vapor flux. Therefore, among the various MD methods, most of researches have been conducted by DCMD. However, DCMD operation consumes a lot of energy because heat conduction through the membrane is easy to occur [46,66]. Regarding membrane types for DCMD, both flat sheet membrane and hollow fiber membrane are used [45].

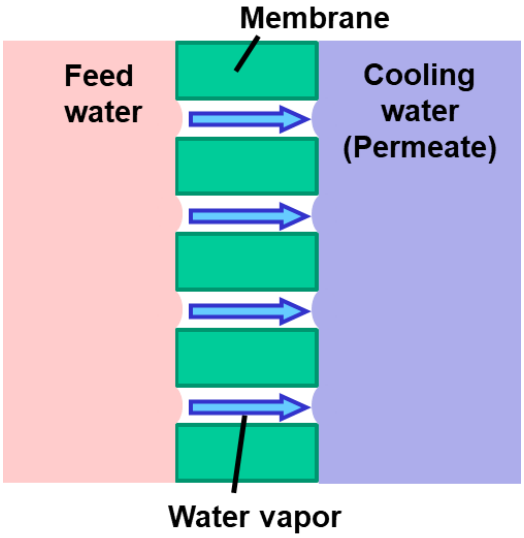

Figure I-12 Schematic of direct contact membrane distillation (DCMD).

I. 4. 4. 2. Air gap MD

Air gap MD (AGMD) is a method which has an air gap between the membrane and the cooling water (Figure I-13) [68]. Heat energy can be used more efficiently than DCMD because heat conduction is reduced by the air gap [35,69]. In addition, it is possible to use the feed water as the cooling water and recover the latent heat for vaporization since the cooling water and the condensed water are separated from each other [70]. However, the vapor pressure difference is difficult to obtain, and vapor flux tend to be lower than DCMD [35]. Regarding membrane types for AGMD, flat sheet membrane is more suitable than hollow fiber membrane because it is easier to assemble the membrane module with the airgap which has constant distance between membrane and cooling water.

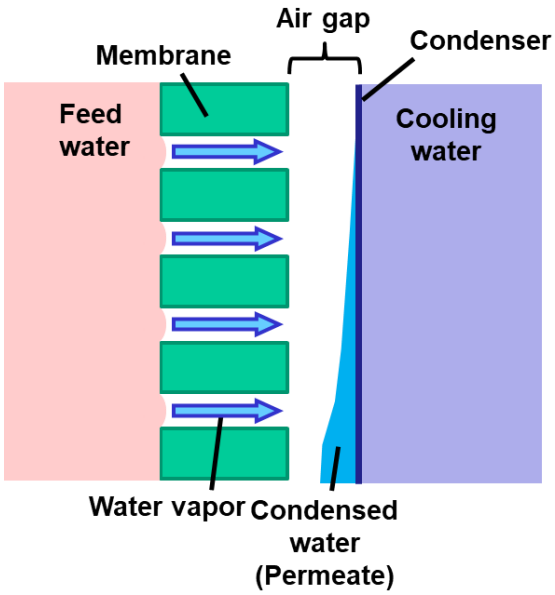

Figure I-13 Schematic of air gap MD (AGMD).

I. 4. 4. 3. Sweep gas MD

Sweep gas MD (SGMD) is a method in which sweep gas flows through the airgap part of AGMD for activating the diffusion of vapor molecule from the membrane surface at air gap part to the condenser (Figure. I-14) [35,71,72]. So, a high flux can be obtained in SGMD even if the cooling water and the membrane are separated from each other. In addition, heat energy consumption can be decreased due to low heat conduction like AGMD [71,73]. Both flat sheet membranes and hollow fiber membranes can be applied

to SGMD, because the wide tolerance of SGMD for the distance between the membrane and the cooling section.

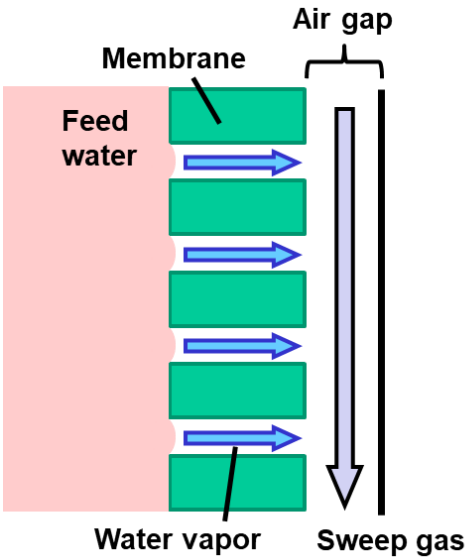

Figure I-14 Schematic of sweep gas MD (SGMD).

I. 4. 4. 4. Vacuum MD

Vacuum MD (VMD) is a method in which the airgap part of AGMD is decompressed for activating the diffusion of vapor molecule from the feed to the condenser through the membrane (Figure. I-15) [35,53,74]. As same as SGMD, a high vapor flux can be obtained. In addition, heat conduction becomes very low because one side of the membrane is decompressed in VMD, and it leads high energy efficiency of MD operation [53]. On the other hand, in VMD, TMP becomes higher than any other MD methods, due to the decompression of permeate side of the membrane [74]. Therefore, the risk of membrane wetting will increase. For a stable VMD operation, the membrane with high LEP is needed [35,74]. As long as membrane has an efficient LEP, both flat sheet membranes and hollow fiber membranes can be applied to VMD because the wide tolerance of VMD for the distance between the membrane and the cooling section, like SGMD.

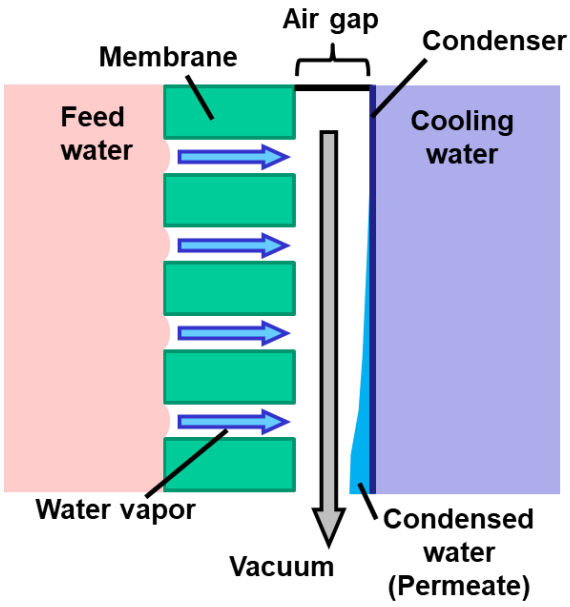

Figure I-15 Schematic of vacuum MD (VMD).

I. 4. 5. Application of MD

Almost all MD applications target aqueous solutions by using the hydrophobic membranes. In treating with aqueous solutions, MD can produce very pure water from various feed solutions. In addition, MD can make pure water even from very high concentration feed solution which cannot be treated by RO [39]. Regarding energy consumption for water production, it can be reduced by utilizing low-grade waste heat and solar energy, as mentioned above. In the previous researches of MD, the applications that can make use of such characteristics of MD have been studied as below.

- Water production

  Water production has been considered as a major application of MD since the beginning of MD research. In particular, desalination has been studied as the main application of MD for a long time. Therefore, applications for desalination of seawater or brackish water have been reported most in MD researches [35,66,75,76]. Compared with RO, MD can improve the water recovery rate by treating with a higher concentration of feed water. In addition, the required electricity for pump can be reduced in MD [40,66]. Furthermore, it is possible to reduce the risk of membrane fouling because TMP of MD is much lower than RO [67].

- Concentration (recovery of valuable solute)

MD can squeeze water from high-concentration solutions as long as the vapor pressure difference is obtained. Taking advantage of this feature, the applications for concentrating solutions have been studied. For example, zero liquid discharge (ZLD), which is a technology to reduce the amount of wastewater, have been studied from the viewpoint of environmental perspective [77–79]. Currently, conventional distillation technologies such as vacuum distillation have been applied to the industrial processes [80]. MD has a potential to reduce energy consumption by using waste heat which is difficult to use by other distillation technologies. Some studies have also been conducted to apply MD in food process [9,81]. It is expected that MD can concentrate food process solution in lower temperature than conventional distillation [82]. In addition, MD can reduce membrane fouling because of lower TMP than any other membrane technologies, such as MF, UF, and RO [67].

I. 5. Purpose of this study

In this thesis, first, I investigated the required membrane properties for the stable long-term MD operation, from the viewpoint of avoiding membrane wetting [83]. As described in section I. 4. 1., MD has many merits that conventional technologies do not have. However, despite years of research, there are no examples of MD being commercialized, as far as I know. One of the biggest reasons of that is the membrane wetting. The membrane wetting makes the stable long-term MD operation difficult, and the life of MD membrane short. A stable long-term operation and a long membrane life are essential for commercialization. Many researches have been conducted to improve the membrane performance of MD, but few studies have been conducted to investigate the required properties of MD membrane from the viewpoint of stable long-term operation. In this study, I chose VMD as the ideal MD operating method because VMD has high heat efficiency, so that it is possible to reduce heat energy for water production. Furthermore, it is expected to obtain a higher flux in VMD, compared to other methods. Moreover, the risk of membrane wetting in VMD operation is highest in four MD setups, as mentioned in section I. 4. 4. 4. Therefore, if the enough anti-wetting property is obtained as VMD

membrane, this membrane is possible to apply for other processes. I investigated the membrane characteristics required for long-term stable operation for VMD by using four types of PVDF HF membranes. PVDF was used because of its high chemical and heat resistance, and ease of fabrication. HF membrane was used because the HF membrane has a larger specific membrane surface area per volume than the flat membrane, and it is possible to emphasize the compactness, which is one of the strengths of the membrane technologies.

Secondly, I attempted to apply VMD process for a seawater desalination [84]. In seawater desalination, a scale precipitation often occurs on the membrane surface, and it may lead a fatal problem for MD in seawater desalination [85,86]. This is because the scale precipitated on the surface of the membrane forms the scale layer and prevents vapor permeation [87,88]. In addition, precipitated scale makes membrane surface hydrophilic and then decreases LEP of the membrane, so that membrane wetting is likely to be occurred [87]. Therefore, I focused on the Reynolds number, and conducted research on the optimum membrane characteristics and operating method for preventing scale precipitation for VMD seawater desalination.

Lastly, I further investigated the recovery of valuable solutes from organic solvent/water mixtures as a new application of MD [89]. The organic solvent/water mixtures are treated in various processes such as chemical, food, and pharmaceutical processes. In addition, the demand for non-heated concentration technologies has increased due to the abundance of heat-sensitive valuable solutes. It is considered that MD has many merits in the recovery the valuable solute, because MD uses the vapor pressure difference as a driving force for vapor permeation [35]. For example, membrane fouling can be reduced compared to the conventional method using TMP as the driving force [67]. Furthermore, it would be possible to use MD as the non-heated concentration technology due to the ease of obtaining vapor pressure difference by MD. However, it is difficult to treat the organic solvent/water mixtures with MD because they decrease the surface tension of aqueous solution and increase the risk of membrane wetting of MD. So, I have applied high hydrophobic PVDF HF membrane, which was obtained in the above investigation, to the recovery of valuable solutes from organic solvent/water mixtures.

I. 6. Scope of this study

This paper describes the improvement of MD membranes and applications of MD process. This thesis is divided into five parts.

Chapter I:

The overall introduction for MD. This section contains the theory, the status of research and development, and application candidates of MD.

Chapter II:

In this section, the effect of membrane characteristics on the long-term stability of VMD system were evaluated [83]. For this evaluation, four different types of polyvinylidene difluoride hollow fiber membranes were fabricated, and used for the VMD operation with 3.5 wt% NaCl aqueous solution at 65 °C as a feed under 11 kPa of air gap pressure. As a result of the evaluation, it was found that the liquid entry pressure (LEP) is the most important factor in the proposed VMD system. The pilot-scale module was also investigated by using the membrane with LEP higher than 0.37 MPa. It was revealed that the pilot-scale module was very stable for long-term operations, and the vapor flux was approximately 19.3 $kg/m^2 \cdot h$ with a total salt retention factor of over 99.9% during the 300-h operation.

Chapter III:

This section shows how to avoid membrane scaling during VMD operation for seawater desalination [84]. Membrane scaling is one of the biggest issues which decrease vapor permeability and hydrophobicity of MD membrane, and lead membrane wetting and flux degradation [85–88]. To solve the scaling issue, the relationship between Reynolds number of feed and the amount of scale precipitation was evaluated. In the evaluation, vacuum MD (VMD) operations with super hydrophobic polyvinylidene fluoride (PVDF) hollow fiber (HF) membrane was conducted with a real seawater as a feed at various linear velocity. In addition, two types of HF membranes of different inner diameters were used. From the results of 24-hours VMD operation, it was found that the amount of scale precipitation on the bore surface of the

membrane satisfactorily decreased over 1200 of the Reynolds number. This was due to the decrease of concentration polarization at bulk/membrane interface [46,85,86]. The vapor flux also increased with the Reynolds number. Furthermore, the membrane with larger inner diameter could reduce the amount of scale precipitation and pressure drop, even at same linear velocity. From these results, operating with high linear velocity under which the Reynolds number of the feed is over 1200, and larger inner diameter HF membrane are needed for stable VMD seawater desalination operation.

Chapter IV:

This section shows the study for the new MD application, the recovery of the variable solute from the organic solvent/water mixtures without heating [89]. As mentioned in the section I.5, it is harsh condition in which the feed solution contains organic solvent, because of the effect of organic solvent on decreasing surface tension of the aqueous feed solution. To deal with this situation, the high hydrophobic MD hollow fiber membrane was used in DCMD operating method. The DCMD with 1000 ppm NaCl, which is a model valuable solute and an indicator of membrane wetting, aqueous solution achieved 0.8 $kg/m^2 \cdot h$ of vapor flux and > 99.9% of NaCl retention, even at feed and coolant temperatures of 25 and 10 °C, respectively. In addition, DCMD was conducted under various conditions, including feed temperatures of 25, 35, and 45 °C, and organic solvent concentration of 15, 30, and 50 wt%, using ethanol/water and acetonitrile/water mixtures containing 1000 ppm NaCl. As a result, it was found that the total vapor flux increased with increasing temperature and concentration of organic solvents, as the partial vapor pressure of the organic solvents increased. Additionally, no solute leaked under any condition, even when the surfactant was used as a valuable solute.

Chapter V:

Summarizes the conclusions of this thesis.

Chapter Ⅱ

Effect of the characteristic properties of membrane on long-term stability in the vacuum membrane distillation process

II. 1. Introduction

As mentioned in Section I. 4. 1., membrane distillation (MD) processes have garnered attention as alternative technologies, because the demand for water treatments that cannot be handled by the RO process is increasing [35]. However, MD is not still widely commercialized due to its expensive water production cost [40–42].

In MD process, heat energy and membrane cost are the large portions of the water production cost [41]. To reduce the heat energy cost, waste heat [42] or natural energy, such as sunlight, are considered [43]. In addition, it is important to increase the heat efficiency of the installation [35]. Heat efficiency significantly depends on the operation setup. So, it is important to select a setup with high heat efficiency. In addition, to reduce the practical membrane cost, it is important to increase the vapor flux ($kg/m^2 \cdot h$) and lifetime of the MD membrane.

As illustrated in Figure II-1, the typical MD setups are divided into four systems [83,90]: direct contact MD (DCMD) (Figure II-1a), air gap MD (AGMD) (Figure II-1b), sweep gas MD (SGMD) (Figure II-1c), and vacuum MD (VMD) (Figure II-1d). DCMD is the simplest MD operation method and has been reported in many papers [35]. In DCMD, feed water is in contact with a coolant via a membrane and the pass for its vapor permeation is the shortest. Therefore, the vapor flux of DCMD is very high. However, heat efficiency is not high because heat conduction through the membrane is most likely to occur [46], and the temperature polarization decreases the flux [91]. AGMD suppresses the heat conduction through the membrane by providing an air gap between the membrane and cooling section [68]. Consequently, its heat efficiency was higher than that of DCMD. However, its vapor flux is lower than that of DCMD owing to the lower vapor pressure

difference. To speed up the diffusion transfer of vapor, in SGMD, sweep gas flows through the air gap part [92], while the air gap part is decompressed in the VMD [93]. Therefore, it is possible to achieve high vapor flux and low heat conduction simultaneously by SGMD and VMD. Especially, in VMD, the highest vapor flux is expected since the high vapor pressure difference can be obtained by decompressing the permeate side. In addition, in VMD, the effect of a temperature polarization will be neglected since the vapor pressure in the permeated side is determined by the decompressed pressure of the permeate side. Additionally, VMD systems can prevent feed water from contaminating the permeated water because the membrane and condenser can be placed farther apart than DCMD and AGMD. In the ideal VMD case, it is almost unnecessary to operate the vacuum pump once the air gap part is decompressed during VMD operation. Thus, the energy cost for decompressing will be low.

From the perspective of the total water production cost, VMD is considered to be the most efficient operation system. However, there are some specific problems for VMD. For example, the higher liquid entry pressure (LEP), which is defined as the pressure required for the liquid to penetrate the membrane [53], than other systems will be required since the large transmembrane pressure difference due to decompressing causes a wetting of membrane. It is also considered that the leaked salts through the membrane may crystalize on the permeate side of membrane surface. Thus, it is almost impossible to evaluate the membrane wetting (salt retention) continuously. In this chapter, taking these situations into consideration, I used the VMD as the operating system and I attempted to evaluate the effect of the characteristic properties of membrane on VMD performance, especially on the long-term stability of MD membrane. To achieve this goal, I fabricated four different types of polyvinylidene fluoride (PVDF) hollow fiber (HF) membranes [61,94,95] using the well-known methods. There is no novelty in the membrane fabrication methods, but the understanding on parameters which effectively affect the long-term stability of MD membrane will indicate the guiding principle of developing high performance MD membrane. Such kind of study has not been reported yet, as far as I know.

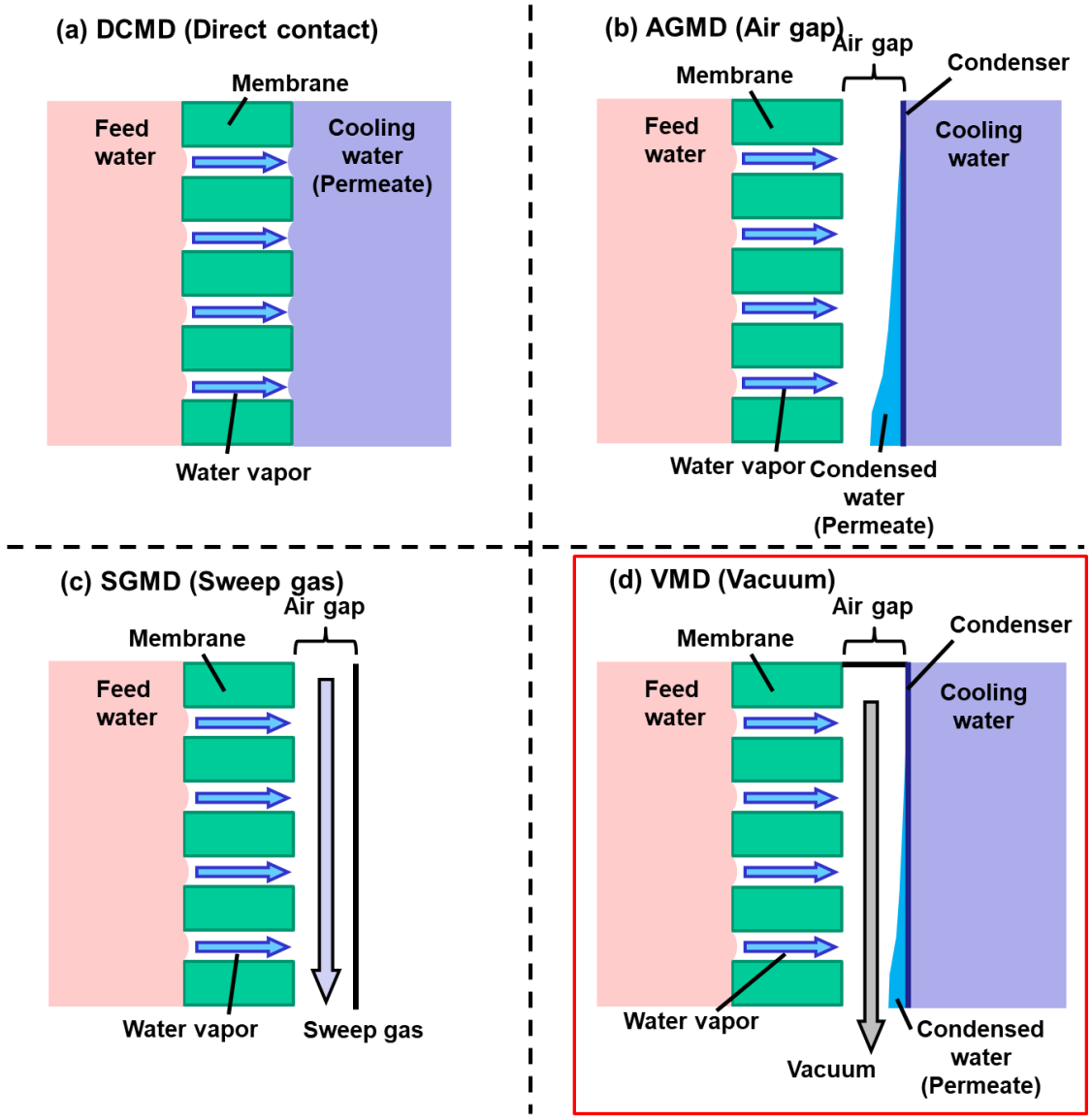

Figure II-1 Schematics of typical membrane distillation (MD) operation setups [83]. (a) Direct contact MD (DCMD), (b) Air gap MD (AGMD), (c) Sweep gas MD (SGMD), (d) Vacuum MD (VMD). VMD was used in this paper.

II. 2. Materials and Methods

II. 2. 1. Materials

Solef 6010 and Solef 6020 (SOLVAY, Brussels, Belgium) were used as PVDF resins for the M-1 [94,95] and M-3 membrane fabrications [61], respectively. AEROSIL-R972 (NIPPON AEROSIL, Tokyo, Japan) was used as the hydrophobic silica which is a pore-forming agent. Di (2-ethylhexyl) phthalate (DOP), dibutyl phthalate (DBP) and glycerol

triacetate (GTA) were used as diluents of the PVDF polymer. Diethyl phthalate (DEP) was used as an extruded solvent in a thermally induced phase separation (TIPS) process. CH_2Cl_2, EtOH, and NaOH were used to wash the membrane after fabrication. 1-Buthanol was used to measure membrane porosity. NaCl was used as a model electrolyte in the feed solution. All these chemicals were purchased from FUJI-FILM Wako Pure Chemical Corporation, Osaka, Japan. A fluoropolymer FS-392B (Fluoro Technology Co. Ltd., Aichi, Japan) was used as the hydrophobic agent.

II. 2. 2. Fabrication of PVDF Membrane

II. 2. 2. 1. Fabrication of PVDF Hollow Fiber Membrane

Four different types of PVDF membranes, M-1–M-4, were fabricated in this chapter. First, I fabricated M-1 and M-3 membranes by TIPS method. Then, M-2 and M-4 membranes were obtained by the hydrophobic treatment of M-1 and M-3, respectively, as discussed in section 2.2.3. The fabricating conditions for M-1 and M-3 are listed in Table II-1.

M-1 was fabricated by the method described in the patent [94]. The dope solution of M-1 was a mixture of hydrophobic silica, DOP, DBP, and PVDF at a weight ratio of 23:31:6:40. This dope solution was melted at 240 °C and extruded through the outer slit of a double-orifice spinneret. Simultaneously, nitrogen gas was discharged as a hollow part formation fluid from the inner slit of the spinneret. The extruded dope was introduced into a water bath (40 °C) through a 20 cm air gap and wound up at a speed of 20 m/min. Then, the stretching process was conducted on the obtained membrane. Initially, tension was applied to the membrane to stretch it to double its length, after which the tension was released. The final membrane length was 1.5 times longer than that of the prepared membrane. Next, the membrane was immersed in CH_2Cl_2 to remove DOP and DBP, and then dried. Subsequently, the membrane was immersed in a 50 wt% EtOH aqueous solution and then immersed in 5 wt% NaOH aqueous solution at 40 °C for 1 h to remove silica. It was revealed that silica particles were removed completely by the analysis of the membrane composition. After washing with water and drying, the PVDF hollow fiber membrane M-1 was obtained.

M-3 was also fabricated by TIPS using the triple-orifice spinneret. M-3 was fabricated according to the method described in a previous study [61]. Briefly, GTA was used as the

bore liquid and DEP as the solvent extruded through the outermost channel of the triple-orifice spinneret. The dope solution of M-3 was a mixture of GTA and PVDF at a weight ratio of 67:33.

Table II-1 Fabricating conditions for PVDF hollow fiber membrane M-1 and M-3.

Spinning conditions	M-1	M-3
Dope solution	PVDF/Si/DOP/DBP = 23/31/6/40	PVDF/GTA = 33/67
Spinneret	Double-orifice	Triple-orifice
Melting Temp. (°C)	240	190
Bore fluid	N_2	GTA
Extruded solvent	None	DEP
Length of air gap (cm)	20	5
Take-up speed (m/min)	20	20
Elongation rate	150%	None

II. 2. 2. 2. Preparation of Membrane Modules

The modules are distinguished by membranes; for example, the module installed by M-1 is called the M-1 module. The M-1 lab-scale module was fabricated by inserting 35 of M-1 membranes, 11 cm in length, into a pipe and both ends were cured with a urethane adhesive. The effective bore surface area of the membrane in the lab-scale module was 0.006 m^2 (Figure II-2) [83]. The M-3 lab-scale module with the same bore surface area was made by introducing 55 of M-3 membranes, 11 cm in length, into a pipe. A pilot-scale module was fabricated in the same way as the lab-scale modules using 700 M-1 membranes with lengths of 50 cm. The effective bore surface area of the membrane in the pilot-scale module was 0.44 m^2.

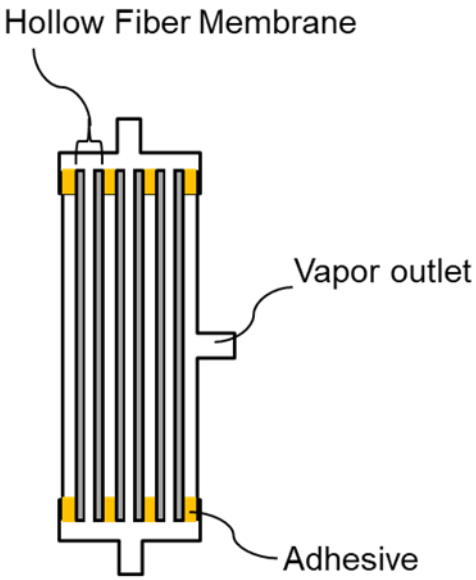

Figure II-2 Schematic of membrane modules for VMD [83].

II. 2. 2. 3. Hydrophobic Treatment

One side of the M-1 lab-scale module was sealed, and then a hydrophobic agent was injected into the inside of the hollow fiber membranes from another side of the module to wet the whole membrane (Figure II-3) [83,95]. The outer surface of the HF membranes were also wetted by a permeated hydrophobic agent (fluoropolymer FS-392B). After the entire membrane was wetted, excess hydrophobic agent was removed. Then, the membrane was dried overnight at around 25 °C by dry air flowing into the module. This operation was repeated twice and the M-2 lab-scale module was obtained. Using this operation, entire parts, including bore surface, shell surface, and cross section of the membrane, were hydrophobized. The same hydrophobic treatment was performed on the M-3 lab-scale and M-1 pilot-scale modules to fabricate the M-4 lab-scale and M-2 pilot-scale modules, respectively.

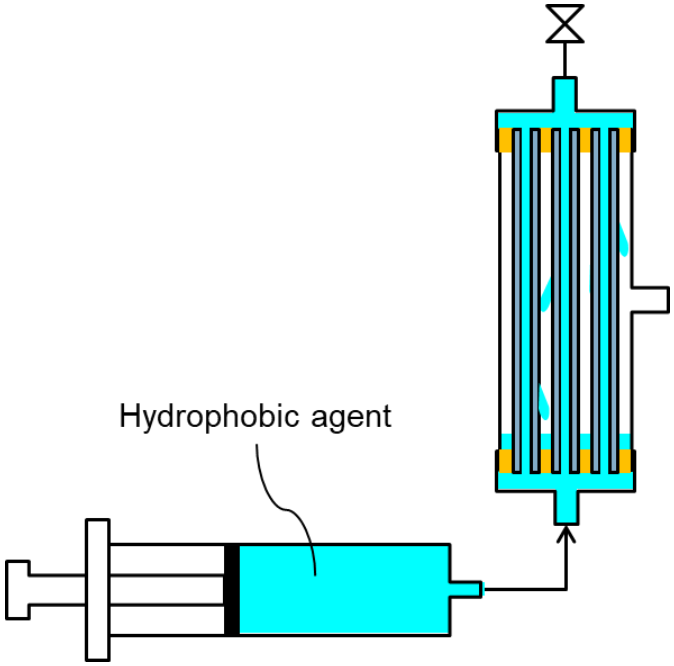

Figure II-3 Schematic diagram of hydrophobic treatment [83].

II. 2. 3. Characterization of PVDF Membrane

II. 2. 3. 1. Pore size Distribution and Porosity

The pore size distributions of all the hollow fiber membranes were measured using a liquid-liquid porometer (LLP-1100A, Porous Materials, Inc., Ithaca, NY, USA) [61]. In this method, pore presence was detected by sensing an increase in the flow rate at a given applied differential pressure, after which "mean flow pore size" was calculated.

The porosity of each hollow fiber membrane was measured via the gravimetric method [96].

II. 2. 3. 2. LEP Measurement

To measure the liquid entry pressure (LEP) of each membrane, both the bore and shell sides of the membrane installed in the lab-scale module were filled with water, and then pressure was applied to the bore side (Figure II-4) [83]. Pressure was gradually in-creased while observing the water level in the tube attached to the shell outlet of the module. LEP was determined as the pressure at which the water level in the tube began to rise [97].

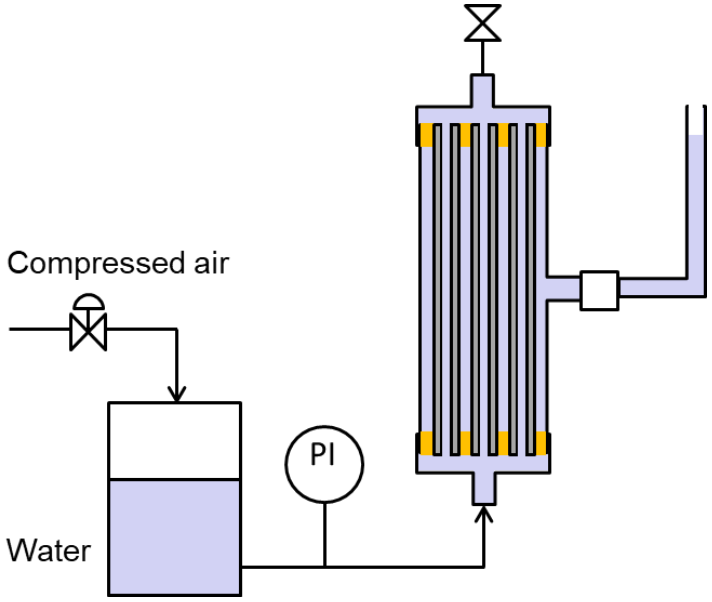

Figure II-4 How to measure LEP of membrane [83].

II. 2. 3. 3. Polymer Composition of Membrane Surface

To confirm the change of surface condition before and after hydrophobic treatment, polymer composition of M-1 and M-2 were observed by XPS (ESCALAB250, Thermo Fisher Scientific, Inc., Massachusetts, MA, USA). AlKα (15kV x 10mA) was used as the X-ray source. Membrane sample was prepared by cutting into around 1 mm size and open the hollow fiber to be able to analyze bore surface. Bore surface of M-1 and M-2 were analyzed, and shell surface of M-2 was also analyzed. The presence of fluoropolymers derived from hydrophobic agent was identified by comparing the peak at 292eV which is considered to be derived from a fluoroethylene carbon of the hydrophobic agent.

II. 2. 3. 4. VMD Evaluation

In the evaluation of the MD performance, especially long-term operation, an increasing feed concentration greatly affects the result, because of the change of water activity coefficient in the feed. Furthermore, if precipitation of the salt occurs with condensation of feed, it may cause a clogging of membrane pore resulting in a decreasing flux. Thus, in this study, the feed concentration was kept constant to avoid such effects, and to evaluate the effect of characteristic property of membrane accurately.

The evaluation of the MD performance of the lab-scale module was conducted using the equipment shown in Figure II-5 [83]. A 3.5 wt% NaCl aqueous solution was used as the feed and heated to 65 °C, then it was circulated to the bore side of the membrane module at a flow rate of 600 mL/min. When the feed volume was reduced via the MD operation, a liquid level sensor installed in the feed tank switched on the pump to supply distilled water and maintain a constant NaCl concentration. The condenser connected to the membrane module was cooled below 20 °C by circulating cooling water at a flow rate of 1000 mL/min. The condenser was also connected to a temporary saving chamber for the permeated water. The shell side of the membrane module, inside the condenser, and saving chamber were maintained at a pressure of 11 kPa using a vacuum pump. The permeate water stored in the temporary saving chamber was dis-charged into the water sampling tank, while the salt concentration of the permeated water was measured by the in-line conductivity meter. The vapor flux through the membrane is given by Equation (II-1):

$$J_w = \frac{W_p}{A\,t} \tag{II-1}$$

where J_w (kg/m^2·h), W_p (kg), A (m^2), and t (h) represent water vapor flux, weight of the permeated water, effective membrane bore surface area, and operating time, respectively [98].

Leaking salt flux (g/m^2·h) was obtained from the operating time and weight of salt permeated through the membrane. Generally, VMD membrane performances were solely evaluated by permeated water quality [57,98–101]. However, during VMD operation, leaking salt exists not only in permeated water alone but also on the membrane shell surface. In this study, to evaluate membrane performance more accurately, I washed the shell side of the membrane module after the VMD operation to determine the amount of salt on the shell surface of the membrane. Then, the total amount of leaking salt was calculated using Equations (II-2)–(II-4),

$$J_{st} = J_{sp} + J_{sr} \tag{II-2}$$

$$J_{sp} = \frac{1000 m_p}{A\,t} = \frac{1000 W_p C_p}{A\,t} \tag{II-3}$$

$$J_{sr} = \frac{1000 m_r}{A\,t} = \frac{1000 W_w C_w}{A\,t} \quad \text{(II-4)}$$

where J_{st} (g/m^2·h), J_{sp} (g/m^2·h), and J_{sr} (g/m^2·h) represent the total leakage salt flux, leaking salt flux into permeated water, and leaking salt flux remaining on the shell surface of the membrane, respectively. J_{sp} and J_{sr} are given by Equations (II-3) and (II-4), respectively, where m_p (kg), C_p (wt%), m_r (kg), W_w (kg), and C_w (wt%) represent the weight of salt in permeated water, salt concentration in permeated water, weight of the salt remaining on the shell surface of the membrane, weight of washing water, and salt concentration in the washing water, respectively. Additionally, C_p and C_w were obtained from the electrical conductivity of the permeated water and washing water, respectively. The salt retention factor, r_F (%), is calculated using Equations (II-5)–(II-7),

$$r_F = \left\{1 - \frac{\mathrm{C}_p^0}{C_f}\right\} \times 100 \quad \text{(II-5)}$$

$$\mathrm{C}_p^0 = \frac{m_p^0}{W_p} \times 100 \quad \text{(II-6)}$$

$$m_p^0 = m_p + m_r \quad \text{(II-7)}$$

where C_f (wt%), $C_p{}^0$ (wt%), and $m_p{}^0$ (kg) represent the salt concentration in the feed, accurate salt concentration of permeated water given by Equation (II-6), and weight of the totally permeated salt given by Equation (II-7), respectively.

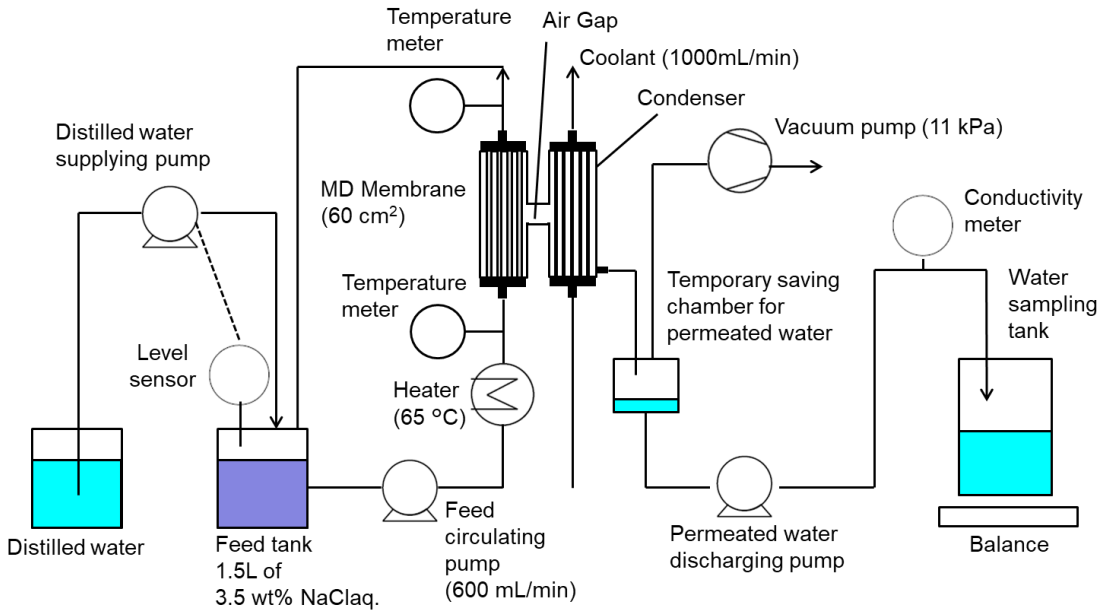

Figure II-5 Schematic of lab-scale VMD system.

The evaluation of the M-2 membrane pilot-scale module was conducted using the equipment illustrated in Figure II-6 [83]. Here, 10 L of 3.5 wt% NaCl aqueous solution was used as the feed. The feed was heated to 65 °C and supplied to the bore side of the M-2 membrane at a flow rate of 7 L/min. The pressure in the condenser was maintained at 11 kPa by a vacuum pump. Tap water (< 40 °C) was used as the coolant and supplied to the condenser at a flow rate of 10 L/min. The permeate was stored in the temporary saving chamber once. The chamber had a level sensor to monitor the level of the permeate in the camber. When the certain amount (around 3 L) of the permeate accumulated in the chamber, the level sensor turned on the permeate discharging pump to return the permeate to the feed tank until the level reaches below lower limit of the sensor to maintain the constant salt concentration of the feed. The volume of accumulated permeated water and its salt concentration were measured by an integrated flow meter installed at the permeated water discharging pump, and a conductivity meter, respectively, when the permeate was returned to the feed tank. Flux was obtained from the operating time and the volume of permeated water. The weight of permeated water was calculated using its density as 1.0 g/mL because the permeated water was almost pure, as mentioned later. The total amount of leaking salt was calculated as a sum of the amount of salt contained

in the permeated water and the amount of salt remaining on the shell surface of the membrane. These were obtained similar to that of the lab-scale VMD evaluation.

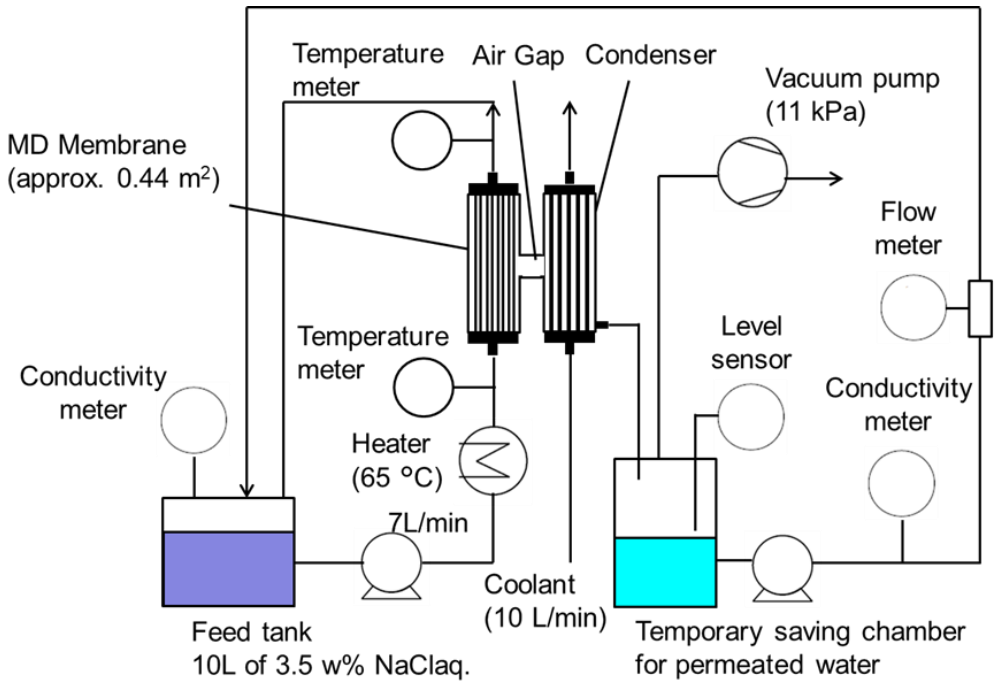

Figure II-6 Schematic of pilot-scale module. The salt concentration of feed water was kept constant by returning the permeated water to the feed tank.

II. 3. Results and Discussion

II. 3. 1. Membrane Morphology

Figure II-7 shows SEM images of M-1–M-4 [83]. It is found from Figure II-7 that M-1 has a highly porous and uniform sponge-like structure throughout its cross section. Its bore surface porosity is higher than that of the shell surface. In contrast, M-3 consists of spherulites with a diameter of approximately 10 μm. There are several micron pores on the bore surface. Although the number of pores on the shell surface is less than that on the bore surface, there are crack-like gaps between spherulites. Comparing SEM images of M-1 with M-3, the pore size of M-1 appears to be more uniform than that of M-3, and the porosity on the bore surface of M-1 seems to be higher than that of M-3. This is due to the silica particles added as a pore forming agent in fabricating M-1. Additionally, from these SEM images, it can be also seen that silica does not remain in the M-1 and M-2 [94]. Regarding the difference of membrane morphology of M-1 and M-3, it is mainly due to

the difference of the bore fluid, and existence of the extent solvent. In M-1 fabrication, the concentration of PVDF polymer arise rapidly by evaporation of the diluent as it passes through the air gap, resulting in small pore [96]. On the other hand, in M-3 fabrication, the extent solvent prevents evaporation of diluent, and the PVDF concentration becomes lower than M-1, resulting in larger pore than that of M-1. M-2 and M-4 were obtained by the hydrophobic treatment of M-1 and M-3, respectively. There is no clear difference in the SEM images between M-1 and M-2, and between M-3 and M-4. Therefore, the hydrophobic agent apparently formed a very thin layer on the polymer surface of the hollow fiber. Figure II-8 shows the results of XPS analysis of the surface of M-1 and M-2 [83]. It is found that a peak at 292 eV which is considered to be derived from a fluoroethylene carbon of the hydrophobic agent is observed only on the bore and shell surfaces of M-2, although the intensity from bore surface is higher than that from shell surface.

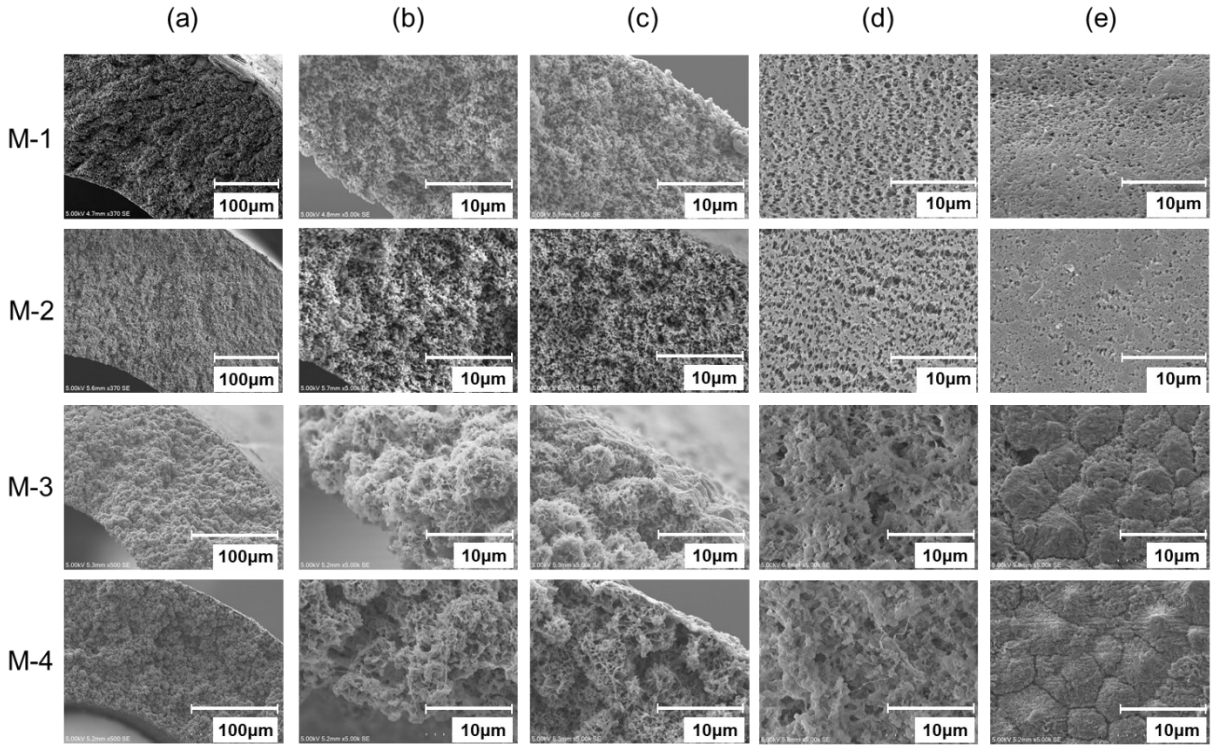

Figure II-7 SEM images of M-1 - M-4 membrane [83]. (a) Cross section, (b) Near the bore side of the cross section, (c) Near the shell side of the cross section, (d) Bore surface, (e) Shell surface.

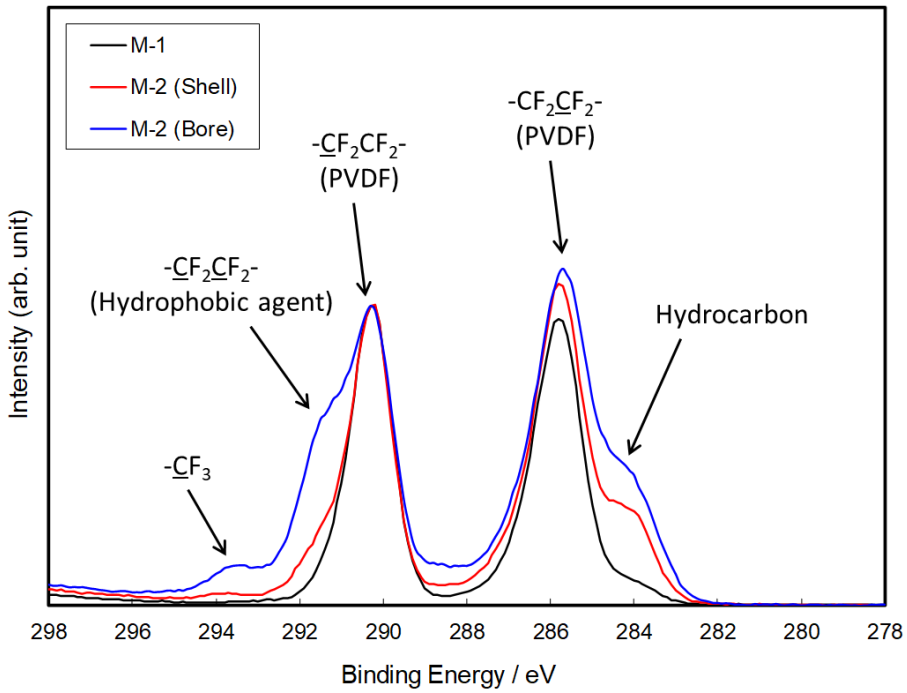

Figure II-8 The results of XPS analysis of M-1 and M-2 [83].

II. 3. 2. Evaluation of Physical Properties of Membranes

Table II-2 presents the properties of each membrane. The outer and inner diameters of M-1 are 1.22 and 0.66 mm, respectively, and its membrane thickness is 0.28 mm. In comparison, the outer and inner diameters of M-3 are 0.75 and 0. 47 mm, respectively, and its membrane thickness is 0.14 mm. The mean pore size of M-1 is 0.10 μm, which is smaller than that of M-3 (0.19 μm). The porosity of M-1 is 72% and higher than that of M-3 (49%). The hydrophobic silica used in the membrane fabrication as a pore-forming agent may contribute to the fabrication of such a highly porous membrane [94]. The maximum pore size of M-1 is 0.12 μm, which is smaller than that of M-3 (0.23 μm). Consequently, the LEP of M-1 is 0.25 MPa, and higher than that of M-3 (0.17 MPa). Figure II-9 shows the pore size distribution of M-1–M-4 [83]. In comparison, the pore size distribution of M-1 is narrower than that of M-3. In summary, from the perspective of obtaining the flux, M-1 has both an advantage (higher porosity) and disadvantages (thicker membrane and smaller mean pore size) when compared with M-3. In contrast, from the perspective of salt retention in the MD process, M-1 is superior to M-3 because M-1 has a higher LEP because its maximum pore size is smaller than that of M-3.

When compared with M-2 fabricated by the hydrophobic treatment of M-1 [95], there were no changes in the outer diameter, inner diameter, and thickness of M-1. Furthermore, other properties such as pore size and porosity are also approximately the same. Only the contact angle of M-2 was increased from 103° for M-1 to 132° by the hydrophobic treatment, as presented in Table II-2. Therefore, the LEP of M-2 also improved from 0.25 to 0.37 MPa. As mentioned above, there is very thin layer of the hydrophobic agent on the shell surface of M-2, revealed from the XPS analysis. This improvement of contact angle of the shell surface of the membrane indicates that hydrophobic treatment has remarkable effect on the hydrophobicity of the membrane surface even by the very thin layer of the hydrophobic agent.

Regarding the M-3 and M-4 fabricated by the hydrophobic treatment of M-3, both the contact angle and LEP of M-4 were also increased by the hydrophobic treatment without any change in other properties. From these results, it is expected that M-1 and M-2 exhibit the same vapor flux and deferent salt retention. Similarly, M-3 and M-4 are expected to have the same flux and deferent salt retention. By comparing these membranes, it is possible to discuss the effect of each physical property on stability during long-term VMD operation.

Table II-2 Membrane properties of M-1 – M-4.

Membrane	OD [1]	ID [2]	Thickness	Mean pore size [3]	Maximum pore size	Porosity	Contact angle	LEP
	[mm]	[mm]	[mm]	[μm]	[μm]	[%]	[°]	[MPa]
M-1	1.22	0.66	0.28	0.10	0.12	72	103	0.25
M-2	1.22	0.66	0.28	0.10	0.14	72	132	0.37
M-3	0.75	0.47	0.14	0.19	0.23	49	113	0.17
M-4	0.75	0.47	0.14	0.20	0.22	54	134	0.19

[1] Outer diameter.

[2] Inner diameter.

[3] Mean flow pore size.

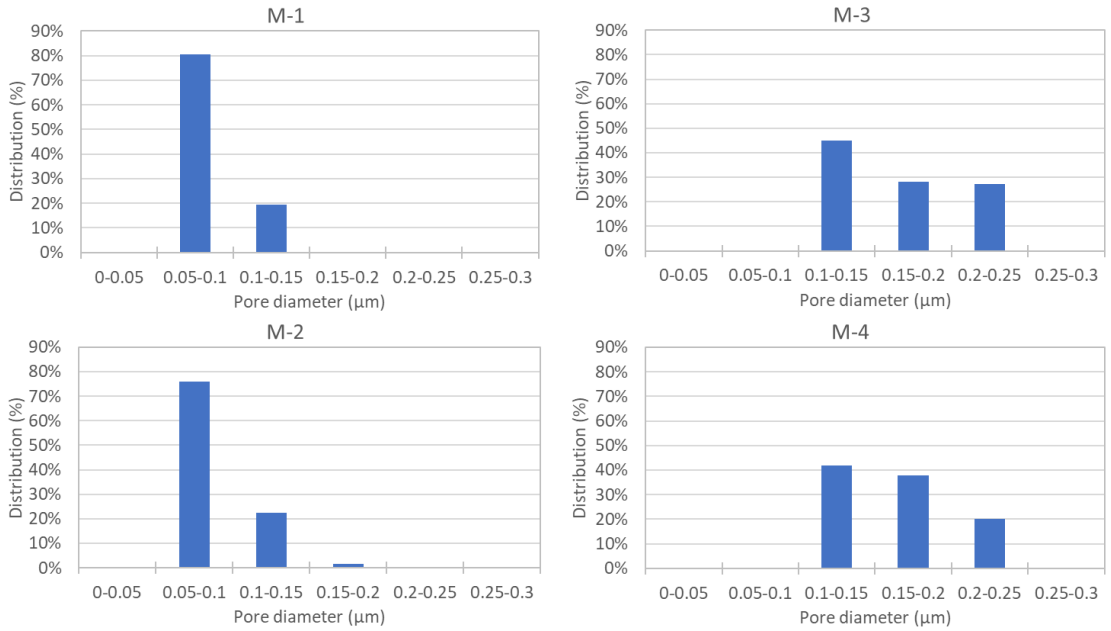

Figure II-9 Pore size distribution of each membrane, M-1–M-4 [83].

II. 3. 3. VMD Performance

II. 3. 3. 1. VMD Performance of Lab-scale Module

M-1, M-2, M-3, and M-4 lab-scale modules were evaluated to confirm the relationship between vacuum MD (VMD) performance, membrane morphology, and their physical properties such as porosity, pore size distribution, and LEP. In this evaluation, 3.5 wt% of NaCl aqueous solution was used as the feed, and the lab-scale module with a 0.006 m^2 effective bore surface area (Figure II-3) was used. The VMD operation of all four modules was performed for 100 h because M-3 was wetted over 100 h, making it impossible to evaluate the performance. Table II-3 presents the results of the VMD test. In the column of water vapor flux, "Initial" represents the flux during 1 h after starting operation, "Last" represents the flux from 99 to 100 h, and "Average" indicates the flux during the entire operating terms of 100 h. The leaking salt flux was obtained at the end of the operation. In the column of leaking salt flux, "Salt in permeated water" indicates the leaking salt flux calculated from the amount of salt in permeated water, "Salt remaining on membrane" represents the flux calculated from the amount of salt retained on the shell surface of the membrane, and "Total" represents the sum of "Salt in permeated water" and "Salt

remaining on membrane." "Leaking salt flux" represents the flux during a 100-h operation. The retention factor was obtained at the end of the operating term.

Table II-3 VMD operation results for M-1 – M-4 lab-scale module.

Membrane	Water vapor flux				Leaking salt flux			Retention factor [6]
	Initial [1]	Last [2]	Last / Initial	Average [3]	Salt in permeated water [4]	Salt remaining on membrane [5]	Total	
	[kg/m^2·h]	[kg/m^2·h]	[%]	[kg/m^2·h]	[g/m^2·h]	[g/m^2·h]	[g/m^2·h]	[%]
M-1	43.2	37.2	86.1	38.7	0.05	3.39	3.44	99.7
M-2	43.9	40.3	91.7	42.0	0.04	0.64	0.68	>99.9
M-3	33.7	21.0	62.5	28.8	0.06	34.33	34.39	96.6
M-4	33.2	24.1	72.6	26.5	0.06	13.60	13.67	98.5

[1] Obtained from the weight of permeated water during one hour after starting operation.

[2] Obtained from the weight of permeated water during one hour before ending operation.

[3] The flux during whole operating terms.

[4] Obtained from the amount of salt in permeated water during whole operating term. (Equation (II-3)).

[5] Obtained from the amount of salt remaining on membrane shell surface during whole operating term and operation time. (Equation (II-4)).

[6] Obtained from the weight of salt in the feed and the total amount of permeated salt at the end of operation. (Equation (II-5)).

From Table II-3, the order of the initial flux was determined to be M-2≧M-1>>M-3 ≧ M-4. As earlier mentioned, compared to M-3, M-1 has both advantages and disadvantages with respect to vapor flux. However, it is clear that M-1 exhibits a higher initial vapor flux than M-3. This was possibly because a higher porosity had a larger impact on the initial vapor flux than membrane thickness in this experiment. For the stability of the flux, the order of the last flux/initial flux is given as M-2>M-1>>M-4>M-3. This order correlates with the order of LEP presented in Table II-2. This indicates that the membrane with higher LEP, which is mainly determined by higher hydrophobicity and/or smaller maximum pore size [53], is stably operated for a longer time.

Figure II-10 shows the time course of the vapor flux of the four membranes over the entire operation period of 100 h [83]. It is clear that the vapor flux of M-2 was the most stable among the four membranes during the 100-h VMD operation. The fluxes of M-1 and M-4 gradually decreased in the first 40 h, and then became constant. The flux of M-3 continued to decrease during the 100-h operation. These results suggest that some pores with low LEP in the M-3 membrane became wet, which led to a pore clogging due to leaked salts and then, a decrease in vapor flux.

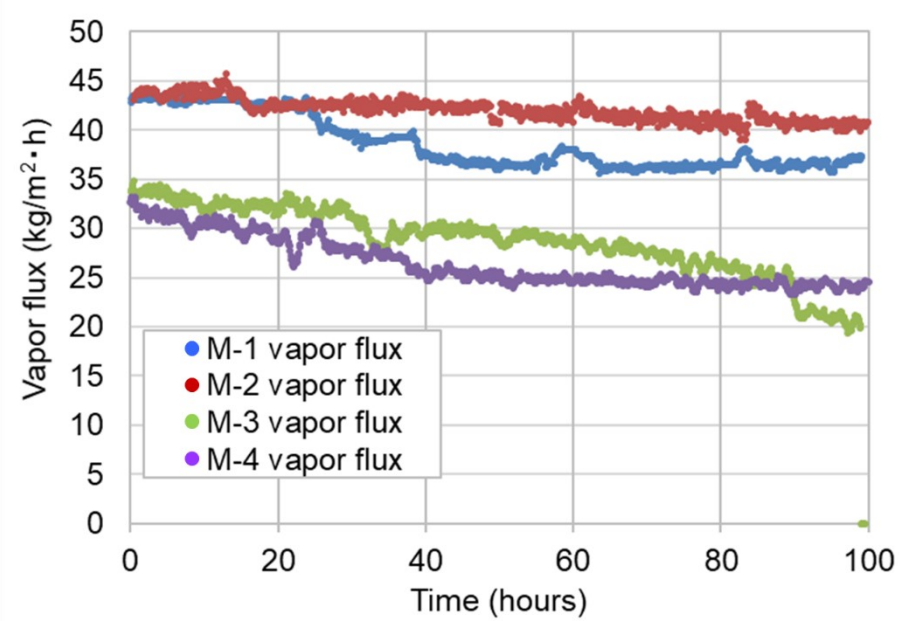

Figure II-10 Time course of vapor flux of four membranes [83].

Figure II-11 shows the time course of the permeate water conductivity of each membrane over the entire operation period [83]. During the 100-h of operation M-1, M-3, and M-4 exhibited "spikes" in their conductivity, while M-2 did not. Figure II-12 shows the shell surface after 100 h of VMD operation [83]. From Figure II-12, it is evident that in M-1, M-3, and M-4, the shell surface of each membrane was significantly or less significantly covered by the salt after the end of the operation, whereas the shell surface of M-2 was scarcely covered with salts. Therefore, it is reasonable to consider that a part of accumulated salt on the shell surface flakes from the surface occasionally, and melts in the permeate resulting in the spike in permeate conductivity. The accumulation of salt on the shell surface will also be the cause of flux decline. This indicates that the larger the LEP, the smaller the leaking salt flux. Interestingly, the salt amounts in permeated

water of all membranes were almost the same, despite the significant differences in LEP, as shown in Table II-3.

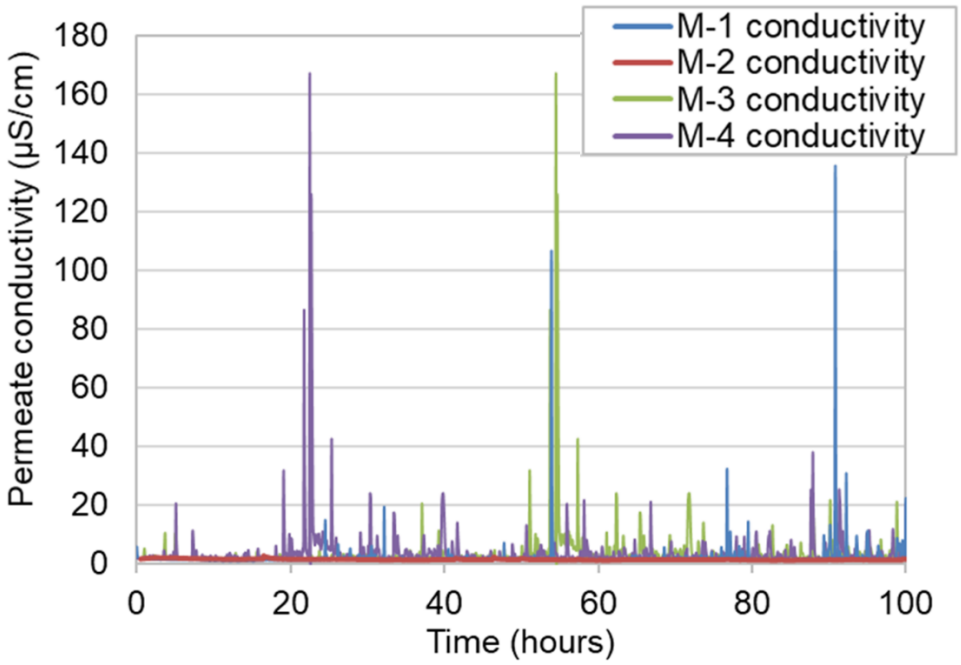

Figure II-11 Time course of permeate water conductivity of four membranes [83].

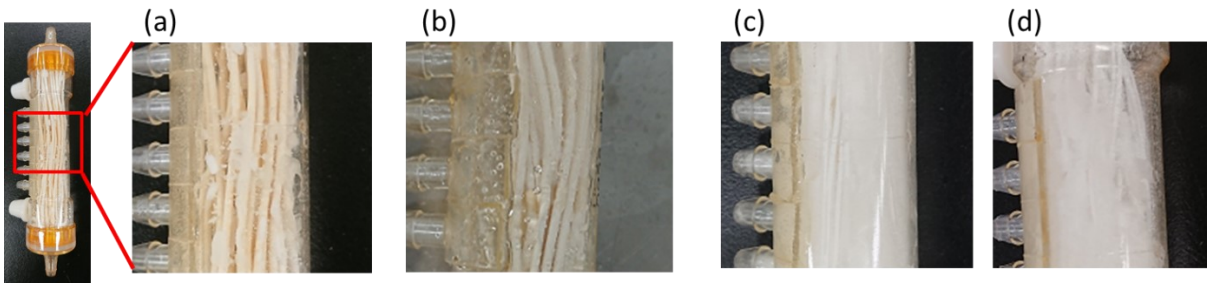

Figure II-12 The pictures of the M-1 to M-4 lab-scale modules after 100-h VMD operation [83]. (a) M-1, (b) M-2, (c) M-3 and (d) M-4.

Figure II-13 shows three kinds of leaking salt flux of four lab-scale membrane modules during the 100-h operation that were calculated from the permeated water conductivity, amount of salt attached on the shell surface of membrane, and total leaking salt flux (their total sum), respectively [83]. The order for the total leaking salt flux is M-3 (34.39 $g/m^2 \cdot h$) > M-4 (13.67 $g/m^2 \cdot h$) > M-1 (3.44 $g/m^2 \cdot h$) > M-2 (0.68 $g/m^2 \cdot h$). This order is opposite that of the LEP. Therefore, it is evident that the higher the LEP, the lower the salt leakage. Interestingly, from Figure II-13, it is determined that most of the salt that permeated

through the membrane remained on the shell surface of the membrane. Even in the M-3 and M-4 cases, the proportion of remaining salt on the shell surface were over 99% of the entire amount of permeated salt, as shown in Table II-3. Provided it is calculated solely with the salt in permeated water, 96.6% of the retention factor of M-3 increases to over 99.9%. In other words, it is one of merits of VMD that the conductivity of permeated water does not increase so much even with such a severe membrane wetting.

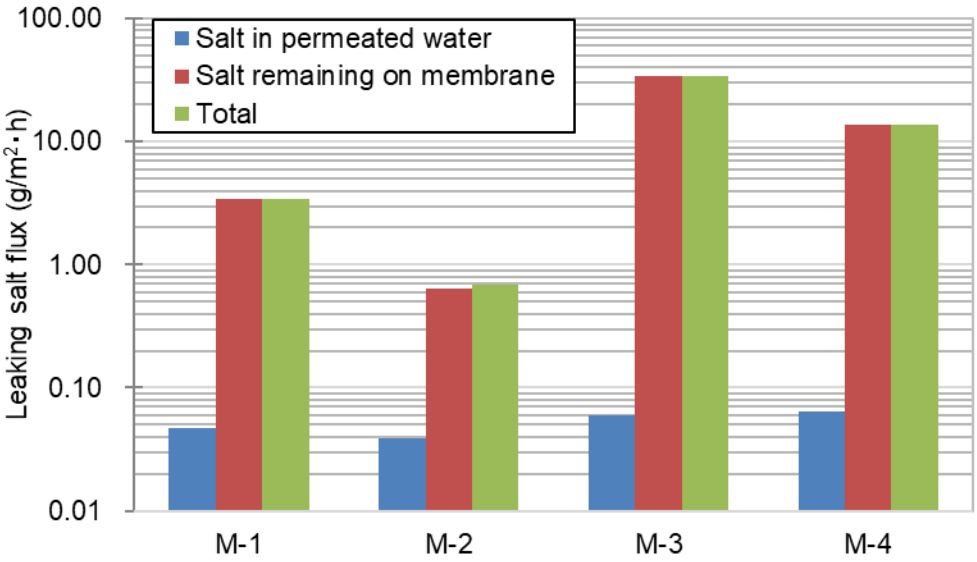

Figure II-13 Comparison of leaking salt flux of four membrane modules during the 100-h operation [83].

Figures II-14 (a) and (b) present the salt retention factor and last/initial ratio of water vapor flux as a function of LEP, respectively, during the 100-h VMD operation [83]. Owing to insufficient data, it is challenging to quantitatively discuss the relationship between LEP and salt retention, and between LEP and the last/initial ratio of water vapor flux. Nevertheless, it is evident from Figures II-14 (a) and (b) that the higher the LEP, the higher the salt retention factor and vapor flux stability. In the VMD system reported here, it is found that if the LEP is higher than approximately 0.32 MPa, the decline in the vapor flux is less than 10%, and the total salt retention factor is over 99.8% during the 100-h VMD operation.

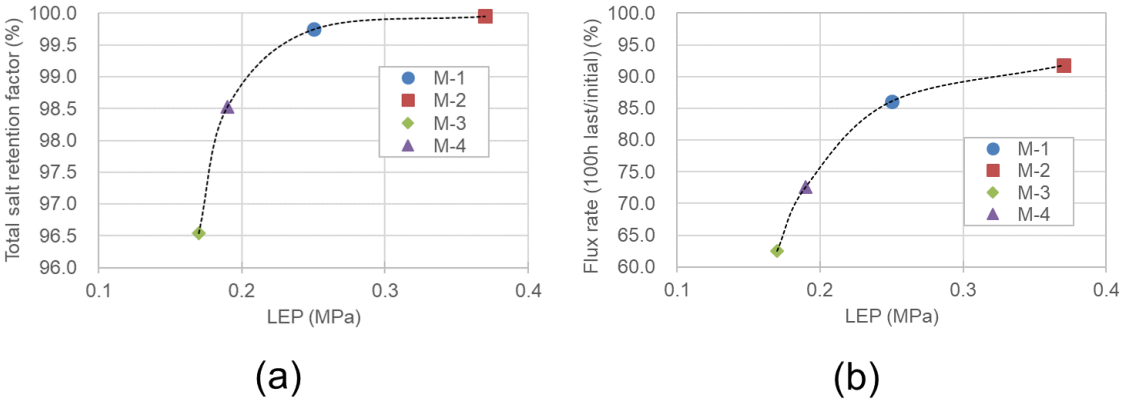

Figure II-14 The LEP dependency of (a) the total salt retention factor and (b) the stability of water vapor flux of M-1 – M-4 after the 100-h VMD operation [83].

II. 3. 3. 2. Scale-up and Long-term Operation

Figure II-15 (a) shows the results of the VMD long-term operation performed with the M-2 pilot-scale module [83]. The operation conditions were the same as those for the lab-scale module, except for the feed flow rate of 7 L/min. The initial vapor flux was 19.3 kg/ m^2·h.

After 300 h of operation, the flux was 16.8 kg/m^2·h, which maintained 87% of the initial flux. The conductivity of the permeated water was 8 μS/cm or less throughout the entire operation period, which corresponds to less than 6.4 ppm of the total NaCl concentration of the permeated water. The total leaking salt flux, which was obtained from the sum of salt contents in the permeated water and on the shell surface, was less than 0.1 g/m^2·h, as shown in Figure II-15 (b) [83]. These results suggest that the M-2 pilot-scale module is very stable for long-term operations.

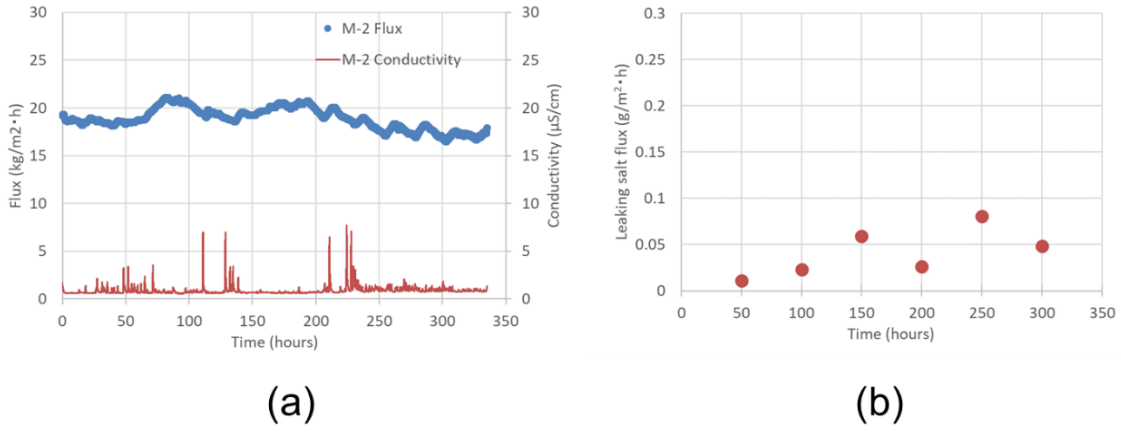

Figure II-15 Time course of (a) the vapor flux and the conductivity of permeate and (b) the total leaking salt flux determined from the sum of salt contents in the permeated water and on the shell surface during VMD operation of M-2 pilot-scale module [83].

II. 4. Conclusions

In this chapter, I attempted to evaluate membrane properties that affect the long-term stability of membranes using a VMD system. First, I fabricated two different types of PVDF hollow fiber membranes, M-1 and M-3, then obtained M-2 and M-4 by treating M-1 and M-3 with hydrophobic agents, respectively. Regarding salt retention, I evaluated the salt retention factor using both the salt in the permeate, and also the salt retained on the shell surface of the membrane. Consequently, it was evident that the higher the LEP, the higher the salt retention and vapor flux stability. Theoretically, it should be possible to operate MD without wetting if the LEP of the membrane is higher than the pressure difference between the feed and permeate. However, practically, a much higher LEP than the practical pressure difference was necessary to operate the VMD stably. In the VMD system reported here, in which the vapor pressure difference was approximately 0.1 MPa, it was found that in the case where the LEP was higher than approximately 0.32 MPa, the decrease in vapor flux was less than 10% and the total salt retention factor was over 99.8% during the 100-h VMD operation. Furthermore, I attempted the 300-h VMD operation using a pilot-scale MD system, which installed the membrane with an LEP of 0.37 MPa (M-2), and demonstrated that the M-2 pilot-scale module was very stable for long-term operations.

Chapter III

Effect of hollow fiber membrane properties and operating conditions on preventing scale precipitation in seawater desalination with vacuum membrane distillation

III. 1. Introduction

As mentioned in Section I. 4. 5., desalination of seawater has been studied as the main application of MD for a long time [35,66,75,76]. In seawater desalination, salt precipitation is one of the most severe challenges [85,86]. Scaling occurs when the saline concentration in the feed solution exceeds the saturated solubility of the salts. In particular, the salt concentration on the membrane surface readily increases because of concentration polarization, owing to the difficulty of renewing the feed solution in the boundary layer on the membrane surface [46,48,73]. The scaling on the membrane surface often forms a scale layer and cover the membrane surface, leading clogging of membrane pores and preventing vapor permeation [87,88]. As a result, the vapor flux decreases significantly.

In addition, scaling generally hydrophilizes the membrane surface, resulting in a decline in the liquid entry pressure (LEP) [87]. LEP (MPa) is the pressure required for the liquid to penetrate the membrane [53]. The decline of LEP causes membrane wetting and deterioration of the stability of long-term operation [83]. Moreover, the solubility of some salts, such as calcium carbonate ($CaCO_3$), which is the main component of scale in seawater desalination, decreases as the temperature increases [102]. Therefore, the risk of precipitation of such salts in MD operation will increase from other typical membrane desalination technologies such as RO.

To date, various attempts have been made to address the problems of scaling in MD operations. For example, chemical and physical cleaning have been explored to remove the scale layer. In most cases of chemical cleaning, acid solutions such as hydrochloric acid, citric acid, humic acid, and acetic acid are used to dissolve basic salts such as $CaCO_3$

[86,102–105]. Regarding physical cleaning, flushing, backwashing, and bubbling are applied to physically remove the scale layer physically [106–109]. Some pretreatment processes have also been investigated to decrease the scale. For example, antiscalants used in the RO process can prevent various types of scaling, such as carbonate, sulfate, and fluoride [85,86,110,111]. However, these processes have several disadvantages. For instance, frequent membrane cleaning may damage the membrane. In addition, the cost of chemicals and equipment increases the water production cost, and the actual operation time is reduced because the operation must be stopped during cleaning.

Another approach is to solve the scaling problem [106]. Guan et al. demonstrated that a large Reynolds number makes scaling less likely to occur by computational fluid dynamics simulation for DCMD operation with a PVDF flat sheet membrane and various concentrations of NaCl aqueous solution. However, this problem is not very simple. The Reynolds number is generally increased by increasing the linear velocity of the feed. Thus, the transmembrane pressure (TMP) increases, which increases the possibility of membrane wetting.

When the fluid flows in the pipe-shaped flow path, such as the bore side of the hollow fiber (HF) membranes, the Reynolds number *Re* can be calculated using Equation (III-1) [112,113].

$$Re = \frac{\rho v d_h}{\mu} = \frac{\rho v d}{\mu} \qquad \text{(III-1)}$$

Where ρ (kg/m^3), v (m/s), d_h (m), and μ (Pa·s) denote the density of the fluid, linear velocity of the fluid, hydraulic diameter of the flow pass, and viscosity of the fluid, respectively. When the flow pass is a pipe shape, d_h is the diameter of the flow path, d (m). From the Equation (III-1), the Reynolds number increases with linear velocity. However, as discussed above, the pressure applied to the inlet of the HF membrane must be increased to increase the linear velocity, resulting in an increase in TMP, especially in VMD, in which the permeate side of the membrane is under vacuum. Membrane wetting occurs when TMP exceeds the LEP of the membrane [53]. In addition, an increase in the linear velocity causes a larger pressure drop. The pressure drop is the energy loss when a fluid passes through the flow path; it is represented by the pressure difference between the inlet and outlet of the flow path. When the fluid flows into the pipe-shaped flow path, such as the bore side of the hollow fiber membranes, the pressure drop (ΔP) (Pa) can be

calculated using the Darcy–Weisbach equation given by Equation (III-2) [112,113],

$$\Delta P = \frac{f \rho v^2 L}{2d} \quad \text{(III-2)}$$

where f (-) and L (m) denote the friction coefficient and length of the HF membrane, respectively.

There are two types of flow, the laminar flow and the turbulent flow. With the increase of Reynolds number, the type of flow changes from the laminar flow to the turbulent flow. In addition, the friction coefficient f also varies depending on the types of flow. In general, the pressure drop of the turbulent flow was larger than that of the laminar flow. Therefore, even if scale precipitation is reduced by an increase in the Reynolds number, there remains challenges of membrane wetting and high energy loss. Moreover, the pressure drop increases with the scaling-up of the module because the pressure drop is proportional to the length of the flow path. When there is a large pressure drop, a high pressure must be applied to the inlet of the HF membrane to flow the fluid through the membrane while maintaining a high linear velocity. This results in a high TMP and increases the possibility of membrane wetting. Therefore, it is very important to use a membrane with high LEP, that is a highly hydrophobic membrane, to avoid the membrane wetting. It is also very important to avoid excessive increases in the pressure drop when increasing the Reynolds number of the feed.

In this study, we used a hydrophobized polyvinylidene fluoride (PVDF) HF membrane for seawater desalination by VMD [83,84]. We focused on the Reynolds number of the feed to solve the scaling problem. Then, we aimed to resolve membrane scaling without an excessive increase in pressure drop by optimizing the membrane properties and operating conditions. In particular, we focused on the inner diameter of the HF membrane because as the diameter increases, the Reynolds number increases (Equation (III-1)), whereas the pressure drop decreases (Equation (III-2)). Thus, we attempted to evaluate the pressure drop, the vapor flux, and the scale precipitation using hydrophobized HF membrane with similar morphology and physical properties, but different inner diameters in order to evaluate the effect of inner diameter. To the best of our knowledge, no previous study has addressed the scaling problem using the same approach in real seawater desalination by VMD with HF membranes.

III. 2. Materials and Methods

III. 2. 1. Materials

Solef 6010 (SOLVAY, Brussels, Belgium) was used as the PVDF resin. AEROSIL-R972 (Nippon Aerosol, Tokyo, Japan) was used as the hydrophobic silica, which is a pore-forming agent [83,84,89]. Di(2-ethylhexyl) phthalate (DOP) and dibutyl phthalate (DBP) were used as diluents for the PVDF polymer. CH_2Cl_2, EtOH, and NaOH were used to wash the membranes after fabrication. 1-Buthanol was used to measure the membrane porosity. HCl solution was used to dissolve the scale precipitated on the membrane surface. All chemicals were purchased from FUJI-FILM Wako Pure Chemical Corporation (Osaka, Japan). Fluoropolymer FS-392B (Fluoro Technology Co. Ltd., Aichi, Japan) was used as the hydrophobic agent. Seawater was collected from a 1 m depth of the sea, ~2 km off the coast of Suruga Bay (Shizuoka, Japan). The total dissolved solids (TDS) of the seawater was 3.5 wt%, which was determined by evaporating the seawater and then measuring the weight of the obtained residue. In addition, no organic compounds were detected in seawater using a total organic carbon analyzer (TOC-V CSN, Shimadzu Corporation, Kyoto, Japan).

III. 2. 2. Fabrication of hydrophobized PVDF Membrane

III. 2. 2. 1. Fabrication of PVDF Hollow Fiber Membrane, and Membrane Modules

First, a PVDF HF membrane was fabricated by the thermally induced phase separation method described in the patent and treated with a hydrophobic agent, resulting in a PVDF HF membrane with a high LEP [94,95,114]. High LEP is essential requirement for long-term stable MD operation as discussed in Section II. 3. 3. 1. [83]. It is also necessary to use high LEP membrane in order to evaluate the impact of scaling on the stability of VMD operation accurately. A mixture of hydrophobic silica, DOP, DBP, and PVDF (weight ratio, 23:31:6:40) was melted at 240 °C and used as the dope solution. Two types of HF membranes, M-5 and M-6, with different inner and outer diameters (Table III-1) were fabricated using two types of spinnerets using nitrogen gas as a hollow part formation fluid. The extruded dope was introduced into a water bath (40 °C) through a 20 cm air

gap and wound up at a speed of 20 m/min. Next, the membrane was immersed in CH_2Cl_2 to remove DOP and DBP, and then dried. Subsequently, the membrane was immersed in a 50 wt% EtOH aqueous solution and then immersed in a 5 wt% NaOH aqueous solution at 40 °C for 1 h to remove silica. Analysis of the membrane composition revealed that the silica particles were completely removed. After washing with water and drying, a PVDF HF membrane was obtained.

The fabricated membranes were inserted into a pipe to make VMD module shown in Figure III-1 [83,84]. For M-5 VMD module, 10 or 20 M-5 membranes (length: 11 cm) were inserted into the pipe and curing both ends with a urethane adhesive. The total bore surface area of the membrane in M-5 VMD modules was 0.0017 or 0.0034 m^2. For M-6 VMD module, 7 or 14 M-6 membranes (length: 11 cm) was inserted into a pipe and curing both ends with a urethane adhesive. The total bore surface area of the membrane in M-6 VMD modules was 0.0018 or 0.0036 m^2. The long modules to measure the pressure drop of M-5 and M-6 were made by inserting three M-5 or M-6 membranes (length: 65 cm) into a nylon tube (~60 cm) and curing both ends with an epoxy adhesive, respectively. These modules were used in experiments after the hydrophobic treatment explained in the next section. The feed solution was flowed through the bore side to make the feed flow uniform through the module.

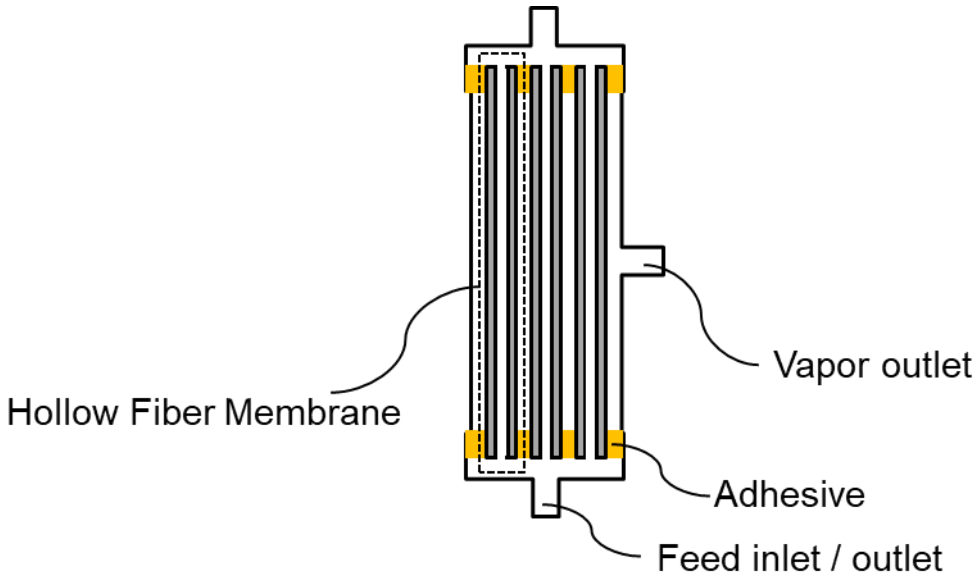

Figure III-1 Schematic of VMD modules [83,84,89].

III. 2. 2. 2. Hydrophobic Treatment

Hydrophobic treatment of M-5 and M-6 membranes was conducted using VMD module shown in Figure III-1 [83,84]. One side of the VMD module was sealed, and then hydrophobic agent was injected by a syringe into the inside of the hollow fiber membranes from another side of module to wet the whole membrane. The hydrophobic agent, fluoropolymer FS-392B was concentrated up to three times by evaporator before injection. By this operation, the hydrophobic agent physically adsorbed and hydrophobized the whole parts of membrane including bore surface, shell surface, and cross section. After the entire membrane was wetted by the concentrated hydrophobic agent, excess hydrophobic agent was removed by draining from feed inlet/outlet and vapor outlet. Then, the membrane was dried overnight at around 25 °C by dry air flowing into the module, and hydrophobized PVDF HF membrane module was obtained. M-5 and M-6 membranes in the long modules were also hydrophobized by the same procedure.

III. 2. 3. Characterization of hydrophobized PVDF membrane

III. 2. 3. 1. Porosity

The hydrophobized hollow fiber membranes M-5 and M-6 were obtained by disassembling the module. The porosity of each membrane was then measured via the gravimetric method [96].

III. 2. 3. 2. Liquid entry pressure (LEP) measurement

To measure the LEP of the membrane, both the bore and shell sides of the membrane were filled with 20 wt% ethanol aqueous solution, and then pressure was applied to the bore side (Figure III-2) [84,89]. The pressure was gradually increased while observing the liquid level in the tube attached to the shell outlet of the module. The LEP was measured as the pressure at which the liquid level in the tube began to increase. In this study, a 20 wt% ethanol aqueous solution was used as the solution for measuring the LEP of the membrane because the LEPs of M-5 and M-6 membranes for pure water were too high, leading to module breakage.

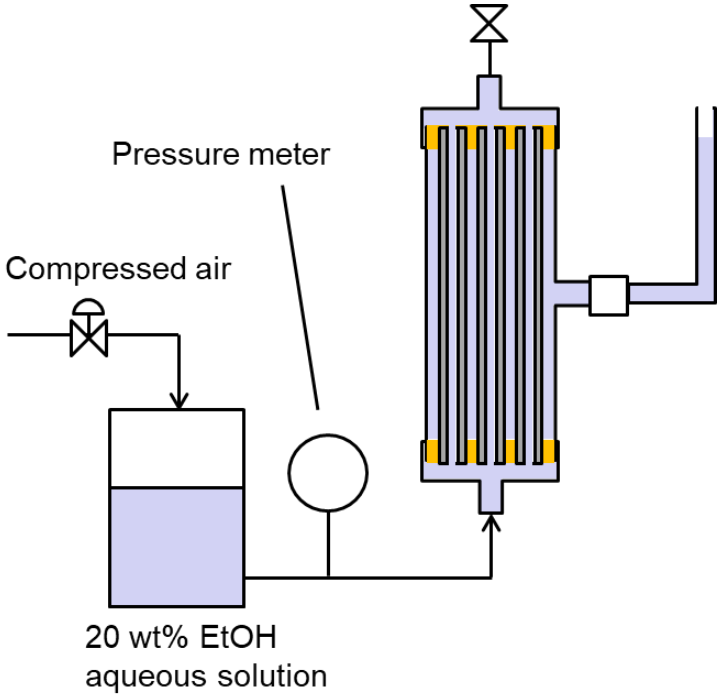

Figure III-2 Measurement apparatus for the LEP of the membrane [84,89].

III. 2. 3. 3. Pressure drop measurement

The pressure drop of the feed solution between the module inlet and outlet was measured to confirm the relationship between the linear velocity of the feed solution and the membrane property, and the pressure drop, using long modules and pure water (Figure III-3) [84]. The flow rate of pure water was measured by weighing the retentate returned to the feed tank for a certain period. The pressure drop was observed as the difference between the pressures at the inlet and outlet of the module by gradually increasing the flow rate. In addition, the measured pressure drop was compared with the theoretical pressure drop in order to recognize the type of flow under all conditions. The theoretical pressure drop can be calculated by using Equation (III-2), but the friction coefficient f (-) varies depending on the type of flow. For the laminar flow, the friction coefficient f_l (-) is given by the Hagen–Poiseuille law shown in Equation (III-3) [112]:

$$f_l = \frac{64}{Re} \tag{III-3}$$

For the turbulent flow in a smooth pipe, f_t (-) is given by the Nikuradse equation, Equation (III-4) [115]:

$$\frac{1}{\sqrt{f_t}} = 2log\left(Re\sqrt{f_t}\right) - 0.8 \quad \text{(III-4)}$$

In addition, the friction coefficient of turbulent flow for a Reynolds number less than 2×10^4 is given by the Blasius equation, Equation (III-5):

$$f_t = \frac{0.316}{Re^{\frac{1}{4}}} \quad \text{(III-5)}$$

Notably, the f_t obtained from Equation (III-5) is larger than that obtained using Equation (III-3) for Reynolds numbers greater than ~2×10^3. Generally, the laminar flow changes to turbulent flow when the Reynolds number exceeds ~2×10^3. The pressure drop of the laminar flow (ΔP_l) (Pa) is given by Equation (III-6) from Equations (III-1), (III-2), and (III-3), and that of the turbulent flow (ΔP_t) (Pa) is given by Equation (III-7) from Equations (III-1), (III-2), and (III-5):

$$\Delta P_l = \frac{32\mu L v}{d^2} \quad \text{(III-6)}$$

$$\Delta P_t = 0.158\,\frac{\rho v^2 L}{d}\left(\frac{\mu}{\rho v d}\right)^{\frac{1}{4}} \quad \text{(III-7)}$$

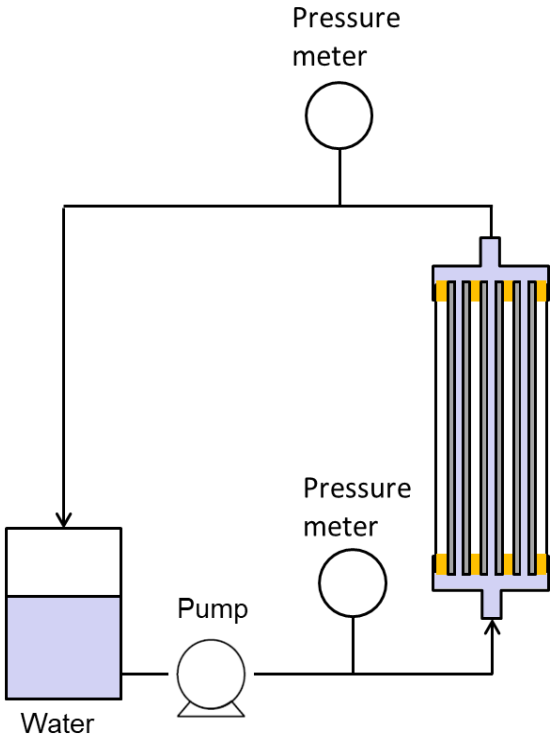

Figure III-3 Measurement apparatus for the pressure drop of membrane modules [84].

III. 2. 3. 4. Vacuum MD (VMD) Evaluation

Evaluation of the MD performance revealed that the increase in feed salt concentration greatly affects the result because of the change in the water activity coefficient in the feed [83]. Furthermore, if salt precipitation occurs due to the condensation of feed, the membrane pores may be clogged, resulting in a decreasing flux. Thus, in this study, the feed concentration was kept constant to avoid such effects and evaluate the impact of the operating conditions and characteristic properties of the membrane.

The MD performance of the VMD modules was evaluated using the equipment shown in Figure (III-4) [84]. Real seawater (1.5 L) was used as the feed and heated to 90 °C, which was measured at the module inlet, and then circulated to the bore side of the membrane module at an arbitrary flow rate. When the feed volume was reduced via the MD operation, a liquid level sensor installed in the feed tank was switched on the pump to supply distilled water and maintained the feed concentration constant. The condenser connected to the membrane module was cooled by circulating the cooling water of 10 - 20 °C at a flow rate of 1000 mL/min. The condenser was connected to a temporary saving chamber for the permeated water. The shell side of the membrane module, inside the condenser, and the saving chamber were maintained at a pressure of 29 kPa using a vacuum pump. Under this condition, once the pressure of permeate side was decompressed to 29 kPa, the vacuum dawn scarcely take place even if the vacuum pump was turned off. Thus, we considered that 100% of vapor condensed in the temporary chamber. The flow rate of permeated water discharging pump was set at higher than the water vapor flux of permeated water, and was running during whole time of VMD operation. The salt concentration of the permeated water was measured using an in-line conductivity meter which was installed between the temporary saving chamber and the sampling tank. The vapor flux through the membrane, J_w (kg/m^2·h), is given by Equation (III-8)

$$J_w = \frac{W_p}{A\,t} \tag{III-8}$$

where W_p (kg), A (m^2), and t (h) are the weight of the permeated water, effective membrane bore surface area, and operating time, respectively.

The leaking salt flux (g/m^2·h) was obtained from the operating time and the weight of salt permeated through the membrane. To evaluate the membrane performance more

accurately, the shell side of the membrane module was washed after the VMD operation to determine the amount of salt on the shell surface of the membrane. J_{st} was calculated using Equations (III-9)–(III-11) [83]:

$$J_{st} = J_{sp} + J_{sr} \quad \text{(III-9)}$$

$$J_{sp} = \frac{1000 m_p}{A\,T} = \frac{1000 W_p C_p}{A\,T} \quad \text{(III-10)}$$

$$J_{sr} = \frac{1000 m_r}{A\,T} = \frac{1000 W_w C_w}{A\,T} \quad \text{(III-11)}$$

where J_{sp} (g/m^2·h) and J_{sr} (g/m^2·h) are the leaking salt flux into the permeated water and the leaking salt flux remaining on the shell surface of the membrane, respectively. J_{sp} and J_{sr} are given by Equations (III-10) and (III-11), respectively, where m_p (kg), C_p (wt%), m_r (kg), W_w (kg), and C_w (wt%) are the weight of salt in permeated water, salt concentration in permeated water, weight of the salt remaining on the shell surface of the membrane, the weight of washing water, and the salt concentration in the washing water, respectively. To determine C_p and C_w, the calibration curve between the TDS of seawater and the electrical conductivity was obtained. In the MD process, salt permeates through the partially wetting pores of the membrane in a liquid state. Therefore, the composition of the leaking salt was considered to be approximately the same as that of seawater. Therefore, C_p and C_w could be obtained from the calibration curve by measuring the electrical conductivity of permeated water and washing water, respectively.

r_F is given by Equation (III-12):

$$r_F = \left\{1 - \frac{C_p^0}{C_f}\right\} \times 100 \quad \text{(III-12)}$$

$$C_p^0 = \frac{m_p^0}{W_p} \times 100 \quad \text{(III-13)}$$

$$m_p^0 = m_p + m_r \quad \text{(III-14)}$$

where $C_p{}^0$ (wt%) and $m_p{}^0$ (kg) are the accurate salt concentrations of permeated water given by Equation (III-13), and the weight of the total permeated salt, given by Equation (III-14), respectively.

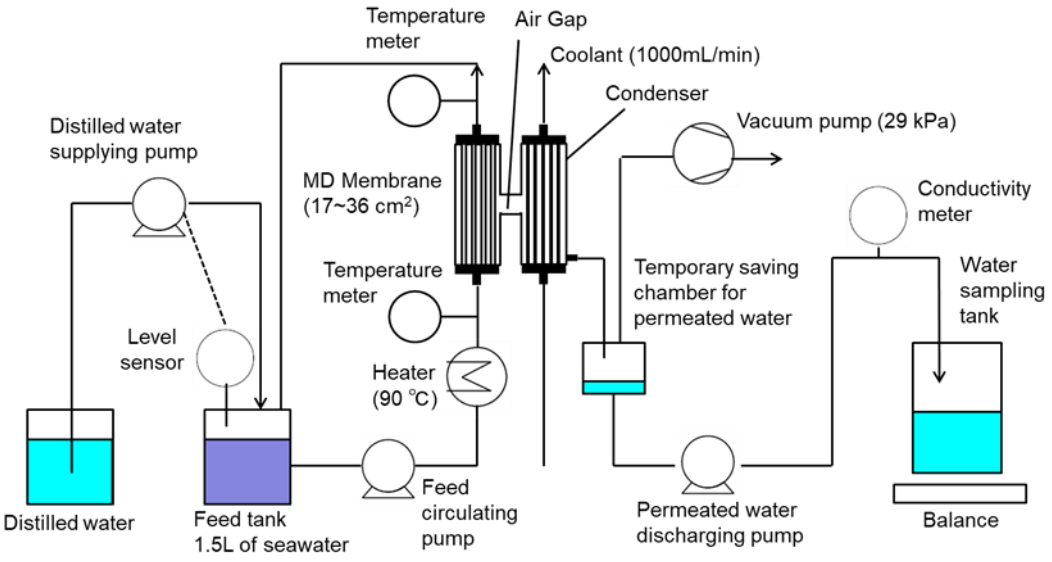

Figure III-4 Schematic of VMD system [84].

III. 2. 3. 5. Measurement of the amount of scale on the bore surface

To measure the amount of precipitated salt on the bore surface of the membrane, 50 mL of 0.1 M HCl aqueous solution was used to dissolve the precipitated salt. The 0.1 M HCl aqueous solution was passed through the bore and circulated in the system (Figure III-5) at 100 mL/min for 1 min [84]. This cleaning process was repeated five times to completely dissolve the scale. We previously confirmed that the Ca^{2+} concentration in fifth acid cleaning solution was zero. Then, all cleaning solutions were combined, and the Ca^{2+} concentration in the cleaning solution was measured by inductively coupled plasma-optical emission spectrometry (ICP-OES) (SPS6100, Hitachi High-Tech Science Corporation, Tokyo, Japan). The scale amount, m_s (g), was calculated using Equation (III-15), assuming that the scale is $CaCO_3$, because $CaCO_3$ is the main component of scale in seawater desalination [116].

$$m_s = \frac{W_a C_i M_s}{100\ M_i} \qquad \text{(III-15)}$$

where W_a (g) is the total amount of cleaning solution, C_i (wt%) is the concentration of dissolved cations in cleaning water, M_i (g/mol) is the molecular weight of dissolved cations, and M_s (g/mol) is the molecular weight of the scale. Thus, in this study, M_i was 40.078 g/mol (Ca^{2+}), and M_s was 100.087 g/mol ($CaCO_3$).

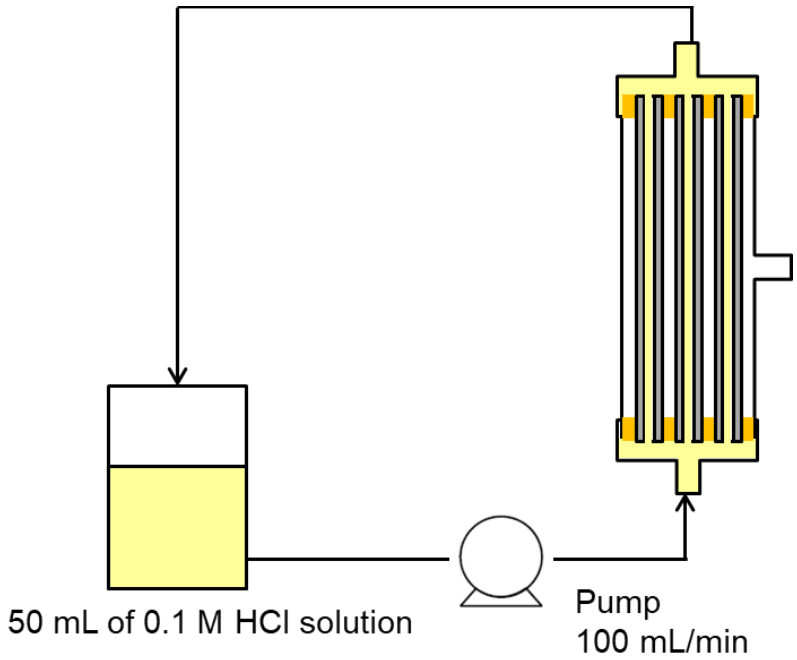

Figure III-5 Dissolution of the scale precipitated on the bore surface of the membrane [84].

III. 3. Results and Discussion

III. 3. 1. Morphology and Physical Properties of Membranes

Figure III-6 depicts the SEM images of M-5 and M-6 membranes; both membranes revealed a highly porous and uniform sponge-like structure throughout its cross section [84]. In addition, the morphology of M-5 and M-6 membranes are almost the same. Table III-1 shows the physical properties of each membrane and indicates that the membrane properties of the M-5 and M-6 membranes such as porosity, contact angle, and LEP were almost the same except for inner and outer diameters. By using these membranes, it will be possible to evaluate the effect of inner diameter on the pressure drop, the vapor flux, and the scales precipitation, avoiding membrane wetting, because of high LEP of the membrane.

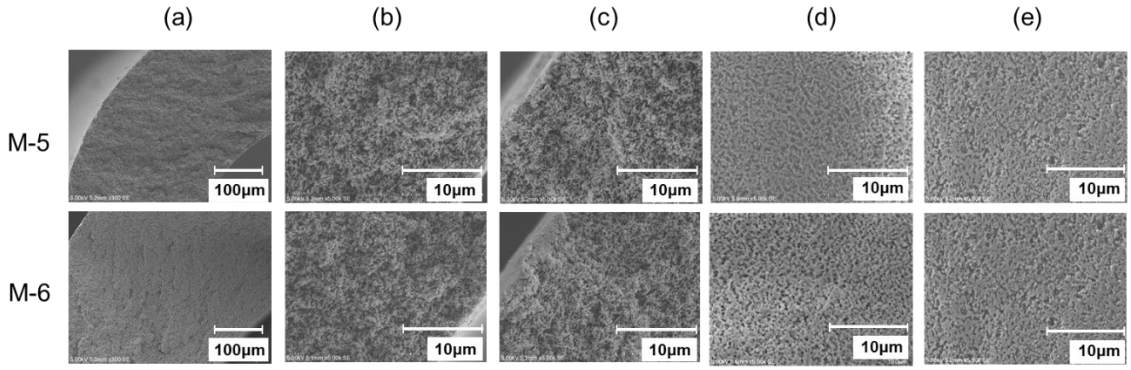

Figure III-6 SEM images of M-5 and M-6 membrane [84]. (a) Cross section, (b) near the bore side of the cross section, (c) near the shell side of the cross section, (d) bore surface, and (e) shell surface.

Table III-1 Membrane properties of M-5 and M-6.

Membrane	OD [1] [mm]	ID [2] [mm]	Thickness [mm]	Porosity [%]	Contact angle [°]	LEP [MPa]
M-5	1.25	0.68	0.29	72	132	0.24
M-6	1.83	1.02	0.41	73	133	0.23

[1] Outer diameter.

[2] Inner diameter.

III. 3. 2. Relationship between the linear velocity of feed solution and membrane property, and pressure drop

Long modules were used to investigate the relationship between the Reynolds number of the feed flow and the pressure drop. In this experiment, the feed was pure water at 25 °C, and thus, ρ and μ were 997 kg/m^3 and 0.00089 Pa·s, respectively [117].

Figures III-7(a)-1 and 7(a)-2 show the pressure drop as a function of linear velocity, and as a function of Reynolds number for the M-5 module, respectively. Figures III-7(b)-1 and 7(b)-2 show similar results for M-6. In these figures, the Reynolds number was calculated with Equation (III-1). The solid line shows the theoretical pressure drop calculated with Equation (III-6) assuming the laminar flow. The dashed line shows the theoretical pressure drop calculated with Equation (III-7) assuming turbulent flow. Figure III-7 shows that the theoretical curve calculated assuming laminar flow fits with the experimental data under a Reynolds number of 1000 (linear velocity of ~1.31 m/s for M-5 and ~0.88 m/s for M-6) but deviates from the experimental data over a Reynolds number of 1000. In contrast, the theoretical curve calculated assuming turbulent flow satisfactorily fits the experimental data over a Reynolds number of 1000. These results indicate the flow through the module changes from the laminar flow to the turbulent flow at a Reynolds number of ~1000 with an increase in linear velocity. Moreover, Figure III-7 shows that the pressure drop of M-5 is larger than that of M-6 at the same linear velocity and Reynolds number. This is because the inner diameter of the M-6 membrane was 1.5 times larger than that of the M-5 membrane. Equations (III-1), (III-6), and (III-7) show that the larger the inner diameter of the flow path, the larger the Reynolds number and the smaller the pressure drop.

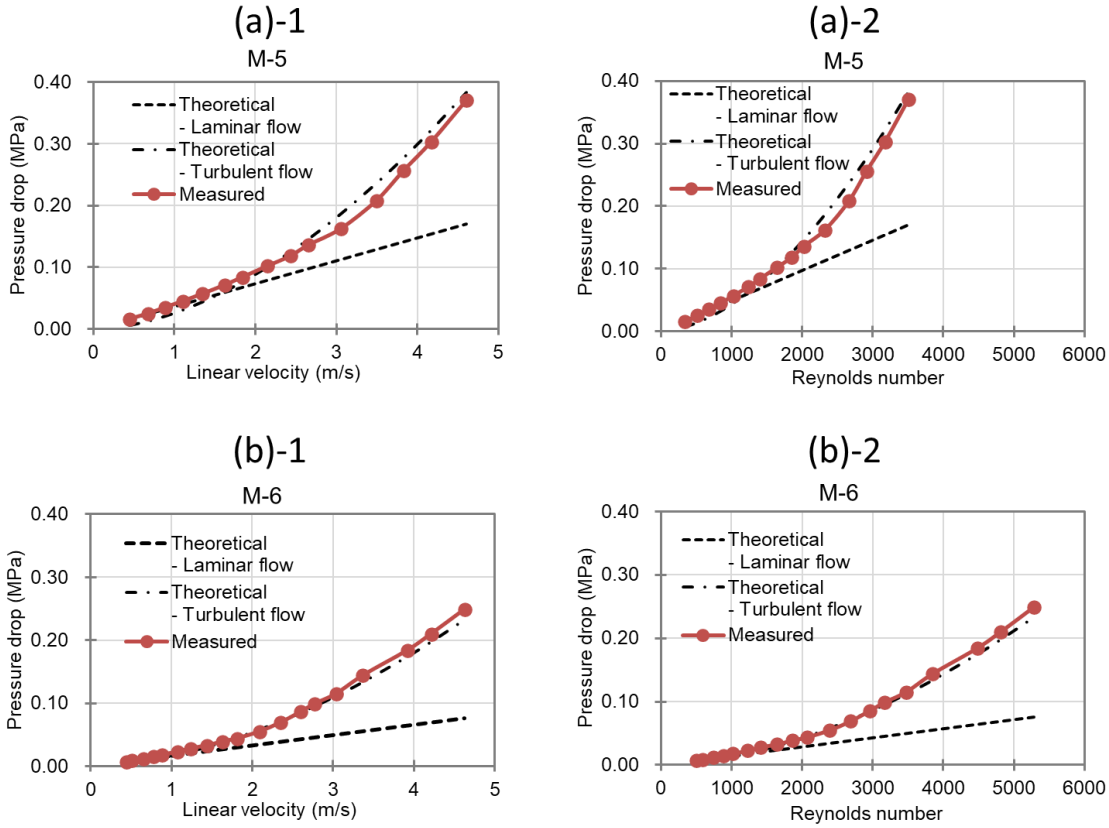

Figure III-7 Pressure drop as a function of (a)-1: linear velocity of the feed, and (a)-2: Reynolds number for M-5 long module. Pressure drop as a function of (b)-1: linear velocity of the feed, and (b)-2: Reynolds number for the M-6 long module [84].

III. 3. 3. Performance of the VMD Module

The effect of the linear velocity of the feed and Reynolds number on preventing scale precipitation was evaluated using real seawater as a feed with M-5 and M-6 VMD modules. In addition, their effect on vapor flux was also investigated. In this experiment, the feed-in temperature was raised to 90 °C to create severe conditions for scaling because the solubility of $CaCO_3$ decreases with temperature [102]. In this evaluation, the effective bore surface area was 0.0017 or 0.0034 m^2 for the M-5 module and 0.0018 and 0.0036 m^2 for the M-6 module. In calculating the Reynolds number, the feed was the seawater at 90 °C, and 991 kg/m^3 and 0.000345 Pa·s were used as ρ and μ, respectively [118]. The VMD operation of the two modules was performed for ~24 h. During VMD operation, the feed concentration was kept almost constant by the method explained in Section III.2.3.4. After VMD operation, modules were cleaned with a 0.1 M HCl solution to detect

the amount of scale precipitated on the bore surface of the membrane. In this experiment, the VMD operation was performed three times under each condition, and the average value and probable error were obtained. We used a new module in each experiment, since the bore surface was fouled by scale after the operation. Table III-2 shows the results of the VMD test for each operating condition. The amount of precipitated scale ($mg/m^2 \cdot h$) was obtained as the $CaCO_3$ corresponding value.

Table III-2 VMD operation results for the M-5 and M-6 VMD modules with the probable errors of the three operations.

Membrane	Linear velocity [m/s]	Reynolds number	Operation time [h]	Feed-in temp. [°C]	Feed-out temp. [°C]	Vapor flux [kg/m²·h]	Leaking salt flux [g/m²·h]	Salt retention rate [%]	$CaCO_3$ [mg/m²·h]
M-5	0.37 ± 0.02 [1, 2]	720 ± 41	25.2 ± 0.8	90.5 ± 0.1	82.2 ± 0.8	40.6 ± 5.4	0.17 ± 0.06	99.986 ± 0.002	106 ± 41
	0.46 [*2]	896	24.0	90.78 ± 0.02	81.6 ± 0.2	53.9 ± 0.9	0.10 ± 0.02	99.992 ± 0.002	51 ± 33
	0.5961 ± 0.0003 [1, 2]	1164 ± 1	21.4 ± 1.2	90.65 ± 0.04	83.7 ± 0.5	57.2 ± 1.4	0.1 ± 0.02	99.993 ± 0.001	0.45 ± 0.06
	0.76 ± 0.02 [1, 2]	1483 ± 37	23.0 ± 0.7	90.3 ± 0.1	84.6 ± 0.5	59.8 ± 1.8	0.26 ± 0.12	99.985 ± 0.007	0.5 ± 0.1
	1.39 ± 0.01 [1, 2]	2716 ± 18	24.0	90.8 ± 0.2	87.3 ± 0.6	67.9 ± 3.2	0.24 ± 0.07	99.988 ± 0.003	0.22 ± 0.04
M-6	0.316 ± 0.003 [3, 4]	925 ± 10	24.0	90.5 ± 0.1	84.2 ± 0.1	40.7 ± 0.9	0.029 ± 0.004	99.9935 ± 0.0002	74 ± 49
	0.4079 [4]	1195	24.0	91.37 ± 0.04	84.86 ± 0.05	45.6 ± 0.3	0.010 ± 0.001	99.9951 ± 0.0001	1.9 ± 0.2
	0.47 ± 0.01 [3, 4]	1368 ± 32	24.5 ± 0.3	90.6 ± 0.1	85.8 ± 0.2	44.8 ± 1.7	0.11 ± 0.05	99.990 ± 0.002	1.9 ± 0.9
	1.40 [3]	4098	24.0	90.36 ± 0.02	88.14 ± 0.02	58.0 ± 0.4	0.10 ± 0.03	99.991 ± 0.001	0.9 ± 0.1

[1] 0.0017 m^2 of M-5 module was used.

[2] 0.0034 m^2 of M-5 module was used.

[3] 0.0018 m^2 of M-6 module was used.

[4] 0.0036 m^2 of M-6 module was used.

Figures III-8(a) and III-8(b) show the amount of scale ($CaCO_3$) precipitated on the bore surface of the membrane as a function of the linear velocity of the feed, and Reynolds number, respectively [84]. It is found from Figures III-8(a) and III-8(b) that the amounts of precipitated scales decrease significantly with the linear velocity, and the Reynolds number. It stands to reason that scale precipitation depends both the linear velocity, and the Reynolds number, since the Reynolds number depends on the linear velocity. However, it is found that the decrease of precipitated scale in M-5 and M-6 modules are not on the same line as a function of the linear velocity, but are almost on the same line as a function of the Reynolds number. This means that scale precipitation is mainly affected by the Reynolds number, i.e., the type of flow. This probably because the Reynolds number reflects the type of flow, and the turbulent flow significantly decreases the scale precipitation. The flow through the module changes from laminar flow to turbulent flow at a Reynolds number of ~1000 with an increase in the linear velocity, as discussed in Section III.3.2.

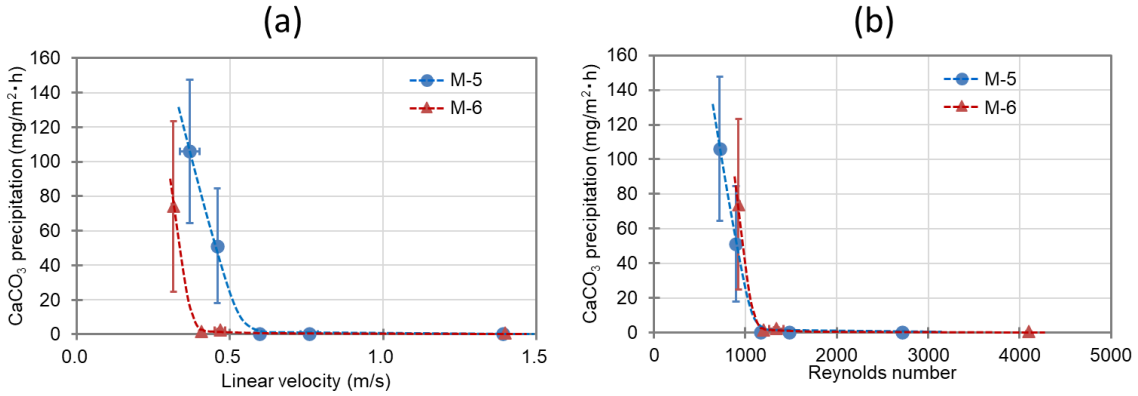

Figure III-8 Amount of scale ($CaCO_3$) precipitated on the bore surface in M-5 and M-6 VMD modules as a function of (a) linear velocity of the feed and (b) Reynolds number [84].

Figures III-9(a) and 9(b) show the time course of vapor flux under high and low linear velocity conditions through (a) M-5 and (b) M-6 membranes, respectively [84]. Figure III-9 shows that the vapor flux under high linear velocity conditions is higher than that under low linear velocity conditions and does not depend on the inner diameter of the HF membrane. This is because the feed-out temperature under high linear velocity conditions is higher than that under low linear velocity conditions, as shown in Table III-2, resulting in higher vapor pressure differences as the driving force of vapor permeation under high

linear velocity conditions than under low linear velocity conditions. The vapor fluxes through the M-5 and M-6 membranes under high linear velocity conditions are much more stable than those under low linear velocity conditions during 24-h operation. This is because scale precipitation on the bore surface of the membrane easily occurs under low linear velocity conditions, in which the Reynolds number is <1200, as shown in Figures III-9. This precipitated scale prevents vapor permeation through the MD membrane and causes a decrease in the vapor flux. These results indicate that the higher the linear velocity of the MD operation, the higher the flux and the more stable the operation.

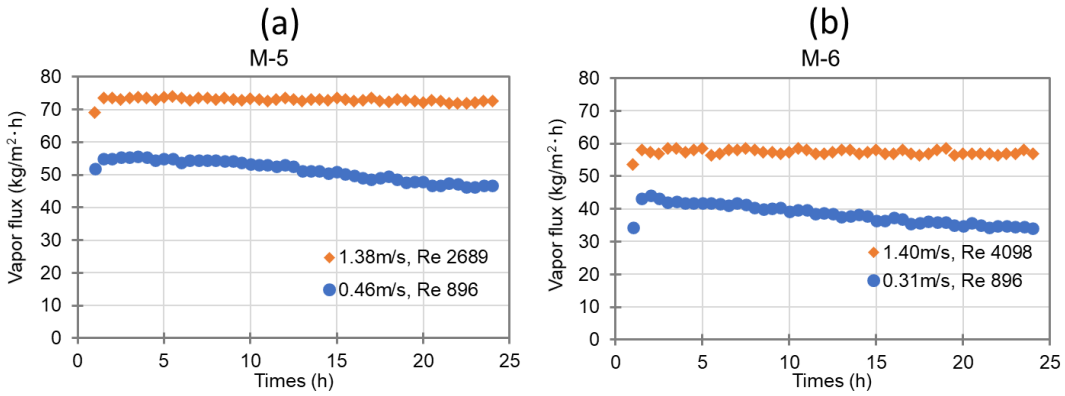

Figure III-9 Time course of vapor flux of (a) M-5 and (b) M-6 membranes under high and low linear velocity conditions [84].

Figures III-10(a) and III-10 (b) depict the vapor flux as a function of the linear velocity and Reynolds number, respectively [84]. Vapor flux increases with the linear velocity of the feed and Reynolds number because, as seen in Table III-2, the difference between the feed-in and feed-out temperatures decreases with the linear velocity of the feed or Reynolds number, and the average temperature of the feed in the module increases. Thus, the mean vapor pressure difference between the feed and permeate increases with the linear velocity of the feed or Reynolds number, resulting in a high vapor flux. In addition, the vapor flux through the M-5 membrane (circles) was higher than that through the M-6 membrane (triangles). This is probably because the difference in the membrane thickness. The membrane thickness of M-5 was 1.5 times thinner than that of M-6. If VMD is operated under the same condition, the vapor flux depends on the membrane thickness.

Thus, if the VMD operation condition for M-5 is the same as that of M-6, the ratio of vapor flux between M-5 and M-6 should be constant and 1.5 in this experiment. However, in Figures III-10(a), the vapor flux ratio increases with the linear velocity, while that in Figures III-10(b) is approximately 1.3, and constant even though it is not 1.5. It means that the operation condition for M-5 is the same as that of M-6 if we consider the vapor flux as a function of Reynolds number. Thus, it is reasonable to consider that the vapor flux is mainly affected by the Reynolds number of the feed flow, as well as the scale formation, as discussed above.

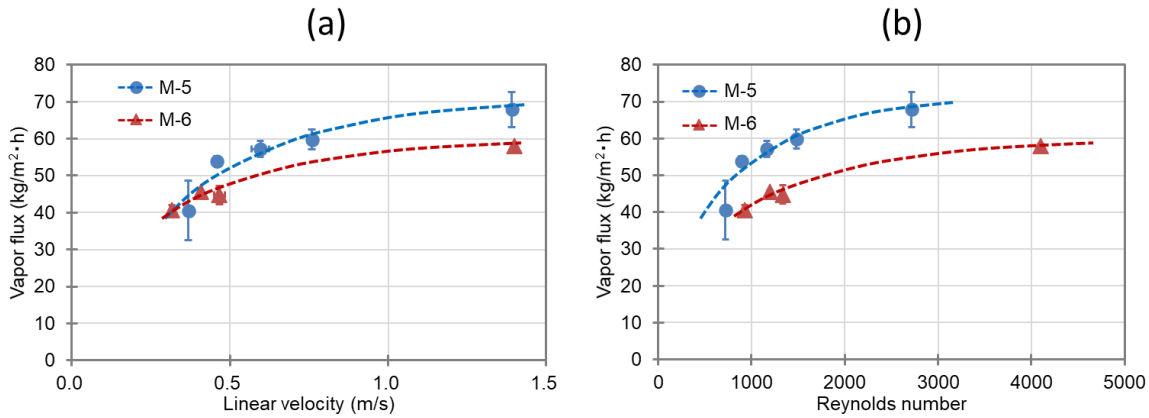

Figure III-10 Vapor fluxes of the M-5 and M-6 VMD modules as a function of (a) linear velocity of the feed and (b) Reynolds number. Circles and triangles denote M-5, and M-6, respectively [84].

The phenomenon in which the amount of scale precipitation depends on the Reynolds number of the feed flow is qualitatively explained as follows: the amount of scale precipitation is closely related to the concentration polarization at the bulk/bore surface interface [46,73,85,86]. In general, the concentration polarization coefficient (CPC) was used to determine the concentration polarization effect on the surface of the membrane. CPC was given by Equation (III-16). [46,48,85],

$$CPC = \frac{C_{m,f}}{C_{b,f}} = exp\left(\frac{J_w}{\rho k}\right) \quad \text{(III-16)}$$

$$k = \frac{D}{\delta_B} \quad \text{(III-17)}$$

where $C_{m,f}$ (wt%) and $C_{b,f}$ (wt%) are the solute concentration at the bulk/membrane

interface and in the bulk feed solution, respectively. k (m/s) is the solute mass transfer coefficient for the diffusive mass transfer through the boundary layer and given by Equation (III-17). D (m^2/s) and δ_B (m) are the diffusion coefficient of the solute and the thickness of the boundary layer, respectively. δ_B can be calculated with Equations (III-18)–(III-20) [48].

$$\delta_B = \frac{D}{k} = \frac{d_h}{Sh} = \frac{d}{Sh} \quad \text{(III-18)}$$

$$Sh = \frac{kd_h}{D} = \frac{kd}{D} = a_1 Re^{a_2} Sc^{a_3} \left(\frac{d}{l}\right)^{a_4} \quad \text{(III-19)}$$

$$Sc = \frac{\mu}{\rho D} \quad \text{(III-20)}$$

where Sh (-) is the Sherwood number given by Equation (III-19) and Sc (-) is the Schmidt number given by Equation (III-20). l (m) denotes the length of the feed channel. a_1, a_2, a_3, and a_4 are constants determined by the experimental condition [119–121]. For example, Kanamori et al. reported that the equation derived by Colburn, where a_1 was 1.62, and a_2, a_3, and a_4 were 1/3, is in good agreement with experimental data obtained for HF membranes under laminar flow conditions [121]. In the case turbulent flow (Reynolds number > 10^4), a_1, a_2, a_3, and a_4 become 0.023, 0.8, 1/3 and 0, respectively [122]. In Equations (III-18) and (III-19), the hydraulic diameter, d_h, is equal to the inner diameter of the HF, because the HF membrane with a pipe shaped cross section is treated in this study. Figure III-11(a) shows the calculated Sherwood number of M-5 as a function of Reynolds number in both case of laminar flow and turbulent flow [84]. Figure III-11(b) also shows the calculated Sherwood number of M-6. In calculating the Sherwood number, the feed was the seawater at 90 °C, and 991 kg/m^3 and 0.000345 Pa·s were used as ρ and μ, respectively [34]. D was used 27.4 × 10^{-10} m^2/s, which is the calculated diffusion coefficient of calcium ion in seawater at 90 °C. This was obtained by using Equation (III-21), which can be derived from the Stokes-Einstein equation [123].

$$D = D_0 \frac{\mu_0}{\mu} \frac{T}{T_0} \quad \text{(III-21)}$$

where D_0 (m^2/s) and μ_0 (kg/m^3) are the diffusion coefficient of solute and the viscosity of the fluid at T_0 (K), respectively. In this calculation, 3.73 × 10^{-10} m^2/s and 1028 kg/m^3 were used as D_0 and μ_0, respectively, which are the diffusion coefficient of calcium ion in seawater and the viscosity of seawater at 273.15 K (0 °C), respectively [124]. T is the

absolute temperature of solute, and 363.15 K (90 °C) in this calculation. It is found from Figures III-11(a) and 11(b) that the Sherwood number increases as the increasing of the Reynolds number in both cases of laminar flow and turbulent flow. It is also found that the Sherwood number in turbulent flow becomes much larger than the Sherwood number in laminar flow.

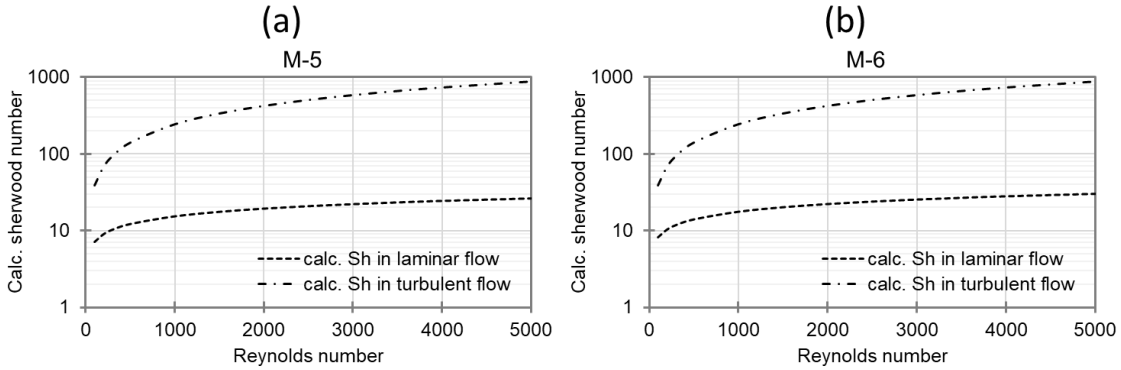

Figure III-11 Calculated Sherwood number as a function of Reynolds number in both case of laminar flow (dotted line) and turbulent flow (chained line) of (a) M-5, and (b) M-6 [84].

Thus, it is found from Equations (III-17) and (III-18) that the solute mass transfer coefficient, k, increases with Sherwood number, that is with Reynolds number. It is found from Equation (III-16) that a larger mass transfer coefficient decreases the CPC, resulting in a lower risk of scale precipitation. In contrast, the vapor flux, J_w, increases with the Reynolds number of the feed, as shown in Fig. 10(b), resulting in an increase in CPC, which increases the risk of scale precipitation. However, the increase in J_w will stop at a certain Reynolds number where the feed-out temperature becomes very close to the feed-in temperature, since the increase of J_w over 1200 of Reynolds number is due to the increase of average temperature of feed in the module. That is, the effect of J_w on CPC is constant above this Reynolds number. However, Equations (III-16)–(III-20) show that the positive effect of the Reynolds number for scale precipitation (i.e., the decrease in scale) continuously increases as the Reynolds number increases. Thus, the decrease in CPC due to the increase in Reynolds number of the feed flow overcomes the increase in CPC due to the increase in vapor flux. Then, the operation at a large Reynolds number prevents scale precipitation by decreasing the concentration polarization.

III. 4. Conclusion

Scale precipitation of the membrane surface is a severe problem for seawater desalination with MD operation. In this chapter, I investigated the Reynolds number of the feed to solve the scaling problem because the feed flow in the module changes from a laminar flow to a turbulent flow at a particular Reynolds number. Turbulent flow decreases the concentration polarization at the bulk/membrane interface and decreases scale formation.

VMD operation was performed using two types of hydrophobized PVDF hollow fibers with similar morphologies and different inner and outer diameters, using real seawater as a feed. Results of the pressure drop in the module reveal that the feed flow changed from laminar flow to turbulent flow at a Reynolds number greater than 1000. Further, the extent of scale precipitation was mainly influenced by the Reynolds number of the feed flow rather than the linear velocity. As expected, the scale precipitation satisfactorily decreased to a Reynolds number of >1200 for the feed flow. This phenomenon was qualitatively explained by the decrease in concentration polarization with the Reynolds number.

The vapor flux increased with the Reynolds number, which is the increase in linear velocity of the feed. This was due to the increase in the mean temperature of the feed in the module, resulting in an increase in the vapor pressure difference as a driving force. In addition, the vapor flux was very stable during 24 h of operation at high Reynolds numbers.

Regarding the membrane size, it was confirmed that the scale precipitation through the HF with a larger inner diameter was less than that through the HF with a small inner diameter under the same linear velocity of feed flow. This was because the Reynolds number of the feed flow through the HF with a larger inner diameter was larger than that through the HF with a small inner diameter, even at the same linear feed velocity. It was also confirmed that the pressure drop in the module with HF with a larger inner diameter was lower than that in the module with HF with a smaller inner diameter.

Selecting a larger inner diameter HF membrane and operating at a higher linear velocity in which a Reynolds number of >1200 is required to prevent scale precipitation without excessive pressure drop. This study provides guidelines for determining suitable membrane properties and VMD operating conditions.

Chapter IV

Recovery of valuable solutes from organic solvent/water mixture by direct contact membrane distillation as non-heated process

IV. 1. Introduction

Recently, the demand for the recovery of valuable solutes from organic solvents/water mixtures have increased in numerous areas, including chemical and pharmaceutical production [125,126]. For instance, organic solvents/water mixtures are used in the synthesis and purification processes of peptides [127]. Since many of these peptides are heat-sensitive, the demand for non-heated concentration technology has increased.

Numerous studies on organic solvent nanofiltration (OSN) as a non-heated concentration technology have been reported [128,129]. OSN is regarded as an energy-efficient concentration method due to the absence of phase transition [130]. Additionally, since OSN is a membrane technology, it is easier to scale up than the conventional distillation technologies [125]. However, because OSN membranes separate solutes by size, it is difficult to concentrate valuable resources that are smaller than the membrane pore size without incurring losses, since they easily pass through the OSN membranes [131–133].

Under such circumstances, I focused on applying MD for the recovery of valuable solutes from organic solvents/water mixtures. Theoretically, MD can separate any solutes from a solvent, as long as the solutes are non-volatile. Thus, MD can separate small solutes which cannot be separated using OSN. In addition, it is possible to concentrate the feed at temperatures below ambient temperature, if the vapor pressure difference between the feed and permeate sides of the membrane is sufficient. Additionally, MD shares many of the same advantages as other membrane technologies, including a simpler system and greater scalability than conventional distillation technologies.

Almost all MD operating conditions reported in previous studies report a feed

temperature higher than 40 °C and a feed solution that did not contain any organic solvents [134]. However, in applications such as chemical and pharmaceutical manufacturing processes, the operating temperature of the MD must be below ambient temperature to avoid the deterioration of valuable resources due to heat. In addition, organic solvents are frequently present in aqueous solutions. Thus, there are two challenges associated with applying MD technology to the process of chemical and pharmaceutical recovery. One issue is low vapor flux through the membrane as a result of a small vapor pressure difference caused by the low feed temperature. The other issue is membrane wetting caused by organic solvents. When the membrane is wet, liquids permeate through the membrane, resulting in the leak of solutes [38].

The vapor flux of MD, J (kg/m^2·h) is proportional to the vapor pressure difference between the feed side and the permeation side and is given by Equation (IV-1) [44,45].

$$J = \alpha(P_{feed} - P_{permeate}) \quad \text{(IV-1)}$$

Here, α (kg/m^2·h· kPa) is the vapor permeation coefficient. P_{feed} (kPa) and $P_{permeate}$ (kPa) are the saturated vapor pressures of the feed side and of the permeation side, respectively. ($P_{feed} - P_{permeate}$) should be positive, since this is the driving force of vapor permeation. Equation (IV-1) suggests that as the temperature of the feed decreases, it becomes more difficult to get enough vapor pressure difference, as the saturated vapor pressure decreases. Therefore, the vapor flux of MD will become extremely low under low feed temperature conditions. Only a few studies of MD operation at low feed temperatures have been reported so far [45]. Furthermore, even if they were successful in MD operation, the vapor flux was extremely low. For example, Macedonio et al. performed direct contact MD (DCMD) operation at 30 °C and 25 °C for the feed and permeate, respectively [44]. Additionally, they used the commercial polypropylene flat sheet membrane and obtained 0.2 kg/m^2·h as the water vapor flux.

Membrane wetting is another severe problem in MD operation. Membrane wetting occurs when a trans-membrane pressure becomes higher than the liquid entry pressure (LEP). LEP (MPa) is the pressure required for the liquid to penetrate into the membrane pore [52]. LEP is given by Equation (IV-2).

$$LEP = \frac{-2B\sigma_L cos\theta}{r_{max}} \quad \text{(IV-2)}$$

Here, B is a geometric factor determined by pore structure, for example, B = 1 for cylindrical pores. σ_L is surface tension of a liquid, θ is a contact angle, and r_{max} is a maximum pore radius of membrane. In general, organic solvents decrease the surface tension of liquid in comparison with water, subsequently decreasing LEP [45]. Thus, MD is difficult to be applied for recovering valuable solutes from organic solvent/water mixtures, since the membrane is easily wetted.

So far, few studies have been conducted that report the use of MD against organic solvent/water mixtures. In a few instances when an organic solvent/water mixture is used, the flux is extremely low as a result of improved LEP to avoid wetting. For example, Banat et al. performed an air gap MD (AGMD) operation using a polyvinylidene fluoride (PVDF) flat sheet membrane and treated an ethanol aqueous solution [135]. They obtain approximately 1 kg/m^2·h flux using 42 °C of 3.3 wt% EtOH aqueous solution as the feed. Additionally, Gupta et al. performed sweep gas MD (SGMD) using a composite membrane containing carbon nanotube to concentrate the iso-propanol aqueous solution [136].

In this chapter, I investigated to improve vapor flux from two perspectives: the membrane and the MD operation method. Regarding MD membrane, a hydrophobized PVDF hollow fiber (HF) membrane with a high vapor flux and high LEP, fabricated in chapter III, was used as the MD membrane [84]. It is expected that by using this membrane, the vapor will permeate efficiently even at low temperatures where the vapor pressure difference is low. Additionally, the membrane will scarcely get wet with the feed, which contains organic solvents, because the membrane will maintain sufficient LEP by the combination of high hydrophobicity and small maximum pore size, even if the surface tension of the feed aqueous solution becomes low due to the contained organic solvents.

Regarding MD operation, it is important to choose the method that allows for a large vapor pressure difference across the membrane while reducing the transmembrane pressure simultaneously. In this chapter, I chose DCMD as the most suitable operation method in typical four MD operation method as described in Figure IV-1 [90].

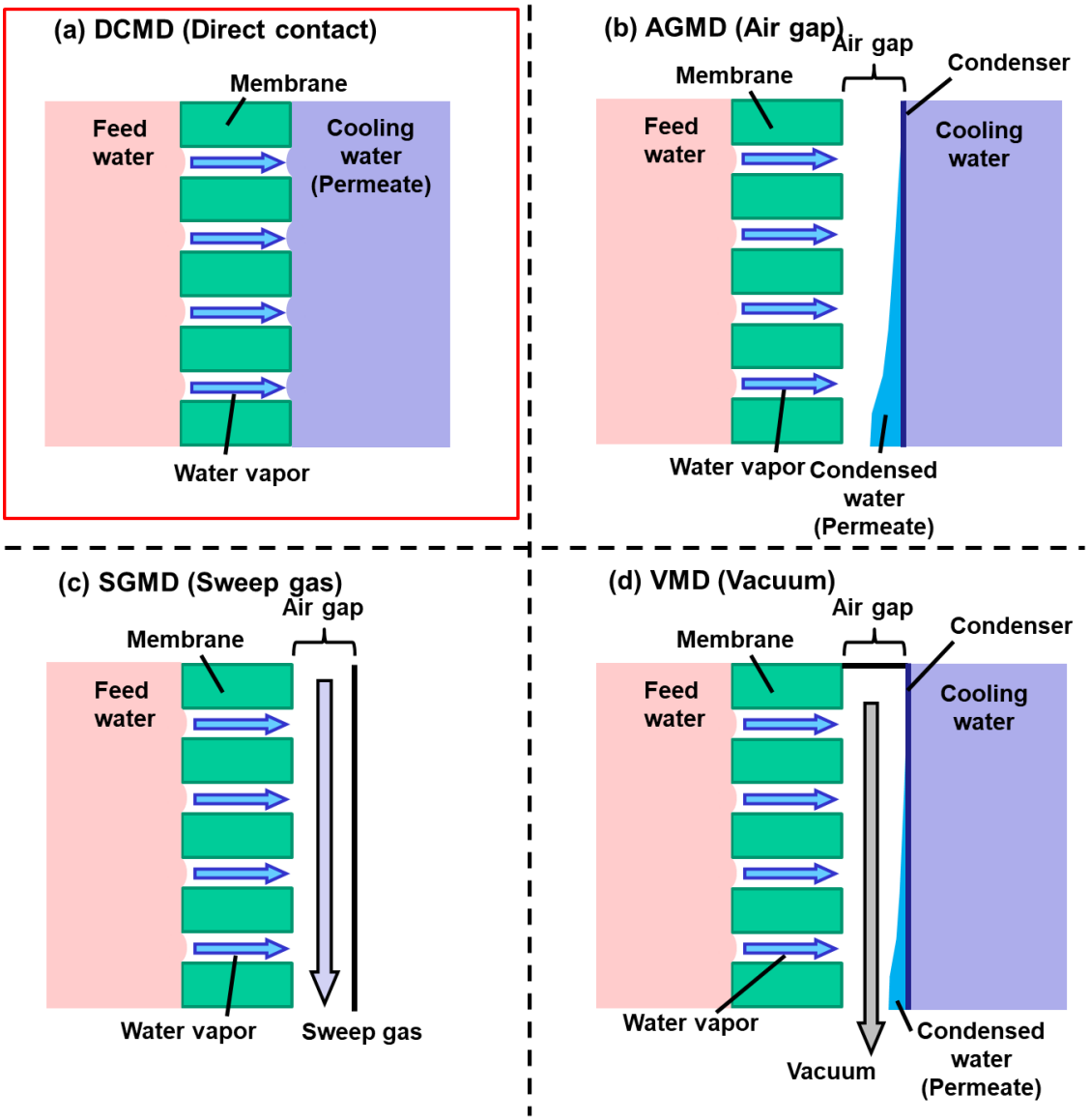

Figure IV-1 Schematics of typical membrane distillation (MD) operation setups. (a) Direct contact MD (DCMD), (b) Air gap MD (AGMD), (c) Sweep gas MD (SGMD), (d) Vacuum MD (VMD). DCMD was used in this chapter.

It is because that the high vapor flux can be obtained in DCMD, simply by flowing water that is cooler than the feed. In terms of membrane wetting, DCMD has a lower transmembrane pressure than other MD processes. Therefore, there is a high possibility that it can be operated even if the LEP decreases due to the organic solvent contained in the feed.

IV. 2. Materials and Methods

IV. 2. 1. Materials

Solef 6010 (SOLVAY, Brussels, Belgium) was used as the PVDF resin [83,89,94]. AEROSIL-R972 (NIPPON AEROSIL, Tokyo, Japan) was the hydrophobic silica, and functioned as a pore-forming agent. The PVDF polymer was diluted using Di (2-ethylhexyl) phthalate (DOP), and dibutyl phthalate (DBP). Following fabrication, CH_2Cl_2, EtOH, and NaOH were used to wash the membrane. The membrane porosity was determined using 1-Butanol., NaCl was used as a model electrolyte in the feed solution. Sodium dodecyl sulfate (SDS) was used as a model surface-active solute. All of these chemicals were purchased from FUJIFILM Wako Pure Chemical Corporation, Osaka, Japan. The fluoropolymer FS-392B (Fluoro Technology Co. Ltd., Aichi, Japan), was used as the hydrophobic agent [95,114].

IV. 2. 2. Fabrication of hydrophobized PVDF Membrane

IV. 2. 2. 1. Fabrication of PVDF Hollow Fiber Membrane

The PVDF hollow fiber (HF) membrane was fabricated by the similar way of fabricating M-5 as described in Section III. 2. 2., in which the thermally induced phase separation method and treatment with a hydrophobic agent were conducted, to produce PVDF HF with a high LEP [83,84]. At first, the PVDF HF membrane was fabricated using the TIPS method described in the patent [83,94]. The dope solution was comprised of hydrophobic silica, DOP, DBP, and PVDF at a weight ratio of 23:31:6:40. This was melted at 240 °C and extruded through the outer slit of a double-orifice spinneret. Simultaneously, nitrogen gas was discharged from the inner slit of the spinneret as a hollow part formation fluid. The extruded dope was then introduced into a water bath (40 °C) through a 20 cm air gap and wound up at a rate of 20 m/min. Following that, the membrane was immersed in CH_2Cl_2 to remove DOP and DBP, and then dried. Subsequently, the membrane was immersed in a 50 wt% EtOH aqueous solution, and 5 wt% NaOH aqueous solution for 1 h at 40 °C to remove silica. The analysis of the membrane composition revealed that silica particles were completely removed. The PVDF HF membrane was finally obtained after washing with water and drying. After

inserting PVDF HF membranes into a lab-scale module, they were treated with a hydrophobic agent as described in section IV. 2. 2. 3..

IV. 2. 2. 2. Preparation of Membrane Modules

A laboratory-scale module was constructed by inserting 70 PVDF HF membranes with a length of 11cm into a pipe and curing both ends with a urethane adhesive [83]. The total bore surface area of the membrane in the lab-scale module was 0.012 m^2 (Figure IV-2) [89].

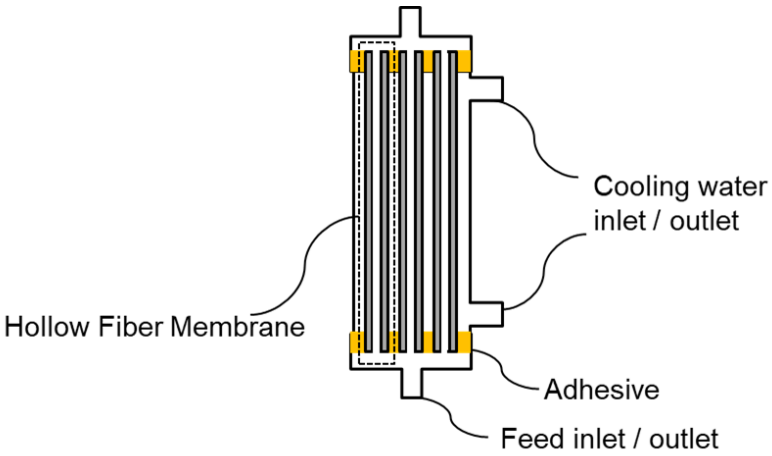

Figure IV-2 Schematic of membrane modules for DCMD [89].

IV. 2. 2. 3. Hydrophobic Treatment

One side of the feed inlet/outlet of the module was sealed, following which a hydrophobic agent was injected by a syringe into the bore side of the hollow fiber membranes from the other side of the feed inlet/outlet of the module to wet the whole membrane (Figure IV-3) [89]. Before injecting, the hydrophobic agent, fluoropolymer FS-392B was concentrated up to three times using an evaporator [114]. Additionally, a permeated hydrophobic agent wet the outer surface of the HF membranes. After wetting the entire membrane, the excess hydrophobic agent was removed. Using dry air flowing into the module, the membrane was then dried overnight at a temperature of ≈25 °C to obtain a hydrophobized PVDF HF membrane module. This operation hydrophobized entire HF membrane, including the bore surface, shell surface, and cross section of the membrane.

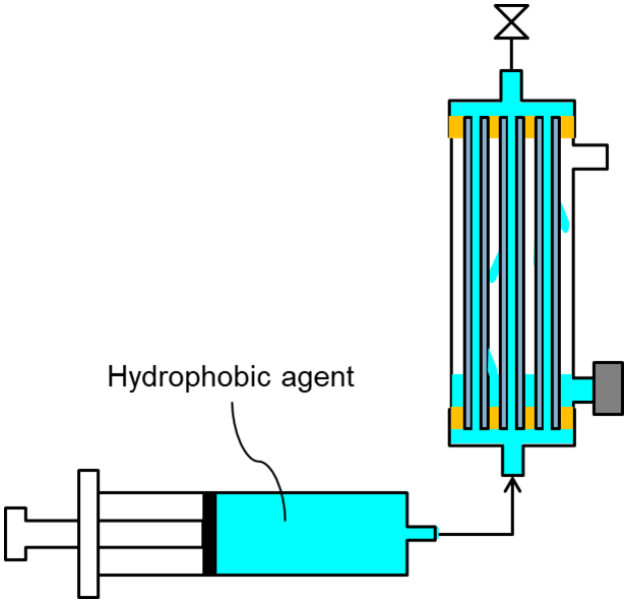

Figure IV-3 Schematic diagram of hydrophobic treatment [89].

IV. 2. 3. Characterization of PVDF Membrane

IV. 2. 3. 1. Liquid entry pressure (LEP) measurement

To measure the LEP of the membrane, both the bore side and the shell sides were filled with 20 wt% ethanol aqueous solution, following which pressure was applied to the bore side (Figure IV-4) [89]. I used a 20 wt% ethanol aqueous solution to simulate actual operating conditions for LEP evaluation. The pressure was gradually increased while the liquid level in the tube connected to the module's shell outlet was monitored. LEP was determined as the pressure at which the liquid level in the tube began to rise [83].

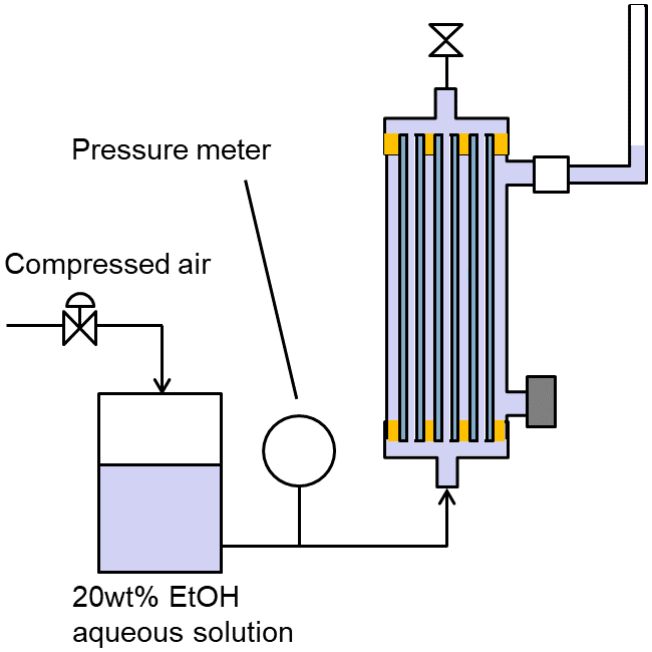

Figure IV-4 How to measure LEP of membrane [89].

IV. 2. 3. 2. DCMD Evaluation

The MD performance was evaluated using the equipment shown in Figure IV-5 [89,114]. The feed organic solvent/water mixture (1000 g) was heated to the desired temperature (25–45 °C) and circulated at a flow rate of 300 mL/min to the bore side of the membrane module. The feed solution contained 1000 ppm NaCl or SDS. The temperature of the cooling water (1000 g) was lowered to <10 °C and circulated at a flow rate of 300 mL/min to the shell side of the membrane module. The higher flow rate of feed and coolant is better to get higher vapor flux, since the effect of heat conduction is decreased. However, an applied pressure to the inlet of the HF membrane must be increased to increase the flow rate, resulting in the increase of transmembrane pressure and the increase of risk of membrane wetting. From the balance between the merit and demerit of high flow rate, 300 mL/min in the flow rate was chosen for the feed and the coolant. The total permeate vapor flux (sum of the water and organic solvents vapor fluxes) through the membrane, J_p (kg/m^2·h) was given by Equation (IV-3):

$$J_p = \frac{W_t}{A\,t} = \frac{W_c - W_c^0}{A\,t} \quad \text{(IV-3)}$$

Here, W_t (kg) is the weight of permeate, W_c^0 (kg) and W_c (kg) are the weights of cooling water before and after the operation, respectively. A (m^2) is the total membrane bore surface area, and t (h) is the operating time.

The flux of total leaking solute, J_s ($g/m^2 \cdot h$) was given by Equation (IV-4):

$$J_s = \frac{1000\Delta m_s}{A\,t} = \frac{1000(W_c\,C_c - W_c^0\,C_c^0)}{A\,t} \quad \text{(IV-4)}$$

here Δm_s (kg) is the difference of the amount of solute contained in cooling water before and after the operation. C_c^0 (wt%), and C_c (wt%) are the solute concentrations in cooling water before and after the operation, respectively, which were obtained from the conductivity of the cooling water.

The concentration factor F, and the solute retention ratio in the feed, β (%) were given by Equations (IV-5) and (IV-6), respectively. β (%) is also confirmed from the leaking solute flux given by Equation (IV-4).

$$F = \frac{C_{sf}}{C_{sf}^0} \quad \text{(IV-5)}$$

$$\beta = \frac{m_{sf}}{m_{sf}^0} \times 100 = \frac{W_f\,C_{sf}}{W_f^0\,C_{sf}^0} \times 100 \quad \text{(IV-6)}$$

Here, m_{sf}^0 (kg) and m_{sf} (kg) are the amounts of solute in the feed before and after the operation, respectively. C_{sf}^0 (wt%) and C_{sf} (wt%) are the solute concentrations in the feed before and after the operation, respectively, which were obtained from the conductivity of the feed. W_f^0 (kg) and W_f (kg) are the weights of the feed before and after the operation, respectively.

The permeate vapor flux of organic solvent, J_{os} ($kg/m^2 \cdot h$) was given by Equation (IV-7):

$$J_{os} = \frac{W_{os}}{A\,t} = \frac{(W_c\,C_{os} - W_c^0\,C_{os}^0)}{A\,t} \quad \text{(IV-7)}$$

here, W_{os} (kg) is the weight of permeated organic solvent through membrane. C_{os}^0 (wt%) and C_{os} (wt%) are the organic solvent concentrations of cooling water before and after the operation, respectively. The organic solvent concentration was measured using the

refractive index meter PAL-RI (ATAGO CO., LTD., Tokyo, Japan). The accuracy of organic solvent concentration is about ± 0.5wt% for ethanol and ± 0.6wt% for acetonitrile due to the measurement accuracy of PAL-RI.

The concentration of organic solvent in vapor C_{osv} (%) was given by Equation (IV-8):

$$C_{osv} = \frac{J_{os}}{J_p} \times 100 \quad \text{(IV-8)}$$

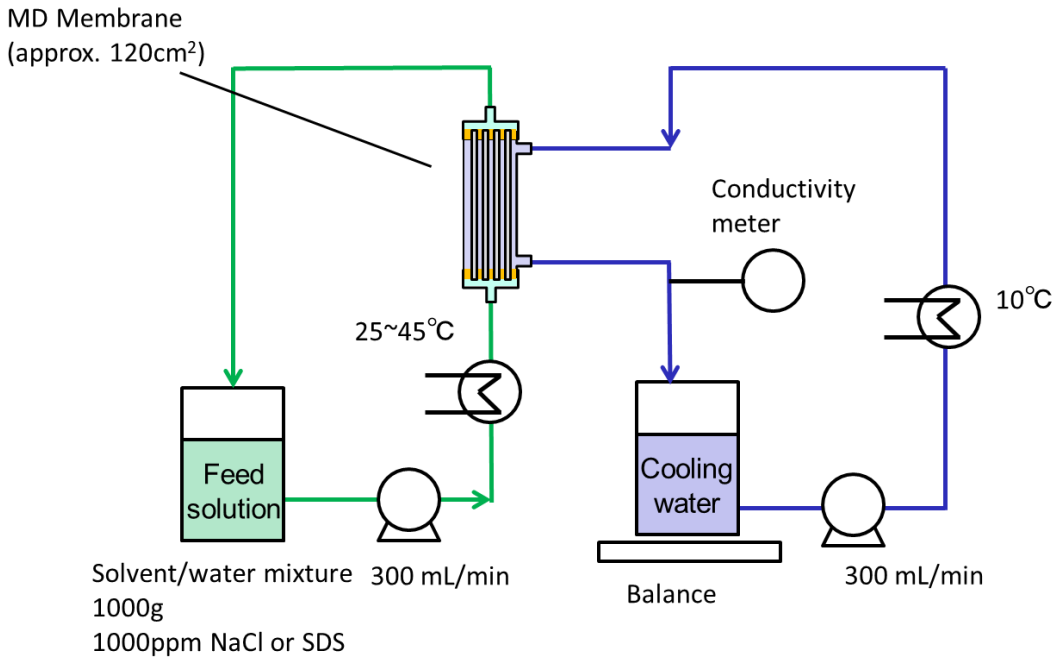

Figure IV-5 The schematic of DCMD system [89].

IV. 3. Results and Discussion

IV. 3. 1. Membrane morphology and membrane properties

Following a hydrophobic treatment, the PVDF HF membrane, described in a previous paper, was used in this study [83]. The morphology of the membrane is depicted in Figure IV-6, and its properties are listed in Table 1 [89]. As illustrated in Figures IV-6(a), IV-6(b), and IV-6(c), the membrane had a highly porous and uniform sponge-like structure throughout its cross-section. Additionally, the bore surface porosity was observed to be higher than that of the shell surface (Figures IV-6(d) and IV-6(e)). Furthermore, due to the hydrophobic treatment, the water contact angle (132°) was higher than that of original

PVDF membranes (103°) (Table IV-1). As a result, the LEP of this membrane was quite high even when used with a 20 wt% ethanol aqueous solution (0.24 MPa), for which the original PVDF membrane was easily wetted.

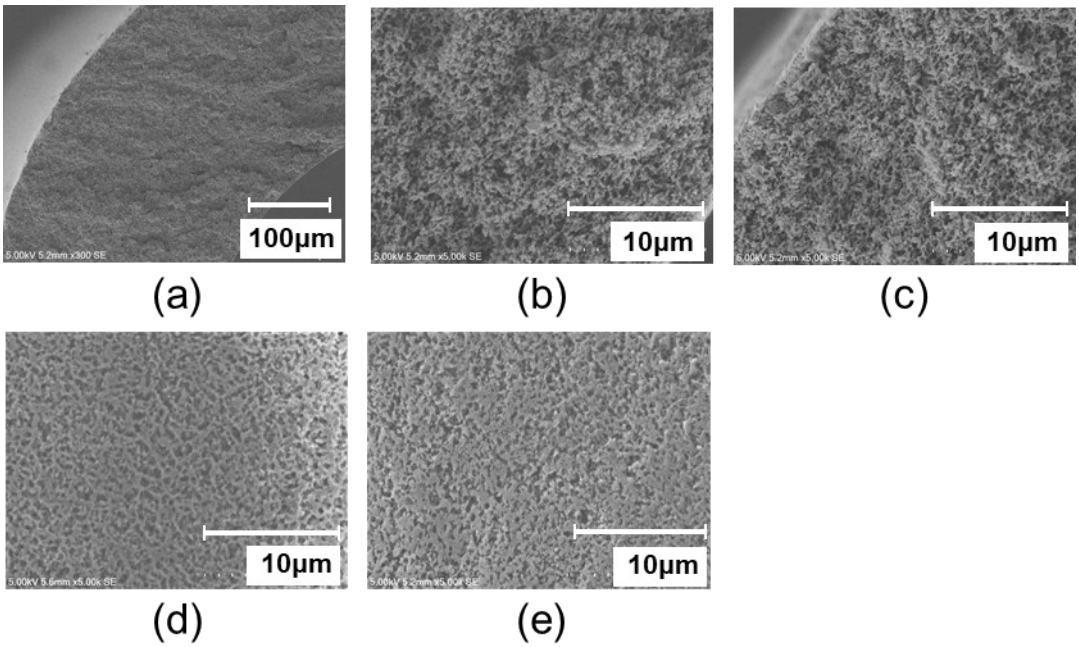

Figure IV-6 Membrane morphology. (a) Cross section, (b) Near the bore side of the cross section, (c) Near the shell side of the cross section, (d) Bore surface, (e) Shell surface [89].

Table IV-1 Membrane properties.

Membrane	OD [1] [mm]	ID [2] [mm]	Thickness [mm]	Contact angle [3] [°]	LEP [4] [MPa]
Before hydrophobic treatment	1.25	0.68	0.28	103	N/A
After hydrophobic treatment	1.25	0.68	0.28	132	0.24

[1] Outer diameter.

[2] Inner diameter.

[3] Measured with water.

[4] For 20 wt% ethanol aqueous solution.

IV. 3. 2. MD performance

IV. 3. 2. 1. Effect of operating temperature on MD performance

DCMD operations were carried out using the DCMD system shown in Figure IV-5 [89]. The effect of feed temperature on DCMD performance was investigated at first, maintaining a coolant temperature of ≈10 °C. The experiment used a 1000 ppm NaCl aqueous solution as feed, with NaCl serving as both a model valuable solute and an indicator of membrane wetting. Because NaCl is difficult to vaporize within the temperature range of MD operation, it is suitable for the valuable model solutes. Furthermore, NaCl is also a suitable indicator of membrane wetting because the size of the NaCl molecule is much smaller than the pore size of MD membrane (≈0.1 μm) [83]. Thus, when the MD is not wet, NaCl does not permeate through the membrane. However, it easily permeates when the membrane is wet. Additionally, NaCl permeation can be detected easily by measuring the conductivity of the coolant.

The results of the DCMD test with various feed temperatures are shown in Table IV-2. In all conditions, the operation time was maintained at 2 hours. When the feed-in temperature was 25.1 °C, the water vapor flux through the membrane was 0.8 kg/m^2·h. It further increased to 3.1 kg/m^2·h as the feed-in temperature increased to 45.4 °C. Thus, the vapor flux increased with the feed temperature when the temperature of the coolant was kept constant. This is due to the increase in the vapor pressure difference between the feed and the cooling water, which is the driving force for vapor permeation across the membrane.

Additionally, the leaking salt flux was less than 0.01 g/m^2·h and the solute retention ratio in the feed was over 99.9%, in all conditions. This demonstrates that solutes, as small as Na^+ and Cl^- ions, can be maintained at a concentration of ≈100% in the feed.

Table IV-2 Results of DCMD operation with 1000 ppm NaCl aqueous solution as feed at various temperature.

Temperature				Operating time	Water vapor flux	Leaking solute (NaCl) flux	Concentration factor	Solute (NaCl) retention ratio in Feed
Feed-in [1]	Feed-out [2]	Coolant-in [3]	Coolant-out [4]					
[°C]	[°C]	[°C]	[°C]	[h]	[kg/m^2·h]	[g/m^2·h]	[-]	[%]
25.1	23.4	11.5	12.9	2.0	0.8	<0.01	1.02	>99.9
35.2	32.3	11.6	13.8	2.0	1.7	<0.01	1.04	>99.9
45.4	40.4	12.8	17.1	2.0	3.1	<0.01	1.08	>99.9

[1] Temperature of the feed at module inlet.

[2] Temperature of the feed at module outlet.

[3] Temperature of the cooling water at module inlet.

[4] Temperature of the cooling water at module outlet.

IV. 3. 2. 2. MD performance with organic solvent/water mixture at various temperatures

To confirm whether DCMD was capable of operating in an aqueous solution containing an organic solvent, ethanol and acetonitrile were used as the model organic solvents and the impact of the feed temperature on the membrane performance was investigated, with a coolant temperature of 10 °C. In all conditions, the feed contained 15 wt% ethanol or acetonitrile, and 1000 ppm NaCl was also used as the model valuable solute. The DCMD operation was performed for 2 hours at three different feed temperatures, 25, 35, and 45 °C.

As shown in Table IV-3, after two hours of operation, the leaking solute flux was less than 0.01 $g/m^2 \cdot h$ and the solute retention ratio was greater than 99.9 % in all conditions. These performances were high enough to apply for solute recovery, and are comparable to the conventional OSN processes [131–133]. The results, thereby indicate that, despite the presence of an organic solvent in the feed, the solute is recovered sufficiently. This strongly suggests that the hydrophobic membrane is easy to maintain high a LEP, and that the DCMD mode can avoid excessive transmembrane pressure.

Furthermore, the total vapor flux increased as the feed-in temperature increased, even in the presence of an organic solvent. Figure IV-7 shows the total vapor flux for three kinds of feeds as a function of feed-in temperature [89]. As illustrated, the total vapor flux was observed to increase due to the inclusion of the organic solvent. Additionally, it was found that the total vapor flux for the mixture of acetonitrile/water mixture is slightly higher than that for ethanol /water.

Table IV-3 Results of DCMD operation at various temperature with the feed which contains 1000 ppm NaCl and 15wt% of ethanol or acetonitrile.

Organic solvent	Temperature				Operating time	Vapor flux		
	Feed-in [1] [°C]	Feed-out [2] [°C]	Coolant-in [3] [°C]	Coolant-out [4] [°C]	[h]	Total [kg/m²·h]	Water [kg/m²·h]	Organic solvent [kg/m²·h]
Ethanol	24.3	22.1	9.8	11.3	2.0	1.6	0.6	1.1
	34.4	30.7	10.7	13.9	2.0	3.2	1.6	1.6
	45.1	39.0	10.5	15.7	2.0	5.4	3.0	2.4
Acetonitrile	25.0	22.8	10.8	12.4	2.0	2.8	0.6	2.2
	34.9	29.8	11.4	15.1	2.0	4.5	1.6	2.9
	45.1	38.9	10.4	15.5	2.0	6.5	3.1	3.3

Organic solvent	Organic solvent conc. in feed		Leaking solute (NaCl) flux	Concentration factor	Solute (NaCl) retention ratio in Feed
	Before operation [wt%]	After operation [wt%]	[g/m²·h]	[-]	[%]
Ethanol	15.0	12.9	<0.01	1.04	>99.9
	15.0	12.2	<0.01	1.08	>99.9
	15.0	10.7	<0.01	1.15	>99.9
Acetonitrile	15.0	10.4	<0.01	1.07	>99.9
	15.0	9.0	<0.01	1.12	>99.9
	15.0	8.3	<0.01	1.18	>99.9

[1] Temperature of the feed at module inlet.

[2] Temperature of the feed at module outlet.

[3] Temperature of the cooling water at module inlet.

[4] Temperature of the cooling water at module outlet.

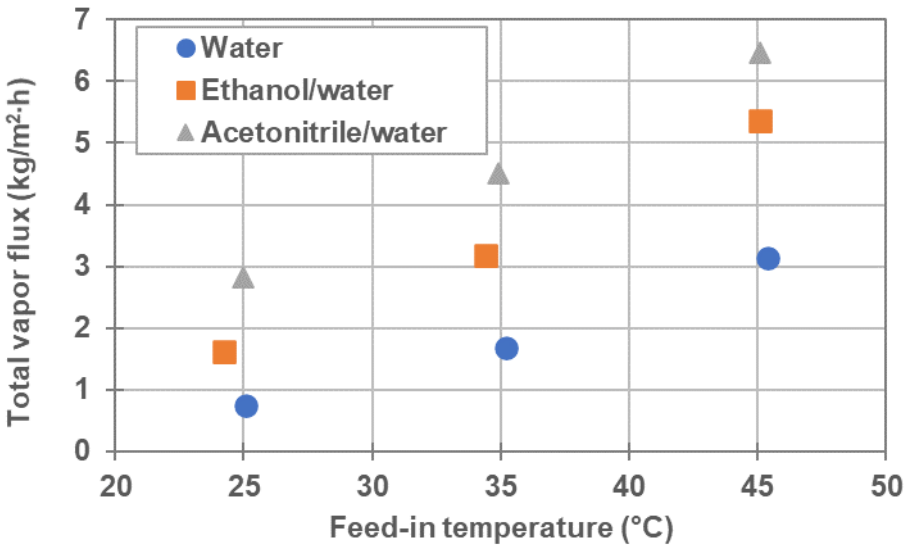

Figure IV-7 Total vapor flux for three kind of feeds, water (Table IV-2), ethanol/water and acetonitrile/water (Table IV-3), as a function of feed-in temperature [89].

These phenomena are qualitatively explained by Raoult's law and Dalton's law. In the case of an ideal solution, according to the Raoult's law, the partial vapor pressure of component *i* in the mixture, P_i (kPa) is given by Equation (IV-9). The total vapor pressure, P_{total} (kPa) is given by Equation (IV-10) according to Dalton's law.

$$P_i = P_i^0 \chi_i \tag{IV-9}$$

$$P_{total} = \Sigma P_i = \Sigma P_i^0 \chi_i \tag{IV-10}$$

where P_i^0 (kPa) indicates the vapor pressure of pure liquid and χ_i the molar fraction of component i. In the case of non-ideal solution like ethanol/water mixture and acetonitrile/water mixture, it is necessary to consider the activity coefficient γ, and Equation (IV-9) is rewritten by Equation (IV-11) [137].

$$P_i = \gamma_i P_i^0 \chi_i \tag{IV-11}$$

where γ_i indicates the activity coefficient of component i. Activity coefficients can be calculate by Wilson equation [138]. In the case of the binary mixture of components *i* and

j, the activity coefficient of those components γ_i and γ_j are given by Equations (IV-12) and (IV-13), respectively.

$$\ln\gamma_i = -\ln(\chi_i + \Lambda_{ij}\chi_j) + \chi_j\left(\frac{\Lambda_{ij}}{\chi_i + \Lambda_{ij}\chi_j} - \frac{\Lambda_{ji}}{\Lambda_{ji}\chi_i + \chi_j}\right) \quad \text{(IV-12)}$$

$$\ln\gamma_j = -\ln(\Lambda_{ji}\chi_i + \chi_j) - \chi_i\left(\frac{\Lambda_{ij}}{\chi_i + \Lambda_{ij}\chi_j} - \frac{\Lambda_{ji}}{\Lambda_{ji}\chi_i + \chi_j}\right) \quad \text{(IV-13)}$$

where Λ_{ij} and Λ_{ji} indicate the Wilson parameters. Those parameters are given by Equation (IV-14).

$$\Lambda_{ij} = exp\left(a_{ij} + \frac{b_{ij}}{T}\right) \quad \text{(IV-14)}$$

where a_{ij} and b_{ij} indicate the parameter coefficients, which are determined by the combination of the components i and j. T indicates absolute temperature [139]. Table IV-4 shows a_{ij}, a_{ji}, b_{ij} and b_{ji} of ethanol/water mixture and acetonitrile/water mixture, which can be obtained from Aspen plus® [140].

Table IV-4 The parameter coefficients for calculation of Wilson parameters of ethanol/water mixture and acetonitrile/water mixture.

Component *i*	**Component *j***	a_{ij}	a_{ji}	b_{ij}	b_{ji}
Ethanol	Water	-2.5035	-0.0503	346.151	-69.6372
Acetonitrile	Water	-0.8487	1.0158	-386.606	-707.346

Figure IV-8(a) shows the vapor pressure, P_i^0, of pure ethanol, acetonitrile and water as a function of temperature, calculated using the Antoine equation, Equation (IV-15) [89,135].

$$log\left(\frac{P_i^0}{100}\right) = \left(A_i - \frac{B_i}{T + C_i}\right) \quad \text{(IV-15)}$$

where A_i, B_i and C_i are constants of Antoine's equation, 100 is a factor to convert "kPa" to "bar", since P_i is in "kPa", and the pressure calculated with parameter shown in Table IV-5 is in "bar". Table 5 shows A_i, B_i and C_i of ethanol, acetonitrile and water, which can be obtained from the website of National Institute of Standards and Technology (NIST). [117]

Table IV-5 The constants of Antoine's equation of ethanol, acetonitrile and water. By using these numbers, the unit of obtained vapor pressure is bar.

Component	A_i	B_i	C_i
Ethanol	5.93296	2345.829	43.815
Acetonitrile	5.37229	1670.409	-40.191
Water	5.40221	1838.675	-31.737

As observed from Figure IV-8(a), the order of vapor pressure of pure liquid is acetonitrile > ethanol > water across all temperature ranges [89].

Furthermore, the activity coefficient and vapor pressure of organic solvent and water were calculated using the feed-in temperature, coolant-in temperature, and molar fraction as operating conditions and are shown in Table IV-6.

Table IV-6 The activity coefficient, vapor pressure of organic solvent and water, calculated from the operating condition of feed-in temperature and coolant-in temperature of the module, and mol-fraction.

Organic solvent	Feed-in [1]								
	Temperature	Organic solvent conc.	Molar fraction		Activity coefficient		Vapor pressure		
			Organic solvent	Water	Organic solvent	Water	Organic solvent	Water	Total
	[°C]	[wt%]	[-]	[-]	[-]	[-]	[kPa]	[kPa]	[kPa]
Ethanol	24.3	15.0	0.065	0.935	3.5	1.0	1.7	2.9	4.6
	34.4	15.0	0.065	0.935	3.6	1.0	3.1	5.2	8.2
	45.1	15.0	0.065	0.935	3.6	1.0	5.4	9.1	14.6
Acetonitrile	25.0	15.0	0.072	0.928	7.9	1.0	6.7	3.0	9.7
	34.9	15.0	0.072	0.928	7.6	1.0	10.1	5.3	15.4
	45.1	15.0	0.072	0.928	7.3	1.0	14.9	9.2	24.1

Organic solvent	Coolant-in [2]							Vapor pressure difference	
	Temperature	Molar fraction		Activity coefficient		Vapor pressure			
		Organic solvent	Water	Organic solvent	Water	Organic solvent	Water	Organic solvent	Water
	[°C]	[-]	[-]	[-]	[-]	[kPa]	[kPa]	[kPa]	[kPa]
Ethanol	9.8	0.000	1.000	-	1.0	-	1.2	1.7	1.7
	10.7	0.000	1.000	-	1.0	-	1.3	3.1	3.9
	10.5	0.000	1.000	-	1.0	-	1.3	5.4	7.9
Acetonitrile	10.8	0.000	1.000	-	1.0	-	1.3	6.7	1.7
	11.4	0.000	1.000	-	1.0	-	1.4	10.1	4.0
	10.4	0.000	1.000	-	1.0	-	1.3	14.9	7.9

[1] The property of the feed at module inlet.

[2] The property of the cooling water at module inlet.

Figure IV-8(b) illustrates the vapor pressure differences between the feed and permeate sides of ethanol/water and acetonitrile/water systems, as a function of feed-in temperature at startup under the experimental conditions specified in Table IV-3 [89]. In Figure IV-8(b), the vapor pressure is calculated using the feed-in temperature and the coolant-in temperature. The molar fractions of organic solvents in the feed were set to 0.072 and 0.065 for acetonitrile and ethanol, respectively, based on a 15 wt% aqueous solution. As the solvent concentration is zero at startup, the molar fractions of the organic solvents were put as zero on the permeate side. To simplify the calculation, a small contribution of the vapor pressure drop by NaCl in the feed was ignored. According to Figures IV-8(a) and IV-8(b), the total vapor pressure difference between the feed and permeate sides of the organic solvent/water mixture was greater than that between the feed and permeate sides of pure water, at the corresponding temperature under the experimental conditions listed in Table IV-3. In addition, the total vapor pressure difference of acetonitrile/water mixture was greater than that of ethanol/water. As a result, it is qualitatively understood that the reason for the increase in total vapor flux, caused by the addition of the organic solvent, is that the total vapor pressure difference increases. In addition, the reason for the total vapor flux for the acetonitrile/water mixture being slightly larger than that for the ethanol /water mixture was attributed to the difference in the total vapor pressure difference. As shown in Table IV-6 and Figure IV-8(b), the partial vapor pressure difference for acetonitrile was greater than that of ethanol. This is ascribed to the larger fraction of acetonitrile (0.072) in the mixture in comparison to ethanol (0.065), as well as, to the larger activity coefficient of acetonitrile. Thus, as shown in Table IV-3, the vapor flux of acetonitrile was higher than that of ethanol at similar feed-in temperatures. Moreover, the ratio of organic solvent vapor flux to the total vapor flux was comparable to or greater than that of water vapor flux, even though the molar fraction of organic solvent was lower than that of water. When DCMD was operated at around 25 °C of feed-in temperature, the ratio of the acetonitrile and ethanol vapor fluxes to the total vapor flux exceeded 60%. This is because ethanol and acetonitrile have a much higher activity coefficient than water in an organic solvent/water mixture, as a result of which the partial vapor pressure of organic solvents becomes comparable or higher than that of water.

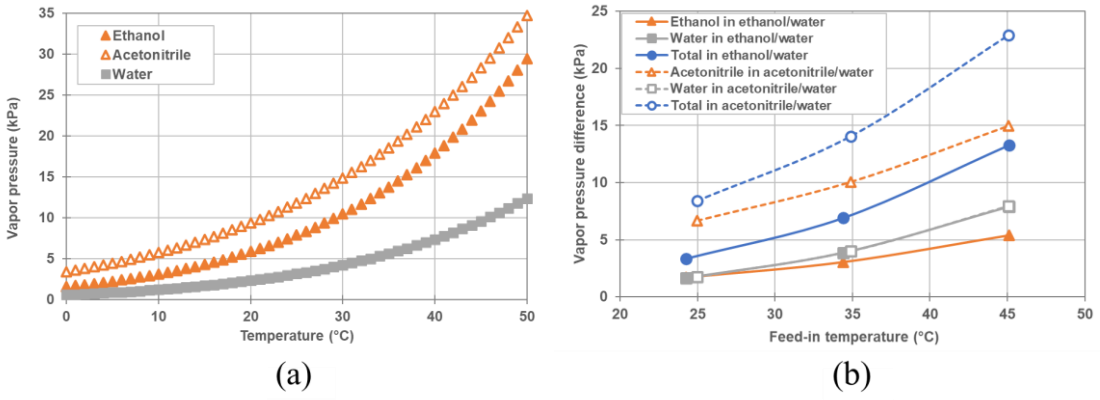

Figure IV-8 (a) Vapor pressure of acetonitrile, ethanol, water as a function of temperature. (b) Vapor pressure differences for etha-nol/water and acetonitrile/water systems between feed side and permeate side in the beginning of operation under the condition shown in Table IV-3 [89]. Open and closed symbols show the vapor pressure difference of acetonitrile/water mixture, and ethanol/water mixture, respectively. Triangles shows the partial vapor pressure difference of organic solvent, squares the partial vapor pressure difference of water, and circles the total vapor pressure difference.

IV. 3. 2. 3. MD performance with various compositions of organic solvent

The effect of the concentration of organic solvents in the feed was also investigated. Herein, the organic solvent/water mixture containing 1000 ppm NaCl was used as the feed, and the feed-in temperature and the coolant-in temperature were set to ≈25 °C and ≈10 °C, respectively. The concentrations of ethanol and acetonitrile in the mixture were varied from 15–50 wt%. The experimental conditions and results are listed in Table IV-7. The total vapor flux is plotted in Figure IV-9 as a function of the concentration of organic solvents, including pure water [89]. As observed, the total vapor flux of organic solvent/water mixture was higher than that of pure water, and increased as the organic solvent fraction increased. Additionally, as shown in Table IV-7, the organic solvent flux increased as the organic solvent fraction increased. Moreover, the total vapor flux and the organic solvent flux for the acetonitrile/water mixture were higher than for the ethanol/water mixture.

Table IV-7 Results of DCMD operation at about 25 °C with the feed which contains 1000 ppm NaCl and various concentration of ethanol or acetonitrile.

Organic solvent	Temperature				Operating time	Vapor flux		
	Feed-in [1]	Feed-out [2]	Coolant-in [3]	Coolant-out [4]		Total	Water	Organic solvent
	[°C]	[°C]	[°C]	[°C]	[h]	[kg/m^2·h]	[kg/m^2·h]	[kg/m^2·h]
Ethanol	24.3	22.1	9.8	11.3	2.0	1.6	0.6	1.1
	24.0	21.9	9.8	11.4	2.0	2.4	0.5	1.9
	24.2	21.9	9.8	11.3	2.0	3.4	0.8	2.6
Acetonitrile	25.0	22.8	10.8	12.4	2.0	2.8	0.6	2.2
	24.3	22.2	9.9	12.0	2.0	4.7	1.2	3.6
	24.3	22.1	9.7	11.7	2.0	5.3	1.0	4.2

Organic solvent	Organic solvent conc. in feed		Leaking solute (NaCl) flux	Concentration factor	Solute (NaCl) retention ratio in Feed
	Before operation	After operation			
	[wt%]	[wt%]	[g/m^2·h]	[-]	[%]
Ethanol	15.0	12.9	<0.01	1.04	>99.9
	30.0	26.9	<0.01	1.06	>99.9
	50.0	47.6	<0.01	1.09	>99.9
Acetonitrile	15.0	10.4	<0.01	1.07	>99.9
	30.0	24.2	<0.01	1.13	>99.9
	50.0	45.6	<0.01	1.14	>99.9

[1] Temperature of the feed at module inlet.

[2] Temperature of the feed at module outlet.

[3] Temperature of the cooling water at module inlet.

[4] Temperature of the cooling water at module outlet.

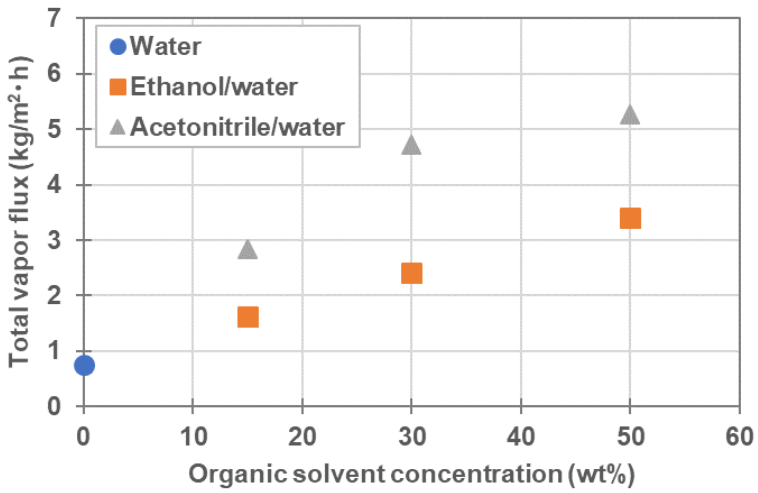

Figure IV-9 The total vapor flux vs organic solvent composition of the feed. The data for water was from Table IV-2 [89].

These phenomena are qualitatively explained as follows: As shown in Equation (IV-11), the partial vapor pressure increases with the molar fraction and the activity coefficient. Table 8 shows the activity coefficient, and vapor pressure of organic solvent and water in the feed and the permeate, which were calculated from the operating conditions of feed-in temperature, coolant-in temperature, and molar fraction shown in Table IV-7. As shown in Table IV-8, the molar fraction of acetonitrile is higher than that of ethanol in the mixture with the same wt%, and the activity coefficient of acetonitrile is higher than that of ethanol. In addition, as shown in Figure IV-8(a), the vapor pressure of pure acetonitrile is higher than that of pure ethanol at the same temperature. Thus, the partial vapor pressure of acetonitrile is higher than that of ethanol in the organic solvent/water mixture with the same wt% at the same temperature. To clearly show this situation, Figure IV-10 shows the vapor pressure difference at the startup of operation, under each condition [89]. It is obvious from Figure IV-10 that the total vapor pressure difference and the partial vapor pressure difference of the organic solvent simultaneously increased with the increase in its molar fraction. In addition, the partial vapor pressure differences of acetonitrile and of ethanol are higher than that of water, and the partial vapor pressure difference of acetonitrile is higher than that of ethanol. Consequently, the total vapor flux and the solvent flux simultaneously increased with the increase of the molar fraction of the organic solvent. Also, the total vapor flux and the solvent flux for

the acetonitrile/water mixture were higher than those of the ethanol/water mixture, since the total vapor pressure difference and the partial vapor pressure difference of the acetonitrile/water organic solvent mixture were higher than those of the ethanol/water mixture.

Surprisingly, as demonstrated in Table IV-7, even when the feed contains 50 wt% ethanol or acetonitrile, the retention ratio of the solute was over 99.9%. This demonstrates that DCMD can be used to recover valuable solutes without losing any solute, even under such harsh conditions for the MD membrane.

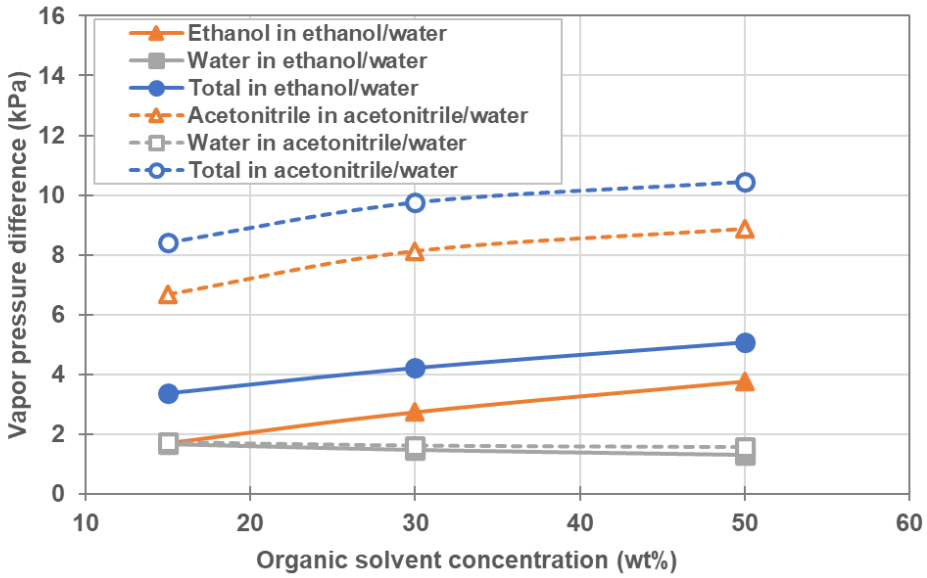

Figure IV-10 Vapor pressure differences between feed side and permeate side of ethanol/water and acetonitrile/water systems in the beginning of operation under the condition shown in Table IV-7 [89]. Open and closed symbols show the vapor pressure difference of ac-etonitrile/water mixture, and ethanol/water mixture, respectively. Triangles show the partial vapor pressure difference of organic solvent, squares the partial vapor pressure difference of water, and circles the total vapor pressure difference.

Table IV-8 The activity coefficient, vapor pressure of organic solvent and water, calculated from the operating conditions of feed-in temperature and mol-fraction.

Organic solvent	Feed-in [1]								
	Temperature	Organic solvent conc.	Molar fraction		Activity coefficient		Vapor pressure		
			Organic solvent	Water	Organic solvent	Water	Organic solvent	Water	Total
	[°C]	[wt%]	[-]	[-]	[-]	[-]	[kPa]	[kPa]	[kPa]
Ethanol	24.3	15.0	0.065	0.935	3.5	1.0	1.7	2.9	4.6
	24.0	30.0	0.143	0.856	2.6	1.0	2.7	2.7	5.4
	24.2	50.0	0.281	0.719	1.8	1.2	3.8	2.5	6.3
Acetonitrile	25.0	15.0	0.072	0.928	7.9	1.0	6.7	3.0	9.7
	24.3	30.0	0.158	0.841	4.5	1.1	8.1	2.8	11.0
	24.3	50.0	0.305	0.695	2.5	1.3	8.9	2.8	11.6

Organic solvent	Coolant-in [2]							Vapor pressure difference	
	Temperature	Molar fraction		Activity coefficient		Vapor pressure			
		Organic solvent	Water	Organic solvent	Water	Organic solvent	Water	Organic solvent	Water
	[°C]	[-]	[-]	[-]	[-]	[kPa]	[kPa]	[kPa]	[kPa]
Ethanol	9.8	0.000	1.000	-	1.0	-	1.2	1.7	1.7
	9.8	0.000	1.000	-	1.0	-	1.2	2.7	1.5
	9.8	0.000	1.000	-	1.0	-	1.2	3.8	1.3
Acetonitrile	10.8	0.000	1.000	-	1.0	-	1.3	6.7	1.7
	9.9	0.000	1.000	-	1.0	-	1.2	8.1	1.6
	9.7	0.000	1.000	-	1.0	-	1.2	8.9	1.6

[1] The property of the feed at module inlet.

[2] The property of the cooling water at module inlet.

IV. 3. 2. 4. Effect of surfactant on MD performance

Polysaccharides [141], phospholipids [142], and peptides [143] comprise valuable surface-active solutes. Surfactants are notoriously difficult to recover using MD because they significantly reduce the surface tension of the aqueous solution, increasing the risk of membrane wetting during MD operation.

The effect of the surfactant in the feed on MD performance was investigated in this section to confirm the possibility of surface-active solute recovery via MD. The DCMD operation was performed for 2 hours with the feed containing 1000 ppm SDS as the model valuable surface-active solute along with 15 wt% acetonitrile, at feed and coolant temperatures of ≈25 °C and ≈10°C, respectively. The experimental condition and result are listed in Table IV-9. No SDS leakage was observed after two hours of operation, as indicated by the change in the cooling water conductivity. This result, therefore, indicates that DCMD with this membrane will be used to effectively recover surface-active solutes.

Table IV-9 Results of DCMD operation at 25 °C with the feed which contains 1000 ppm SDS and 15wt% of acetonitrile.

Organic solvent	Temperature				Operating time	Vapor flux		
	Feed-in [1] [°C]	Feed-out [2] [°C]	Coolant-in [3] [°C]	Coolant-out [4] [°C]	[h]	Total [kg/m²·h]	Water [kg/m²·h]	Organic solvent [kg/m²·h]
Acetonitrile	24.5	22.1	10.1	12.0	2.0	3.2	0.8	2.4

Organic solvent	Organic solvent conc. in feed		Leaking solute (NaCl) flux	Concentration factor	Solute (NaCl) retention ratio in Feed
	Before operation [wt%]	After operation [wt%]	[g/m²·h]	[-]	[%]
Acetonitrile	15.0	10.1	<0.01	1.08	>99.9

[1] Temperature of the feed at module inlet.

[2] Temperature of the feed at module outlet.

[3] Temperature of the cooling water at module inlet.

[4] Temperature of the cooling water at module outlet.

IV. 4. Conclusion

In this chapter, DCMD operation using hydrophobized PVDF HF membranes was investigated to confirm a possibility of recovering heat-sensitive valuable solutes from organic solvents/water mixtures via MD as a non-heated process. At first, the possibility of DCMD operation at low feed temperature was evaluated using 1000 ppm NaCl aqueous solution as the feed, and it was confirmed DCMD could achieve 0.8 kg/m^2·h of vapor flux even at feed and coolant temperatures of 25 °C and 10 °C, respectively. Furthermore, the NaCl retention ratio was observed to be > 99.9%, indicating that it was possible to operate DCMD at low feed temperature. Subsequently, the recovery of solutes from organic solvent/water mixtures was evaluated using ethanol/water and acetonitrile/water mixtures containing 1000 ppm NaCl. As a result, it was confirmed that DCMD could be applied for the recovery of solutes from organic solvent/water mixtures without causing membrane wetting or solute leakage. The effect of feed temperature (25, 35, 45°C) and concentration of organic solvents (15, 30, 50 wt%) were also investigated using ethanol/water and acetonitrile/water mixtures containing 1000 ppm NaCl. The total vapor flux, as well as, the partial vapor flux of organic solvents simultaneously increased with the temperature and concentration of the organic solvents. These phenomena were qualitatively explained by changes in partial vapor pressure of organic solvent in the organic solvent/ water mixtures. Additionally, there was no solute leakage under any of the conditions. Furthermore, investigations using SDS as a model valuable surface-active solute also demonstrated the possibility of recovering surface-active solutes from organic solvent/water mixtures via DCMD. These findings, therefore, indicate that DCMD with a hydrophobic hollow fiber membrane will be applied for the recovery of valuable solutes from organic solvent/water mixtures as a non-heated process even under harsh condition where surface active solutes are included in the feed.

Chapter V

Conclusions

In this thesis, the research on the required membrane properties for the stable long-term MD operation was investigated from the viewpoint of avoiding membrane wetting. It is because that one of the biggest issues on the commercialization of MD is the membrane wetting. To solve the issues of membrane wetting, and to achieve the stable long-term MD operation, I investigated to reveal the required membrane properties for the stable long-term MD operation, by using four PVDF HF membranes. In addition, I investigated to solve the issue of scale precipitation in seawater desalination by VMD. Furthermore, I also investigated the recovery of valuable solutes from organic solvent/water mixtures as a new application of MD. The conclusions of this study are summarized below.

1. Effect of the Characteristic Properties of Membrane on Long-Term Stability in the Vacuum Membrane Distillation Process

In Chapter II, I attempted to evaluate membrane properties that affect the long-term stability of membranes using a VMD system. First, I fabricated two different types of PVDF hollow fiber membranes, M-1 and M-3, then obtained M-2 and M-4 by treating M-1 and M-3 with hydrophobic agents, respectively. Regarding salt retention, I evaluated the salt retention factor using both the salt in the permeate, and also the salt retained on the shell surface of the membrane. Consequently, it was evident that the higher the LEP, the higher the salt retention and vapor flux stability. Theoretically, it should be possible to operate MD without wetting if the LEP of the membrane is higher than the pressure difference between the feed and permeate. However, practically, a much higher LEP than the practical pressure difference was necessary to operate the VMD stably. In the VMD system reported here, in which the vapor pressure difference was approximately 0.1 MPa, it was found that in the case where the LEP was higher than approximately 0.32 MPa, the decrease in vapor flux was less than 10% and the total salt retention factor was over 99.8% during the 100-h VMD operation. Furthermore, I attempted the 300-h VMD operation

using a pilot-scale MD system, which installed the membrane with an LEP of 0.37 MPa (M-2), and demonstrated that the M-2 pilot-scale module was very stable for long-term operations.

2. Effect of membrane properties and operating conditions on preventing scale precipitation in seawater desalination with vacuum membrane distillation

In Chapter III, I investigated the required membrane properties and operating conditions on preventing scale precipitation, which is a severe problem for seawater desalination with MD operation. I focused on Reynolds number of the feed flowing inside of HF membrane because the feed flow in the module changes from a laminar flow to a turbulent flow at a particular Reynolds number. Turbulent flow decreases the concentration polarization at the bulk/membrane interface and decreases scale formation. VMD operation was performed using two types of hydrophobized PVDF hollow fibers with similar morphologies and different inner and outer diameters, using real seawater as a feed. Results of the pressure drop in the module reveal that the feed flow changed from laminar flow to turbulent flow at a Reynolds number greater than 1000. Further, the extent of scale precipitation was mainly influenced by the Reynolds number of the feed flow rather than the linear velocity. As expected, the scale precipitation satisfactorily decreased in the case where Reynolds number of the feed flow was over 1200. This phenomenon was qualitatively explained by the decrease in concentration polarization with the Reynolds number. The vapor flux increased with the Reynolds number, which is the increase in linear velocity of the feed. This was due to the increase in the mean temperature of the feed in the module, resulting in an increase in the vapor pressure difference as a driving force. In addition, the vapor flux was very stable during 24 h of operation at high Reynolds numbers. Regarding the membrane size, it was confirmed that the scale precipitation through the HF with a larger inner diameter was less than that through the HF with a small inner diameter under the same linear velocity of feed flow. This was because the Reynolds number of the feed flow through the HF with a larger inner diameter was larger than that through the HF with a small inner diameter, even at the same linear feed velocity. It was also confirmed that the pressure drop in the module with HF with a larger inner diameter was lower than that in the module with HF with a smaller inner diameter.

Selecting a larger inner diameter HF membrane and operating at a higher linear velocity in which a Reynolds number of >1200 is required to prevent scale precipitation without excessive pressure drop. This study provides guidelines for determining suitable membrane properties and VMD operating conditions.

3. Recovery of Valuable Solutes from Organic Solvent/Water Mixtures via Direct Contact Membrane Distillation (DCMD) as a Non-Heated Process

In Chapter IV, I investigated the recovery of valuable solutes from organic solvent/water mixtures as a new application of MD. The organic solvent/water mixtures are treated in various processes such as chemical, food, and pharmaceutical processes. A treatment of organic solvent/water mixtures with MD has a risk of membrane wetting, since the organic solvent in feed solution decreases the surface tension of the aqueous feed solution. Nevertheless, there would be many merits in applying MD into these processes, such as less membrane fouling than the conventional membrane processes using TMP as the driving force. In addition, MD can treat a heat-sensitive, and pressure sensitive materials. In order to confirm a possibility of recovering heat-sensitive valuable solutes from organic solvents/water mixtures via MD as a non-heated process, I investigated DCMD operation using hydrophobized PVDF HF membranes. At first, the possibility of DCMD operation at low feed temperature was evaluated using 1000 ppm NaCl aqueous solution as the feed, and it was confirmed DCMD could achieve 0.8 $kg/m^2 \cdot h$ of vapor flux even at feed and coolant temperatures of 25 °C and 10 °C, respectively. Furthermore, the NaCl retention ratio was observed to be >99.9%, indicating that it was possible to operate DCMD at low feed temperature. Subsequently, the recovery of solutes from organic solvent/water mixtures was evaluated using ethanol/water and acetonitrile/water mixtures containing 1000 ppm NaCl as a model valuable solute. As a result, it was confirmed that DCMD could be applied for the recovery of solutes from organic solvent/water mixtures without causing membrane wetting or solute leakage, by using a super hydrophobic membrane. The effect of feed temperature (25, 35, 45°C) and concentration of organic solvents (15, 30, 50 wt%) were also investigated using ethanol/water and acetonitrile/water mixtures containing 1000 ppm NaCl. The total vapor flux, as well as, the partial vapor flux of organic solvents simultaneously increased with the temperature and concentration of the organic solvents. These phenomena were

qualitatively explained by changes in partial vapor pressure of organic solvent in the organic solvent/ water mixtures. Additionally, there was no solute leakage under any of the conditions. Furthermore, investigations using SDS as a model valuable surface-active solute also demonstrated the possibility of recovering surface-active solutes from organic solvent/water mixtures via DCMD. These findings, therefore, indicate that DCMD with a hydrophobic hollow fiber membrane will be applied for the recovery of valuable solutes from organic solvent/water mixtures as a non-heated process even under harsh condition where surface active solutes are included in the feed.

Perspective

In this thesis, I investigated to improve the membrane properties and operating methods, from the viewpoint of achieving the stable long-term MD operation. It is because that poor stability is one of the biggest obstacles to commercialization of MD. As a result, I revealed the required membrane characteristics for VMD, in which much higher LEP than TMP is needed. In addition, I also investigated to avoid scale precipitation in seawater desalination, and revealed that the amount of scale precipitation can be reduced significantly under the condition with >1200 of Reynolds number of the feed. It is considered that these results paved the way for commercialization in the desalination application by MD. Regarding the new application of MD, I could demonstrate to handle the organic solvent/water mixtures without heating, which has rarely been conducted in the previous MD studies. So, it is considered that this result can open up new possibilities for MD. I hope that the results of my study will advance the practical application of MD, and help to solve the global issue of water shortage.

Nomenclature

Symbols	Description	Units
a_{ij}, a_{ji}, b_{ij}, b_{ji}	Parameter coefficients determined by the components *i* and *j*	-
A	Total membrane bore surface area	m^2
B	Geometric factor determined by pore structure	-
$C_{b,f}$	Solute concentration in the bulk feed	wt%
C_c	Solute concentrations in cooling water after the operation	wt%
C_c^0	Solute concentrations in cooling water before the operation	wt%
C_f	Salt concentration in feed water	wt%
C_i	Concentration of dissolved cations in cleaning water	wt%
$C_{m,f}$	Solute concentration at the bulk/membrane interface	wt%
C_{os}	Organic solvent concentration of cooling water after the operation	wt%
C_{os}^0	Organic solvent concentration of cooling water before the operation	wt%
C_{osv}	Organic solvent concentration in vapor	wt%
C_p	Salt concentration in permeated water	wt%
C_p^0	Accurate salt concentration of permeated water	wt%
C_{sf}	Solute concentration in the feed after the operation	wt%
C_{sf}^0	Solute concentration in the feed before the operation	wt%
C_w	Salt concentration in washing water	wt%
d	Diameter of the flow path	m
d_h	Hydraulic diameter	m
d_p	Membrane pore diameter	m
D	Diffusion coefficient of the solute	m^2/s
D_W	Diffusion coefficient of water	m^2/s
F	Concentration factor	-
f	Friction coefficient	-
f_l	Friction coefficient of laminar flow	-
f_t	Friction coefficient of turbulent flow	-
J	Vapor flux	$kg/m^2 \cdot h$
J_p	Total permeate vapor flux	$kg/m^2 \cdot h$
J_s	Total leaking solute flux	$g/m^2 \cdot h$
J_{sp}	Leaking salt flux into permeated water	$g/m^2 \cdot h$
J_{sr}	Leaking salt flux remaining on shell surface of membrane	$g/m^2 \cdot h$
J_{st}	Total leaking salt flux	$g/m^2 \cdot h$
J_{os}	Organic solvent vapor flux	$kg/m^2 \cdot h$
J_w	Water vapor flux	$kg/m^2 \cdot h$

k	Solute mass transfer coefficient	m/s
k_B	Boltzmann constant	-
Kn	Knudsen number	-
L	Length of hollow fiber membrane	m
l	Length of the feed channel	m
LEP	Liquid entry pressure	Pa
m_{sf}	Amount of solute in the feed after the operation	kg
m_{sf}^0	Amount of solute in the feed before the operation	kg
m_p	Weight of salt in permeated water	kg
m_p^0	Weight of total permeated salt	kg
m_r	Weight of salt remaining on shell surface of membrane	kg
m_s	Amount of scale precipitation	g
M_i	Molecular weight of dissolved cations	g/mol
M_s	Molecular weight of scale	g/mol
M_W	Molecular weight of water	g/mol
P	Total pressure in the membrane pore	Pa
p_a	Air pressure in the membrane pore	Pa
P_{feed}	Saturated vapor pressure at membrane surface of the feed side	kPa
P_i	Partial vapor pressure of component *i*	kPa
P_i^0	Vapor pressure of pure liquid *i*	kPa
P_m	Mean pressure within the pore	Pa
P_{total}	Total vapor pressure	kPa
$P_{permeate}$	Saturated vapor pressure at membrane surface of the feed side	kPa
ΔP	Pressure drop	Pa
ΔP_l	Pressure drop of laminar flow	Pa
ΔP_t	Pressure drop of turbulent flow	Pa
R	Gas constant	J/K·mol
r	Membrane pore radius	m
r_F	Salt retention factor	%
r_{max}	Maximum pore radius of membrane	m
r_u	Pore size of the membrane composed of uniform size pore	m
Re	Reynolds number	-
Sc	Schmidt number	-
Sh	Sherwood number	-
T	Absolute temperature	K
t	Operation time	h
W_a	Total amount of cleaning solution	g
W_c	Weight of cooling water after the operation	kg

W_c^0	Weight of cooling water before the operation	kg
W_f	Weight of the feed after the operation	kg
W_f^0	Weight of the feed before the operation	kg
W_{os}	Weight of permeated organic solvent through membrane	kg
W_p	Weight of permeated water	kg
W_t	Total weight of permeate	kg
W_w	Weight of washing water	kg
α	Vapor permeation coefficient	kg/m^2·h·kPa
β	Solute retention ratio in the feed	%
γ_i	Activity coefficient of component *i*	-
δ	Membrane thickness	m
δ_B	Thickness of the boundary layer	m
ε	membrane porosity	-
θ	Contact angle of liquid	°
λ	Mean free path of vapor molecule	m
Λ_{ij}, Λ_{ji}	Wilson parameters of the binary mixture of components *i* and *j*	
λ_W	Mean free path of water vapor molecule	m
μ	Viscosity of the fluid	Pa·s
ν	Linear velocity of the fluid	m/s
ρ	Density of the fluid	kg/m^3
σ	Collision diameter of the vapor molecule	m
σ_L	a surface tension of liquid	kg/s^2
τ	Pore tortuosity of the membrane	-
ν	Linear velocity of the fluid	m/s
χ_i	Molar fraction of component *i*	-

References

[1] NASA EARTHDATA, Freshwater availability. Available online: https://earthdata.nasa.gov/learn/toolkits/freshwater-availability (accessed on 13 October 2021).

[2] Z. Huang, X. Yuan, X. Liu, The key drivers for the changes in global water scarcity: Water withdrawal versus water availability, Journal of Hydrology. 601 (2021) 126658. https://doi.org/10.1016/j.jhydrol.2021.126658.

[3] Y. Wada, D. Wisser, S. Eisner, M. Flörke, D. Gerten, I. Haddeland, N. Hanasaki, Y. Masaki, F.T. Portmann, T. Stacke, Z. Tessler, J. Schewe, Multimodel projections and uncertainties of irrigation water demand under climate change, Geophysical Research Letters. 40 (2013) 4626–4632. https://doi.org/10.1002/grl.50686.

[4] Y. Wada, M.F.P. Bierkens, Sustainability of global water use: Past reconstruction and future projections, Environmental Research Letters. 9 (2014) 104003. https://doi.org/10.1088/1748-9326/9/10/104003.

[5] M.M. Mekonnen, A.Y. Hoekstra, Sustainability: Four billion people facing severe water scarcity, Science Advances. 2 (2016) e1500323. https://doi.org/10.1126/sciadv.1500323.

[6] C. Fant, C.A. Schlosser, X. Gao, K. Strzepek, J. Reilly, Projections of water stress based on an ensemble of socioeconomic growth and climate change scenarios: A case study in Asia, PLoS ONE. 11 (2016) e0150633. https://doi.org/10.1371/journal.pone.0150633.

[7] N.A. Eckardt, E. Cominelli, M. Galbiati, C. Tonelli, The Future of Science: Food and Water for Life, The Plant Cell. 21 (2009) 368–372. https://doi.org/10.1105/tpc.109.066209.

[8] D.K. Babi, R. Gani, Hybrid Distillation Schemes, in: Distillation, Elsevier, (2014). https://doi.org/10.1016/B978-0-12-386547-2.00009-0.

[9] A. Cassano, R. Castro-Muñoz, C. Conidi, E. Drioli, Recent Developments in Membrane Technologies for Concentration of Liquid Foods and Food Ingredients, in: Innovative Food Processing Technologies, Elsevier, (2021) 100–121. https://doi.org/10.1016/B978-0-08-100596-5.23036-9.

[10] W.A. Porter, Computational aspects of quadratic signal processing, IEEE Transactions on Acoustics, Speech, and Signal Processing. 38 (1990) 137–144. https://doi.org/10.1109/29.45626.

[11] M. Mulder, Basic Principles of Membrane Technology, Springer Netherlands, Dordrecht, 1996. https://doi.org/10.1007/978-94-009-1766-8.

[12] H. Matsuyama, S. Rajabzadeh, H. Karkhanechi, S. Jeon, 1.7 PVDF Hollow Fibers Membranes, in: Comprehensive Membrane Science and Engineering, Elsevier, (2017) 137–189. https://doi.org/10.1016/b978-0-12-409547-2.12244-9.

[13] S.F. Anis, R. Hashaikeh, N. Hilal, Microfiltration membrane processes: A review of research

trends over the past decade, Journal of Water Process Engineering. 32 (2019) 100941. https://doi.org/10.1016/j.jwpe.2019.100941.

[14] R. Reif, F. Omil, J.M. Lema, Removal of Pharmaceuticals by Membrane Bioreactor (MBR) Technology, Comprehensive Analytical Chemistry. 62 (2013) 287–317. https://doi.org/10.1016/B978-0-444-62657-8.00009-4.

[15] T. Arumugham, N.J. Kaleekkal, S. Gopal, J. Nambikkattu, R. K, A.M. Aboulella, S. Ranil Wickramasinghe, F. Banat, Recent developments in porous ceramic membranes for wastewater treatment and desalination: A review, Journal of Environmental Management. 293 (2021) 112925. https://doi.org/10.1016/j.jenvman.2021.112925.

[16] Y. Huang, X. Feng, Polymer-enhanced ultrafiltration: Fundamentals, applications and recent developments, Journal of Membrane Science. 586 (2019) 53–83. https://doi.org/10.1016/j.memsci.2019.05.037.

[17] A.W. Mohammad, Y.H. Teow, W.L. Ang, Y.T. Chung, D.L. Oatley-Radcliffe, N. Hilal, Nanofiltration membranes review: Recent advances and future prospects, Desalination. 356 (2015) 226–254. https://doi.org/10.1016/j.desal.2014.10.043.

[18] J. Kim, J. Lim, K. Park, S. Hong, Fundamentals and application of reverse osmosis membrane processes, in: Osmosis Engineering, Elsevier, (2021) 17–52. https://doi.org/10.1016/b978-0-12-821016-1.00002-4.

[19] Y.J. Lim, K. Goh, M. Kurihara, R. Wang, Seawater desalination by reverse osmosis: Current development and future challenges in membrane fabrication – A review, Journal of Membrane Science. 629 (2021) 119292. https://doi.org/10.1016/j.memsci.2021.119292.

[20] D.L. Oatley-Radcliffe, M. Walters, T.J. Ainscough, P.M. Williams, A.W. Mohammad, N. Hilal, Nanofiltration membranes and processes: A review of research trends over the past decade, Journal of Water Process Engineering. 19 (2017) 164–171. https://doi.org/10.1016/j.jwpe.2017.07.026.

[21] S. Zhu, S. Zhao, Z. Wang, X. Tian, M. Shi, J. Wang, S. Wang, Improved performance of polyamide thin-film composite nanofiltration membrane by using polyetersulfone/polyaniline membrane as the substrate, Journal of Membrane Science. 493 (2015) 263–274. https://doi.org/10.1016/j.memsci.2015.07.013.

[22] W.-P. Zhu, S.-P. Sun, J. Gao, F.-J. Fu, T.-S. Chung, Dual-layer polybenzimidazole/polyethersulfone (PBI/PES) nanofiltration (NF) hollow fiber membranes for heavy metals removal from wastewater, Journal of Membrane Science. 456 (2014) 117–127. https://doi.org/10.1016/j.memsci.2014.01.001.

[23] M. Kurihara, Y. Ito, Sustainable seawater reverse osmosis desalination as green desalination in the 21st century, Journal of Membrane Science and Research. 6 (2020) 20–29. https://doi.org/10.22079/JMSR.2019.109807.1272.

[24] A. Cassano, N.K. Rastogi, A. Basile, Reverse osmosis in food processing, in: Current Trends and Future Developments on (Bio-) Membranes, Elsevier, 2020. https://doi.org/10.1016/B978-0-12-816777-9.00010-1.

[25] C. Liu, G. Dong, T. Tsuru, H. Matsuyama, Organic solvent reverse osmosis membranes for organic liquid mixture separation: A review, Journal of Membrane Science. 620 (2021) 118882. https://doi.org/10.1016/j.memsci.2020.118882.

[26] D. Dolar, K. Košutić, Removal of Pharmaceuticals by Ultrafiltration (UF), Nanofiltration (NF), and Reverse Osmosis (RO), in: Comprehensive Analytical Chemistry, (2013) 319–344. https://doi.org/10.1016/B978-0-444-62657-8.00010-0.

[27] W.L. Ang, A. Wahab Mohammad, D. Johnson, N. Hilal, Forward osmosis research trends in desalination and wastewater treatment: A review of research trends over the past decade, Journal of Water Process Engineering. 31 (2019) 100886. https://doi.org/10.1016/j.jwpe.2019.100886.

[28] Y.-N. Wang, K. Goh, X. Li, L. Setiawan, R. Wang, Membranes and processes for forward osmosis-based desalination: Recent advances and future prospects, Desalination. 434 (2018) 81–99. https://doi.org/10.1016/j.desal.2017.10.028.

[29] Z. Zhou, Y. Hu, Q. Wang, B. Mi, Carbon nanotube-supported polyamide membrane with minimized internal concentration polarization for both aqueous and organic solvent forward osmosis process, Journal of Membrane Science. 611 (2020) 118273. https://doi.org/10.1016/j.memsci.2020.118273.

[30] E.M. Garcia-Castello, J.R. McCutcheon, M. Elimelech, Performance evaluation of sucrose concentration using forward osmosis, Journal of Membrane Science. 338 (2009) 61–66. https://doi.org/10.1016/j.memsci.2009.04.011.

[31] G. Liu, W. Jin, Pervaporation membrane materials: Recent trends and perspectives, Journal of Membrane Science. 636 (2021) 119557. https://doi.org/10.1016/j.memsci.2021.119557.

[32] X. Feng, R.Y.M. Huang, Liquid Separation by Membrane Pervaporation: A Review, Industrial & Engineering Chemistry Research. 36 (1997) 1048–1066. https://doi.org/10.1021/ie960189g.

[33] L.M. Vane, Review: membrane materials for the removal of water from industrial solvents by pervaporation and vapor permeation, Journal of Chemical Technology & Biotechnology. 94 (2019) 343–365. https://doi.org/10.1002/jctb.5839.

[34] Y.K. Ong, G.M. Shi, N.L. Le, Y.P. Tang, J. Zuo, S.P. Nunes, T.-S. Chung, Recent membrane development for pervaporation processes, Progress in Polymer Science. 57 (2016) 1–31. https://doi.org/10.1016/j.progpolymsci.2016.02.003.

[35] E. Drioli, A. Ali, F. Macedonio, Membrane distillation: Recent developments and perspectives, Desalination. 356 (2015) 56–84. https://doi.org/10.1016/j.desal.2014.10.028.

[36] M. Qasim, I.U. Samad, N.A. Darwish, N. Hilal, Comprehensive review of membrane design and synthesis for membrane distillation, Desalination. 518 (2021) 115168.

https://doi.org/10.1016/j.desal.2021.115168.

[37] P. Wang, T.S. Chung, Recent advances in membrane distillation processes: Membrane development, configuration design and application exploring, Journal of Membrane Science. 474 (2015) 39–56. https://doi.org/10.1016/j.memsci.2014.09.016.

[38] H. Chamani, T. Matsuura, D. Rana, C.Q. Lan, Modeling of pore wetting in vacuum membrane distillation, Journal of Membrane Science. 572 (2019) 332–342. https://doi.org/10.1016/j.memsci.2018.11.018.

[39] S. Adham, A. Hussain, J.M. Matar, R. Dores, A. Janson, Application of Membrane Distillation for desalting brines from thermal desalination plants, Desalination. 314 (2013) 101–108. https://doi.org/10.1016/j.desal.2013.01.003.

[40] A. Al-Karaghouli, L.L. Kazmerski, Energy consumption and water production cost of conventional and renewable-energy-powered desalination processes, Renewable and Sustainable Energy Reviews. 24 (2013) 343–356. https://doi.org/10.1016/j.rser.2012.12.064.

[41] D. González, J. Amigo, F. Suárez, Membrane distillation: Perspectives for sustainable and improved desalination, Renewable and Sustainable Energy Reviews. 80 (2017) 238–259. https://doi.org/10.1016/j.rser.2017.05.078.

[42] S. Goodarzi, E. Jahanshahi Javaran, M. Rahnama, M. Ahmadi, Techno-economic evaluation of a multi effect distillation system driven by low-temperature waste heat from exhaust flue gases, Desalination. 460 (2019) 64–80. https://doi.org/10.1016/j.desal.2019.03.005.

[43] K. Zarzoum, K. Zhani, H. ben Bacha, J. Koschikowski, Experimental parametric study of membrane distillation unit using solar energy, Solar Energy. 188 (2019) 1274–1282. https://doi.org/10.1016/j.solener.2019.07.025.

[44] F. Macedonio, A. Ali, T. Poerio, E. El-Sayed, E. Drioli, M. Abdel-Jawad, Direct contact membrane distillation for treatment of oilfield produced water, Separation and Purification Technology. 126 (2014) 69–81. https://doi.org/10.1016/j.seppur.2014.02.004.

[45] B.B. Ashoor, S. Mansour, A. Giwa, V. Dufour, S.W. Hasan, Principles and applications of direct contact membrane distillation (DCMD): A comprehensive review, Desalination. 398 (2016) 222–246. https://doi.org/10.1016/j.desal.2016.07.043.

[46] M. Khayet, T. Matsuura, Direct Contact Membrane Distillation, in: Membrane Distillation, Elsevier, (2011) 249–293. https://doi.org/10.1016/b978-0-444-53126-1.10010-7.

[47] T. Matsuura, Synthetic Membranes and Membrane Separation Processes, CRC Press, (1994). https://doi.org/10.1201/9781003068037.

[48] K.W. Lawson, D.R. Lloyd, Membrane distillation, Journal of Membrane Science. 124 (1997) 1–25. https://doi.org/10.1016/S0376-7388(96)00236-0.

[49] M. Khayet, K. Khulbe, T. Matsuura, Characterization of membranes for membrane distillation by atomic force microscopy and estimation of their water vapor transfer coefficients in vacuum

membrane distillation process, Journal of Membrane Science. 238 (2004) 199–211. https://doi.org/10.1016/j.memsci.2004.03.036.

[50] S. Kimura, S.-I. Nakao, S.-I. Shimatani, Transport phenomena in membrane distillation, Journal of Membrane Science. 33 (1987) 285–298. https://doi.org/10.1016/S0376-7388(00)80286-0.

[51] M. Khayet, A. Velázquez, J.I. Mengual, Modelling mass transport through a porous partition: Effect of pore size distribution, Journal of Non-Equilibrium Thermodynamics. 29 (2004) 279–299. https://doi.org/10.1515/JNETDY.2004.055.

[52] T.Y. Cath, V.D. Adams, A.E. Childress, Experimental study of desalination using direct contact membrane distillation: A new approach to flux enhancement, Journal of Membrane Science. 228 (2004) 5–16. https://doi.org/10.1016/j.memsci.2003.09.006.

[53] M.A.E.R. Abu-Zeid, Y. Zhang, H. Dong, L. Zhang, H.L. Chen, L. Hou, A comprehensive review of vacuum membrane distillation technique, Desalination. 356 (2015) 1–14. https://doi.org/10.1016/j.desal.2014.10.033.

[54] D. Hou, K.S.S. Christie, K. Wang, M. Tang, D. Wang, J. Wang, Biomimetic superhydrophobic membrane for membrane distillation with robust wetting and fouling resistance, Journal of Membrane Science. 599 (2020) 117708. https://doi.org/10.1016/j.memsci.2019.117708.

[55] J.-M. Li, Z.-K. Xu, Z.-M. Liu, W.-F. Yuan, H. Xiang, S.-Y. Wang, Y.-Y. Xu, Microporous polypropylene and polyethylene hollow fiber membranes. Part 3. Experimental studies on membrane distillation for desalination, Desalination. 155 (2003) 153–156. https://doi.org/10.1016/S0011-9164(03)00292-3.

[56] N. Tang, Q. Jia, H. Zhang, J. Li, S. Cao, Preparation and morphological characterization of narrow pore size distributed polypropylene hydrophobic membranes for vacuum membrane distillation via thermally induced phase separation, Desalination. 256 (2010) 27–36. https://doi.org/10.1016/j.desal.2010.02.024.

[57] S. Simone, A. Figoli, A. Criscuoli, M.C. Carnevale, S.M. Alfadul, H.S. Al-Romaih, F.S. al Shabouna, O.A. Al-Harbi, E. Drioli, Effect of selected spinning parameters on PVDF hollow fiber morphology for potential application in desalination by VMD, Desalination. 344 (2014) 28–35. https://doi.org/10.1016/j.desal.2014.03.004.

[58] J. Zhang, J. de Li, S. Gray, Effect of applied pressure on performance of PTFE membrane in DCMD, Journal of Membrane Science. 369 (2011) 514–525. https://doi.org/10.1016/j.memsci.2010.12.033.

[59] L. Zhao, C. Wu, Z. Liu, Q. Zhang, X. Lu, Highly porous PVDF hollow fiber membranes for VMD application by applying a simultaneous co-extrusion spinning process, Journal of Membrane Science. 505 (2016) 82–91. https://doi.org/10.1016/j.memsci.2016.01.014.

[60] Z. Cui, J. Pan, Z. Wang, M. Frappa, E. Drioli, F. Macedonio, Hyflon/PVDF membranes prepared by NIPS and TIPS: Comparison in MD performance, Separation and Purification Technology.

247 (2020) 116992. https://doi.org/10.1016/j.seppur.2020.116992.

[61] C. Fang, S. Jeon, S. Rajabzadeh, L. Cheng, L. Fang, H. Matsuyama, Tailoring the surface pore size of hollow fiber membranes in the TIPS process, Journal of Materials Chemistry A. 6 (2018) 535–547. https://doi.org/10.1039/C7TA08295A.

[62] L.N. Nthunya, L. Gutierrez, A.R. Verliefde, S.D. Mhlanga, Enhanced flux in direct contact membrane distillation using superhydrophobic PVDF nanofibre membranes embedded with organically modified SiO_2 nanoparticles, Journal of Chemical Technology & Biotechnology. 94 (2019) 2826–2837. https://doi.org/10.1002/jctb.6104.

[63] H. Li, W. Shi, X. Zeng, S. Huang, H. Zhang, X. Qin, Improved desalination properties of hydrophobic GO-incorporated PVDF electrospun nanofibrous composites for vacuum membrane distillation, Separation and Purification Technology. 230 (2020) 115889. https://doi.org/10.1016/j.seppur.2019.115889.

[64] L.D. Tijing, Y.C. Woo, W.-G. Shim, T. He, J.-S. Choi, S.-H. Kim, H.K. Shon, Superhydrophobic nanofiber membrane containing carbon nanotubes for high-performance direct contact membrane distillation, Journal of Membrane Science. 502 (2016) 158–170. https://doi.org/10.1016/j.memsci.2015.12.014.

[65] L. Eykens, K. de Sitter, C. Dotremont, L. Pinoy, B. van der Bruggen, Membrane synthesis for membrane distillation: A review, Separation and Purification Technology. 182 (2017) 36–51. https://doi.org/10.1016/j.seppur.2017.03.035.

[66] S. Al-Obaidani, E. Curcio, F. Macedonio, G. di Profio, H. Al-Hinai, E. Drioli, Potential of membrane distillation in seawater desalination: Thermal efficiency, sensitivity study and cost estimation, Journal of Membrane Science. 323 (2008) 85–98. https://doi.org/10.1016/j.memsci.2008.06.006.

[67] A. Alkhudhiri, N. Darwish, N. Hilal, Membrane distillation: A comprehensive review, Desalination. 287 (2012) 2–18. https://doi.org/10.1016/j.desal.2011.08.027.

[68] I. Janajreh, K. el Kadi, R. Hashaikeh, R. Ahmed, Numerical investigation of air gap membrane distillation (AGMD): Seeking optimal performance, Desalination. 424 (2017) 122–130. https://doi.org/10.1016/j.desal.2017.10.001.

[69] A.S. Alsaadi, N. Ghaffour, J.-D. Li, S. Gray, L. Francis, H. Maab, G.L. Amy, Modeling of air-gap membrane distillation process: A theoretical and experimental study, Journal of Membrane Science. 445 (2013) 53–65. https://doi.org/10.1016/j.memsci.2013.05.049.

[70] J.H. Hanemaaijer, J. van Medevoort, A.E. Jansen, C. Dotremont, E. van Sonsbeek, T. Yuan, L. de Ryck, Memstill membrane distillation - a future desalination technology, Desalination. 199 (2006) 175–176. https://doi.org/10.1016/j.desal.2006.03.163.

[71] I.A. Said, T. Chomiak, J. Floyd, Q. Li, Sweeping gas membrane distillation (SGMD) for wastewater treatment, concentration, and desalination: A comprehensive review, Chemical

Engineering and Processing - Process Intensification. 153 (2020) 107960. https://doi.org/10.1016/j.cep.2020.107960.

[72] Z. Ding, L. Liu, Z. Li, R. Ma, Z. Yang, Experimental study of ammonia removal from water by membrane distillation (MD): The comparison of three configurations, Journal of Membrane Science. 286 (2006) 93–103. https://doi.org/10.1016/j.memsci.2006.09.015.

[73] M. Khayet, Membranes and theoretical modeling of membrane distillation: A review, Advances in Colloid and Interface Science. 164 (2011) 56–88. https://doi.org/10.1016/j.cis.2010.09.005.

[74] M. Khayet, T. Matsuura, Vacuum Membrane Distillation, in: Membrane Distillation, Elsevier, (2011) 323–359. https://doi.org/10.1016/b978-0-444-53126-1.10012-0.

[75] H. Maab, L. Francis, A. Al-saadi, C. Aubry, N. Ghaffour, G. Amy, S.P. Nunes, Synthesis and fabrication of nanostructured hydrophobic polyazole membranes for low-energy water recovery, Journal of Membrane Science. 423–424 (2012) 11–19. https://doi.org/10.1016/j.memsci.2012.07.009.

[76] B. Li, K.K. Sirkar, Novel membrane and device for vacuum membrane distillation-based desalination process, Journal of Membrane Science. 257 (2005) 60–75. https://doi.org/10.1016/j.memsci.2004.08.040.

[77] J.-W. Wang, L. Li, J.-Q. Gu, M.-Y. Yang, X. Xu, C.-S. Chen, H.-T. Wang, S. Agathopoulos, Highly stable hydrophobic SiNCO nanoparticle-modified silicon nitride membrane for zero-discharge water desalination, AIChE Journal. 63 (2017) 1272–1277. https://doi.org/10.1002/aic.15500.

[78] G. Viader, O. Casal, B. Lefèvre, N. de Arespacochaga, C. Echevarría, J. López, C. Valderrama, J.L. Cortina, Integration of membrane distillation as volume reduction technology for in-land desalination brines management: Pre-treatments and scaling limitations, Journal of Environmental Management. 289 (2021) 112549. https://doi.org/10.1016/j.jenvman.2021.112549.

[79] A. Yadav, P.K. Labhasetwar, V.K. Shahi, Membrane distillation crystallization technology for zero liquid discharge and resource recovery: Opportunities, challenges and futuristic perspectives, Science of The Total Environment. 806 (2022) 150692. https://doi.org/10.1016/j.scitotenv.2021.150692.

[80] Muhammad Yaqub, W. Lee, Zero-liquid discharge (ZLD) technology for resource recovery from wastewater: A review, Science of The Total Environment. 681 (2019) 551–563. https://doi.org/10.1016/j.scitotenv.2019.05.062.

[81] X. An, Y. Hu, N. Wang, Z. Zhou, Z. Liu, Continuous juice concentration by integrating forward osmosis with membrane distillation using potassium sorbate preservative as a draw solute, Journal of Membrane Science. 573 (2019) 192–199. https://doi.org/10.1016/j.memsci.2018.12.010.

[82] P. Onsekizoglu Bagci, Potential of Membrane Distillation for Production of High Quality Fruit Juice Concentrate, Critical Reviews in Food Science and Nutrition. 55 (2015) 1098–1113. https://doi.org/10.1080/10408398.2012.685116.

[83] Y. Suga, R. Takagi, H. Matsuyama, Effect of the Characteristic Properties of Membrane on Long-Term Stability in the Vacuum Membrane Distillation Process, Membranes. 11 (2021) 252. https://doi.org/10.3390/membranes11040252.

[84] Y. Suga, R. Takagi, H. Matsuyama, Effect of hollow fiber membrane properties and operating conditions on avoiding scale precipitation in seawater desalination with vacuum membrane distillation, Desalination (in press).

[85] D.M. Warsinger, J. Swaminathan, E. Guillen-Burrieza, H.A. Arafat, J.H. Lienhard V, Scaling and fouling in membrane distillation for desalination applications: A review, Desalination. 356 (2015) 294–313. https://doi.org/10.1016/j.desal.2014.06.031.

[86] H.C. Duong, M. Duke, S. Gray, P. Cooper, L.D. Nghiem, Membrane scaling and prevention techniques during seawater desalination by air gap membrane distillation, Desalination. 397 (2016) 92–100. https://doi.org/10.1016/j.desal.2016.06.025.

[87] M. Gryta, J. Grzechulska-Damszel, A. Markowska, K. Karakulski, The influence of polypropylene degradation on the membrane wettability during membrane distillation, Journal of Membrane Science. 326 (2009) 493–502. https://doi.org/10.1016/j.memsci.2008.10.022.

[88] E. Guillen-Burrieza, R. Thomas, B. Mansoor, D. Johnson, N. Hilal, H. Arafat, Effect of dry-out on the fouling of PVDF and PTFE membranes under conditions simulating intermittent seawater membrane distillation (SWMD), Journal of Membrane Science. 438 (2013) 126–139. https://doi.org/10.1016/j.memsci.2013.03.014.

[89] Y. Suga, R. Takagi, H. Matsuyama, Recovery of Valuable Solutes from Organic Solvent/Water Mixtures via Direct Contact Membrane Distillation (DCMD) as a Non-Heated Process, Membranes. 11 (2021) 559. https://doi.org/10.3390/membranes11080559.

[90] K. Nagata, Introduction of membrane distillation technology., PHARM TECH JAPAN 2016, Vol. 32, No.1. (2016) 61–64.

[91] S. Santoro, I. Vidorreta, I. Coelhoso, J. Lima, G. Desiderio, G. Lombardo, E. Drioli, R. Mallada, J. Crespo, A. Criscuoli, A. Figoli, Experimental Evaluation of the Thermal Polarization in Direct Contact Membrane Distillation Using Electrospun Nanofiber Membranes Doped With Molecular Probes, Molecules. 24 (2019) 638. https://doi.org/10.3390/molecules24030638.

[92] L. Gao, J. Zhang, S. Gray, J. de Li, Experimental study of hollow fiber permeate gap membrane distillation and its performance comparison with DCMD and SGMD, Separation and Purification Technology. 188 (2017) 11–23. https://doi.org/10.1016/j.seppur.2017.07.009.

[93] K.W. Lawson, D.R. Lloyd, Membrane distillation. I. Module design and performance evaluation using vacuum membrane distillation, Journal of Membrane Science. 120 (1996) 111–121.

https://doi.org/10.1016/0376-7388(96)00140-8.

[94] K. Nagata, H. Arai, Membrane distillation apparatus and hydrophobic porous membrane, U.S. Patent No. 10,898,858 B2, (2021).

[95] T. Hashimoto, H. Arai, K. Nagata, H. Takezawa, T. Otoyo, Porous membrane for membrane distillation, and method for operating the MD module, PCT International Publication No. WO2018/174279A1, (2018).

[96] Z. Song, M. Xing, J. Zhang, B. Li, S. Wang, Determination of phase diagram of a ternary PVDF/γ-BL/DOP system in TIPS process and its application in preparing hollow fiber membranes for membrane distillation, Separation and Purification Technology. 90 (2012) 221–230. https://doi.org/10.1016/j.seppur.2012.02.043.

[97] L. Zhao, X. Lu, C. Wu, Q. Zhang, Flux enhancement in membrane distillation by incorporating AC particles into PVDF polymer matrix, Journal of Membrane Science. 500 (2016) 46–54. https://doi.org/10.1016/j.memsci.2015.11.010.

[98] D. Tong, X. Wang, M. Ali, C.Q. Lan, Y. Wang, E. Drioli, Z. Wang, Z. Cui, Preparation of Hyflon AD60/PVDF composite hollow fiber membranes for vacuum membrane distillation, Separation and Purification Technology. 157 (2016) 1–8. https://doi.org/10.1016/j.seppur.2015.11.026.

[99] H. Zhang, B. Li, D. Sun, X. Miao, Y. Gu, SiO_2-PDMS-PVDF hollow fiber membrane with high flux for vacuum membrane distillation, Desalination. 429 (2018) 33–43. https://doi.org/10.1016/j.desal.2017.12.004.

[100] K. Chen, C. Xiao, Q. Huang, H. Liu, H. Liu, Y. Wu, Z. Liu, Study on vacuum membrane distillation (VMD) using FEP hollow fiber membrane, Desalination. 375 (2015) 24–32. https://doi.org/10.1016/j.desal.2015.07.021.

[101] Q. Sun, Z. Yang, C. Hu, C. Li, G. Yan, Z. Wang, Facile preparation of superhydrophobic PVDF microporous membranes with excellent anti-fouling ability for vacuum membrane distillation, Journal of Membrane Science. 605 (2020) 118106. https://doi.org/10.1016/j.memsci.2020.118106.

[102] M. Gryta, Alkaline scaling in the membrane distillation process, Desalination. 228 (2008) 128–134. https://doi.org/10.1016/j.desal.2007.10.004.

[103] M. Gryta, Long-term performance of membrane distillation process, Journal of Membrane Science. 265 (2005) 153–159. https://doi.org/10.1016/j.memsci.2005.04.049.

[104] E. Guillen-Burrieza, A. Ruiz-Aguirre, G. Zaragoza, H.A. Arafat, Membrane fouling and cleaning in long term plant-scale membrane distillation operations, Journal of Membrane Science. 468 (2014) 360–372. https://doi.org/10.1016/j.memsci.2014.05.064.

[105] E. Curcio, X. Ji, G. di Profio, A.O. Sulaiman, E. Fontananova, E. Drioli, Membrane distillation operated at high seawater concentration factors: Role of the membrane on $CaCO_3$ scaling in presence of humic acid, Journal of Membrane Science. 346 (2010) 263–269.

https://doi.org/10.1016/j.memsci.2009.09.044.

[106] G. Guan, H. Lou, C. Yao, J. Li, X. Yang, Achieving sustainable operation for hypersaline membrane distillation applications: A novel strategy based on the critical Reynolds number, Desalination. 499 (2021) 114833. https://doi.org/10.1016/j.desal.2020.114833.

[107] H. Julian, Y. Ye, H. Li, V. Chen, Scaling mitigation in submerged vacuum membrane distillation and crystallization (VMDC) with periodic air-backwash, Journal of Membrane Science. 547 (2018) 19–33. https://doi.org/10.1016/j.memsci.2017.10.035.

[108] G. Chen, X. Yang, Y. Lu, R. Wang, A.G. Fane, Heat transfer intensification and scaling mitigation in bubbling-enhanced membrane distillation for brine concentration, Journal of Membrane Science. 470 (2014) 60–69. https://doi.org/10.1016/j.memsci.2014.07.017.

[109] Y. Ye, S. Yu, L. Hou, B. Liu, Q. Xia, G. Liu, P. Li, Microbubble aeration enhances performance of vacuum membrane distillation desalination by alleviating membrane scaling, Water Research. 149 (2019) 588–595. https://doi.org/10.1016/j.watres.2018.11.048.

[110] M. Gryta, Polyphosphates used for membrane scaling inhibition during water desalination by membrane distillation, Desalination. 285 (2012) 170–176. https://doi.org/10.1016/j.desal.2011.09.051.

[111] F. He, K.K. Sirkar, J. Gilron, Effects of antiscalants to mitigate membrane scaling by direct contact membrane distillation, Journal of Membrane Science. 345 (2009) 53–58. https://doi.org/10.1016/j.memsci.2009.08.021.

[112] A. Ramadhan Al-Obaidi, I. Chaer, Study of the flow characteristics, pressure drop and augmentation of heat performance in a horizontal pipe with and without twisted tape inserts, Case Studies in Thermal Engineering. 25 (2021) 100964. https://doi.org/10.1016/j.csite.2021.100964.

[113] E. Marušić-Paloka, I. Pažanin, Effects of boundary roughness and inertia on the fluid flow through a corrugated pipe and the formula for the Darcy–Weisbach friction coefficient, International Journal of Engineering Science. 152 (2020) 103293. https://doi.org/10.1016/j.ijengsci.2020.103293.

[114] T. Hashimoto, Y. Suga, Raw-Material Liquid Concentration System and Concentration Apparatus, PCT International Publication No. WO2021/070955A1, (2021).

[115] X. Fang, Y. Xu, Z. Zhou, New correlations of single-phase friction factor for turbulent pipe flow and evaluation of existing single-phase friction factor correlations, Nuclear Engineering and Design. 241 (2011) 897–902. https://doi.org/10.1016/j.nucengdes.2010.12.019.

[116] T. Waly, M.D. Kennedy, G.J. Witkamp, G. Amy, J.C. Schippers, Will calcium carbonate really scale in seawater reverse osmosis?, Desalination and Water Treatment. 5 (2009) 146–152. https://doi.org/10.5004/dwt.2009.577.

[117] NIST Chemistry WebBook, SRD69. Available online: https://webbook.nist.gov/chemistry/ (accessed on 20 September 2021).

[118] Thermophysical properties of seawater. Available online: http://web.mit.edu/seawater/ (accessed on 15 December 2021).

[119] T. Nishimura, Y. Ohori, Y. Kajimoto, Y. Kawamura, Mass transfer characteristics in a channel with symmetric wavy wall for steady flow., JOURNAL OF CHEMICAL ENGINEERING OF JAPAN. 18 (1985) 550–555. https://doi.org/10.1252/jcej.18.550.

[120] L. Martínez-Díez, M.I. Vázquez-González, Temperature and concentration polarization in membrane distillation of aqueous salt solutions, Journal of Membrane Science. 156 (1999) 265–273. https://doi.org/10.1016/S0376-7388(98)00349-4.

[121] T. Kanamori, K. Sakai, T. Awaka, M. Fukuda, Mass Transfer in Laminar Flows around Single Hollow-Fiber Membranes for Hemodialysis., JOURNAL OF CHEMICAL ENGINEERING OF JAPAN. 27 (1994). https://doi.org/10.1252/jcej.27.830.

[122] V. Gekas, B. Hallström, Mass transfer in the membrane concentration polarization layer under turbulent cross flow, Journal of Membrane Science. 30 (1987) 153–170. https://doi.org/10.1016/S0376-7388(00)81349-6.

[123] Y. Ma, C. Zhu, P. Ma, K.T. Yu, Studies on the Diffusion Coefficients of Amino Acids in Aqueous Solutions, Journal of Chemical & Engineering Data. 50 (2005) 1192–1196. https://doi.org/10.1021/je049582g.

[124] L. Yuan-Hui, S. Gregory, Diffusion of ions in sea water and in deep-sea sediments, Geochimica et Cosmochimica Acta. 38 (1974) 703–714. https://doi.org/10.1016/0016-7037(74)90145-8.

[125] P. Marchetti, M.F. Jimenez Solomon, G. Szekely, A.G. Livingston, Molecular separation with organic solvent nanofiltration: A critical review, Chemical Reviews. 114 (2014) 10735–10806. https://doi.org/10.1021/cr500006j.

[126] M.G. Buonomenna, J. Bae, Organic Solvent Nanofiltration in Pharmaceutical Industry, Separation & Purification Reviews. 44 (2015) 157–182. https://doi.org/10.1080/15422119.2014.918884.

[127] P. Marchetti, A. Butté, A.G. Livingston, Quality by Design for peptide nanofiltration: Fundamental understanding and process selection, Chemical Engineering Science. 101 (2013) 200–212. https://doi.org/10.1016/j.ces.2013.06.014.

[128] R.B. Merlet, M.A. Pizzoccaro-Zilamy, A. Nijmeijer, L. Winnubst, Hybrid ceramic membranes for organic solvent nanofiltration: State-of-the-art and challenges, Journal of Membrane Science. 599 (2020). https://doi.org/10.1016/j.memsci.2020.117839.

[129] P. Vandezande, L.E.M. Gevers, I.F.J. Vankelecom, Solvent resistant nanofiltration: separating on a molecular level, Chem. Soc. Rev. 37 (2008) 365–405. https://doi.org/10.1039/B610848M.

[130] G. Szekely, M.F. Jimenez-Solomon, P. Marchetti, J.F. Kim, A.G. Livingston, Sustainability assessment of organic solvent nanofiltration: From fabrication to application, Green Chemistry. 16 (2014) 4440–4473. https://doi.org/10.1039/c4gc00701h.

[131] G. Székely, J. Bandarra, W. Heggie, B. Sellergren, F.C. Ferreira, Organic solvent nanofiltration: A platform for removal of genotoxins from active pharmaceutical ingredients, Journal of Membrane Science. 381 (2011) 21–33. https://doi.org/10.1016/j.memsci.2011.07.007.

[132] M. Rabiller-Baudry, G. Nasser, D. Delaunay, A. Keraani, T. Renouard, D. Roizard, H. ben Soltane, C. Fischmeister, J.L. Couturier, D. Dhaler, Interests and challenges of organic solvent nanofiltration for sustainable chemistry: The case of homogeneous catalysis of metathesis, WIT Transactions on Ecology and the Environment. 154 (2011) 141–152. https://doi.org/10.2495/CHEM110141.

[133] R. Othman, A.W. Mohammad, M. Ismail, J. Salimon, Application of polymeric solvent resistant nanofiltration membranes for biodiesel production, Journal of Membrane Science. 348 (2010) 287–297. https://doi.org/10.1016/j.memsci.2009.11.012.

[134] J. Zhang, Z. Song, B. Li, Q. Wang, S. Wang, Fabrication and characterization of superhydrophobic poly (vinylidene fluoride) membrane for direct contact membrane distillation, Desalination. 324 (2013) 1–9. https://doi.org/10.1016/j.desal.2013.05.018.

[135] F.A. Banat, J. Simandl, Membrane distillation for dilute ethanol, Journal of Membrane Science. 163 (1999) 333–348. https://doi.org/10.1016/S0376-7388(99)00178-7.

[136] O. Gupta, S. Roy, S. Mitra, Enhanced membrane distillation of organic solvents from their aqueous mixtures using a carbon nanotube immobilized membrane, Journal of Membrane Science. 568 (2018) 134–140. https://doi.org/10.1016/j.memsci.2018.10.002.

[137] M. Hristova, T. Donchev, D. Kolev, I. Baloch, H. Georgiev, PARAMETER'S ESTIMATE IN WILSON EQUATION, International Electronic Journal of Pure and Applied Mathematics. 7 (2015) 29–35. https://doi.org/10.12732/iejpam.v9i1.4.

[138] G.M. Wilson, Vapor-Liquid Equilibrium. XI. A New Expression for the Excess Free Energy of Mixing, Journal of the American Chemical Society. 86 (1964) 127–130. https://doi.org/10.1021/ja01056a002.

[139] J. Yousefi Seyf, A. Haghtalab, Measurement and Thermodynamic Modeling of the Solubility of Lamotrigine, Deferiprone, Cefixime Trihydrate, and Cephalexin Monohydrate in Different Pure Solvents from 283.1 to 323.1 K, Journal of Chemical & Engineering Data. 61 (2016) 2170–2178. https://doi.org/10.1021/acs.jced.6b00163.

[140] Aspen Technology Inc., Aspen plus®, https://www.aspentech.com/en/products/engineering/aspen-plus (accessed on 31 October 2021).

[141] T. Zhang, R.E. Marchant, Novel Polysaccharide Surfactants: The Effect of Hydrophobic and Hydrophilic Chain Length on Surface Active Properties, Journal of Colloid and Interface Science. 177 (1996) 419–426. https://doi.org/10.1006/jcis.1996.0054.

[142] P. Weschayanwiwat, J.F. Scamehorn, P.J. Reilly, Surfactant properties of low molecular weight phospholipids, Journal of Surfactants and Detergents. 8 (2005) 65–72.

https://doi.org/10.1007/s11743-005-0332-8.

[143] A.F. Dexter, A.P.J. Middelberg, Peptides As Functional Surfactants, Industrial & Engineering Chemistry Research. 47 (2008) 6391–6398. https://doi.org/10.1021/ie800127f.

List of Publications

Chapter II Yuki SUGA, Ryosuke TAKAGI, Hideto MATSUYAMA: Effect of the Characteristic Properties of Membrane on Long-Term Stability in the Vacuum Membrane Distillation Process, Membranes, 11, 252-267 (2021) https://doi.org/10.3390/membranes11040252.

Chapter III Yuki SUGA, Ryosuke TAKAGI, Hideto MATSUYAMA: Effect of hollow fiber membrane properties and operating conditions on avoiding scale precipitation in seawater desalination with vacuum membrane distillation, Desalination (in press).

Chapter IV Yuki SUGA, Ryosuke TAKAGI, Hideto MATSUYAMA: Recovery of Valuable Solutes from Organic Solvent/Water Mixtures via Direct Contact Membrane Distillation (DCMD) as a Non-Heated Process, Membranes, 11, 559-578 (2021) https://doi.org/10.3390/membranes11080559.

Acknowledgement

First of all, I would like to express my sincere gratitude to Prof. Hideto Matsuyama for the opportunity to conduct my research under his supervision. Through your leading and support, I could learn a lot about my study and myself. I am proud to have received your guidance.

I would also like to show my greatest appreciation to Dr. Ryosuke Takagi for the continuous support to my research. You have given me constructive comments and warm encouragement. Without your guidance and persistent support, I would not have been possible to accomplish my PhD thesis.

I sincerely thank Prof. Atsunori Mori and Prof. Chiaki Ogino for your kindness during the reviewing and examining of this thesis and giving constructive comments to improve upon it.

I am also particularly grateful for Dr. Masato Mikawa and Dr. Noboru Kubota in Asahi Kasei Corporation. You have given me this valuable opportunity to challenge the doctoral course. And you have provided me with various support beyond your scope of business for four years. I will never forget this favor as long as my life.

I would like to express my gratitude to Keitaro Suzumura and Mitsuru Fujita in Asahi Kasei Corporation. You have given me as much support as possible in coordinating my work. I would like to return this grace to our business.

I would also like to offer my special thanks to Sachiko Yamashima, Mitsumi Torii, and Yukiko Kimura in Asahi Kasei Corporation for your technical support and cooperation. With your kindly support, I could always carry on the experiments. Thank you for the consecutive support on my research.

Finally, I am forever grateful to my wife. You have continuously supported me so that I can concentrate to my work and research. I would not have accomplished my PhD thesis without you.

Yuki Suga
Graduate school of Engineering
Kobe University, 2022

Doctoral Dissertation, Kobe University
“Study on development of hollow fiber membrane distillation technology and new applications”, 117 pages
Submitted on January, 19, 2022
The date of publication is printed in cover of repository version published in Kobe University Repository Kernel.

© Yuki Suga
All Rights Reserved, 2022